International PhD Program in Biomolecular Sciences

Department of Cellular, Computational and Integrative Biology – CIBIO

XXXII Cycle

"The m6A RNA modification sustains neuroblastoma tumour aggressiveness"

Tutor

Prof. Alessandro Quattrone

Department CIBIO, University of Trento

Ph.D. Thesis of

Giulia Montuori

Department CIBIO, University of Trento

Academic Year 2018-2019

Original authorship:

Declaration:

I, Giulia Montuori, confirm that this is my own work and the use of all materials from other sources has been properly and fully acknowledged.

Trento, 18/09/2020

ACKNOWLEDGEMENT

This thesis represents the work of my PhD. In the past four years, I worked in a stimulating centre and met a lot of great researchers and persons.

First of all, I would like to thank Prof. Alessandro Quattrone for letting me work on this project and for encouraging my research. The opportunity that he gave me has profoundly defined my life both at the professional and personal level.

I thank Dr Luigi Pasini from whom I inherited the project and who guided me at the beginning of my time in CIBIO and in Trento.

A special thanks to all the member of the Laboratory of Translational Genomics that helped me to grow as a scientist and as an individual.

I would like to express my thanks to Internal Committee members, Prof. Alessandro Provenzani and Dr Luca Tiberi for their comments and suggestion which let me improve this manuscript.

Last, but not least a special thanks to Prof. Alessandro Fatica and Prof. Francesca Aguilo for have accepted to be members of my External Committee and for the stimulating discussion that we will have during my PhD defence.

TABLE OF CONTENTS

ABSTRACT

The N6-methyladenosine, also known as m6A, is the most common post-transcriptional modification in mRNAs and long non-coding RNAs and that profoundly influences mRNA biology, from early processing in the nucleus to final steps of translation and decay in the cytoplasm. Taking into consideration the importance of RNA in shaping cell fate, m6A is widely recognized as an additional layer in the regulation of gene expression, also thanks to its dynamic and reversible nature. Therefore, it is not surprising that any misregulation in m6A content might lead to the loss of cellular homeostasis. This effect is particularly evident when it comes to stem cells differentiation, embryo development and cancer. In a tumorigenic context, the m6A could affect the development, progression, cancer stem cells (CSCs) renewal and drug resistance of solid and liquid tumours. So, the m6A is consistently becoming a new attractive pharmacological target.

Neuroblastoma (NB) is a neuroendocrine tumour of early childhood that derives from undifferentiated cells of the sympathoadrenal lineage of the neural crest. About 50% of patients have a very aggressive form of NB, with an overall survival rate of less than 30% despite heavy treatments. Moreover, NB is a challenging druggable tumour due to a low rate of somatic mutations. Somatic mutations at significant frequency have been identified in only five genes that also show detectable expression. Among these, only one is currently a directly validated druggable target.

Two m6A regulators (*METTL14* and *ALKBH5*) are aberrantly expressed in high-risk NB patients, and their alteration in NB cell lines affects tumour aggressiveness. Specifically, the overexpression of the methyltransferase *METTL14* increases cell proliferation and invasion *in vitro* and tumour growth in mice acting as an oncogene, while *ALKBH5* restoration affects cell proliferation, apoptosis and invasion in an opposite fashion. Importantly, the demethylase ALKBH5 impaired tumour formation *in vivo* when costitutively expressed and dramatically slows down tumor progression in mice when is induced by causing massive apoptosis. These data suggest that *ALKBH5* acts as a potent tumour suppressor in NB.

We discovered that METTL14 and ALKBH5 exert their effect on different levels by affecting mRNA stability or translation, respectively. Although the contribution to NB of the altered stability of transcripts related to mRNA processing in *METTL14*-overexpressing cells is less understand, the increase translation of pro-apoptotic genes in the *ALKBH5*-overexpression condition leaves little doubts.

Our results unveil the m6A and its regulators as potential therapeutic targets for treating NB. Indeed, in collaboration with the Laboratory of Genomic Screening of Professor Alessandro Provenzani, we presented an encouraging proof-of-concept of the reader YTHDF1 as a possible pharmacological target.

THESIS ORGANIZATION

This thesis is organized in seven main parts: Introduction, Hypothesis and Aim of the project, Results, Discussion, Ongoing Work, Future Plans and Experimental Procedures.

The Introduction provides the background of the project. It consists of two parts that have been written taking into account the latest publications and the older but historically fundamental literature. The first part centred on the post-transcriptional modification m6A, giving information about its discovery and its role as an additional layer as fine-tuning regulators of gene expression with a specific focus on its link with tumour development and progression. The second part reviews the neuroblastoma tumour, its standard of care depending on its staging (or risk) classification and its development.

The second chapter outlines the hypothesis of the project, which ultimately aims to investigate a possible role of the m6A modification in NB progression. The premise is that NB could at least partially be driven by reversible epitranscriptomics alteration due to its embryonic derivation, robust gene (and so transcriptome) imbalance and the ability of some NB metastatic at the onset to regress spontaneously.

The Results chapter describes the phenotypic and molecular effect of the deregulation of crucial m6A effectors on NB aggressiveness, using both *in vitro* and *in vivo* assays, and provides a list of genes that are most affected by m6A alteration in their stability and translation efficiency.

The fourth and fifth chapters provide a discussion of the obtained results and the conclusion of the work, with a focus on the druggability of the m6A machinery in NB tumour.

The sixth chapter contains an overview of the ongoing work, which sets the basis for future plans outlined in the following section.

Finally, the experimental procedures and methodologies used in this work are presented in the seventh chapter.

INTRODUCTION

1. Beyond the Central Dogma: the multifaceted control of gene expression

The Central Dogma states that genetic information is a forward flow of DNA transcribed into RNA and RNA translated into protein (Crick, 1970). Hence, in the early days of molecular biology, it seemed that only these three macromolecules and two fundamental processes -transcription and translation- were able to explain life as it is. As our knowledge deepened, it became more evident that many more layers of regulation control gene expression. In this change of perspective, RNA began to play a predominant role.

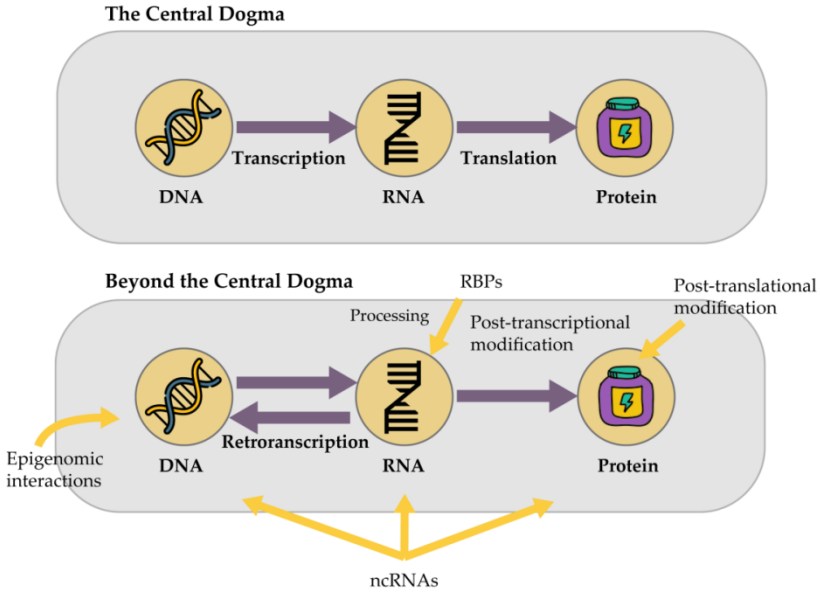

Figure 1| Overcoming the Central Dogma. The central dogma of molecular biology states that the genetic information is a forward flow from DNA that is transcribed in RNA and translated into proteins. Nowadays, is widely established that gene expression is regulated at multiple and interconnected levels.

1.1 Transcriptional control of gene expression

The set of actively transcribed genes, broadly defines the identity of a cell; for this reason, transcription is the first, highly regulated step in gene expression (Jacob & Monod, 1961). Transcriptional regulation occurs mainly through sequence-specific elements on DNA (*cis*-elements) bound by Transcriptional Factors (TFs) that recruits all the other members of the transcriptional apparatus (*trans*-elements) (Istrail & Davidson, 2005). Among thousands of factors that participate in regulating transcriptions (Venter, 2001), most are protein and a growing number appear to be various RNA species (Cech & Steitz, 2014) (Mette, van der Winden, Matzke, & Matzke, 1999) (Matzke, 2001).

Specific DNA sequences , such as : core promoters, proximal regions to the core promoter and distal regions (enhancers), provide information about when, where and at what level specific genes are transcribed. Core promoters favour the assembly of the pre-initiation complex (PIC) composed of General Transcription Factors (GTFs), while specific TFs bind proximal regions and enhancers. TFs exert their activity predominantly through co-activators, which in turn bind to and regulate RNA polymerase II (PolII) and GTFs activity (Adelman & Lis, 2012).

In this context, chromatin and chromatin-regulators play a fundamental and correlative role in the control of gene expression. Chromatin represents a repeating unit of DNA, packed down in histones that form the nucleosome. The amount and the pattern of epigenetic modifications occurring on histone tails (mainly acetylation and methylation) (Bannister & Kouzarides, 2011) and DNA (CpG islands methylation), can alter chromatin condensation and can make it more or less accessible to chromatin remodelling factors, TFs and transcription co-factors (both activator and repressor) to ultimately fine-tuning gene expression in a highly dynamic way (Holliday & Pugh, 1975).

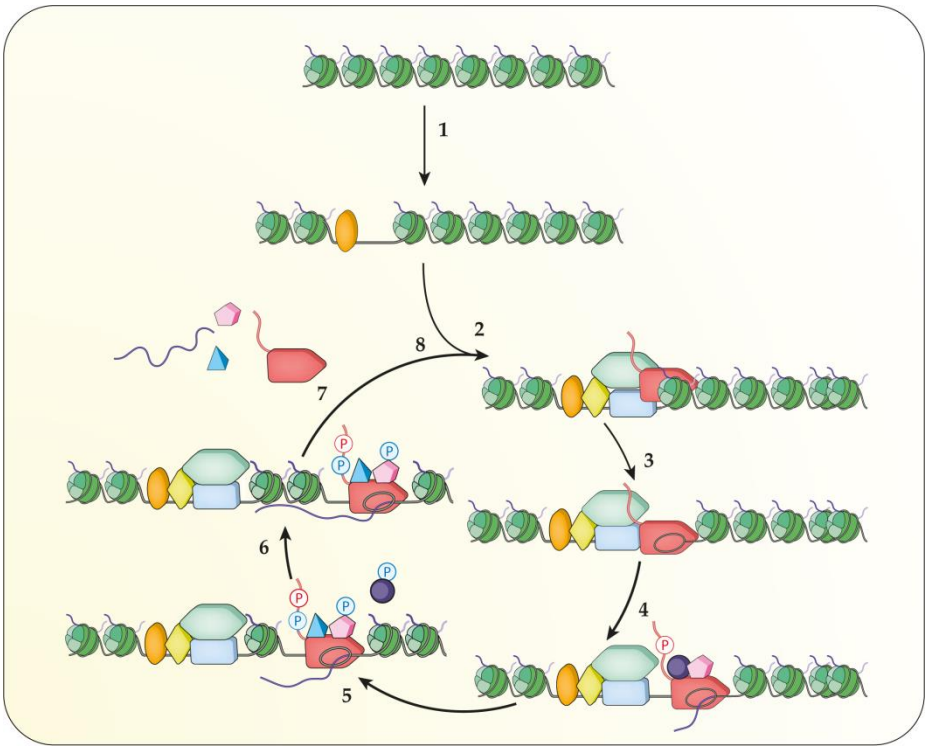

Figure 2| Transcriptional control of gene expression: 1- Chromatin opening. **2**- Formation of the PIC. **3**-Transcription initiation. **4**-Promoter escape/clearance. **5**- Escape from pausing. **6**- Productive elongation. **7**- Termination. **8**- Recycling. *(Adapted from Fuda et al., Nature, 2009).*

The specific regulation of PolII activity is essential for maintaining cell homeostasis and, at a large extent, the programmed development of multicellular organisms. Indeed, mutation and misregulation in regulatory regions, TFs, co-factors, chromatin regulators and ncRNAs might be associated with the development of cancer, autoimmunity disease and neurological disorders, among others.

1.2 Translational control of gene expression: bringing the genome to life

Translational control is the final step in gene expression. It is required to generate the proteome in a time- and space-specific manner in response to several cellular needs, such as proliferation, differentiation, metabolism and embryonic development (Wickens, 2000). Translation can be controlled in two ways: via a 'global' control, during which the

translation of all mRNA is regulated in a nonspecific manner, and a 'selective' control that acts on a specific set of mRNAs.

RNA Translation is an elaborate mechanism that accounts for a large proportion of the energy budget of a cell, and that can be divided into three main phases: initiation, elongation and termination. While elongation and termination involve a limited number of factors, translation initiation is a complex, tightly regulated step, that comprises the activity of numerous elements (Pestova, 2001 and Preiss, 2003). Two significant events take place during **translation initiation**: the recruitment of the mRNA and the assembly of the translational machinery on the correct AUG. Translation is modulated both by c*is*- and *trans*- regulatory elements. *Cis*-elements on mRNA can influence translation initiation: the cap structure at the 5'-end and the poly(A) tail at the 3'-end are canonical elements that promote the translation of an mRNA. IRESs (Internal Ribosome Entry Sequences) can promote a cap-independent translation whereas other secondary structures can block translation. Changes in the phosphorylation status of initiation factors and of other regulators are involved in the global control of protein synthesis. For examples, the activity of the cap-binding protein eIF4F is rate-limiting and depends on the phosphorylation of the 4E-BP (4E-Binding Protein) to released eIF4F (Pause, 1994 and Gingras, 1999). On the other hand *trans*-acting proteins that bind regulatory region on mRNAs can interfere with different steps of translation and affect initiation rates (Gebauer, 2012). Also, small RNA elements (such as miRNA) can play a role in translation regulation of specific mRNAs by base-pairing in the 3'-UTR region and repressing translation (Olsen, 1999). The **elongation** and the **termination** step can also be targets of translational control. The elongation rate affects protein folding (Cabrita, 2010) in fact, if the elongation is too fast, proteins fail to properly fold, unless the overall rate is reduced (Siller, 2010). In some cases, termination can be suppressed, thereby extending the nascent protein to its carboxyl terminus (Atkins and Gesteland, 2002).

In the light of this tight regulation, mutations in genes involved in translation control have been linked with several human diseases, either systemic disorders (Harding, 2000) or a wide range of cancer (Marte, 1997; Shayeste 1999 and Testa, 2001).

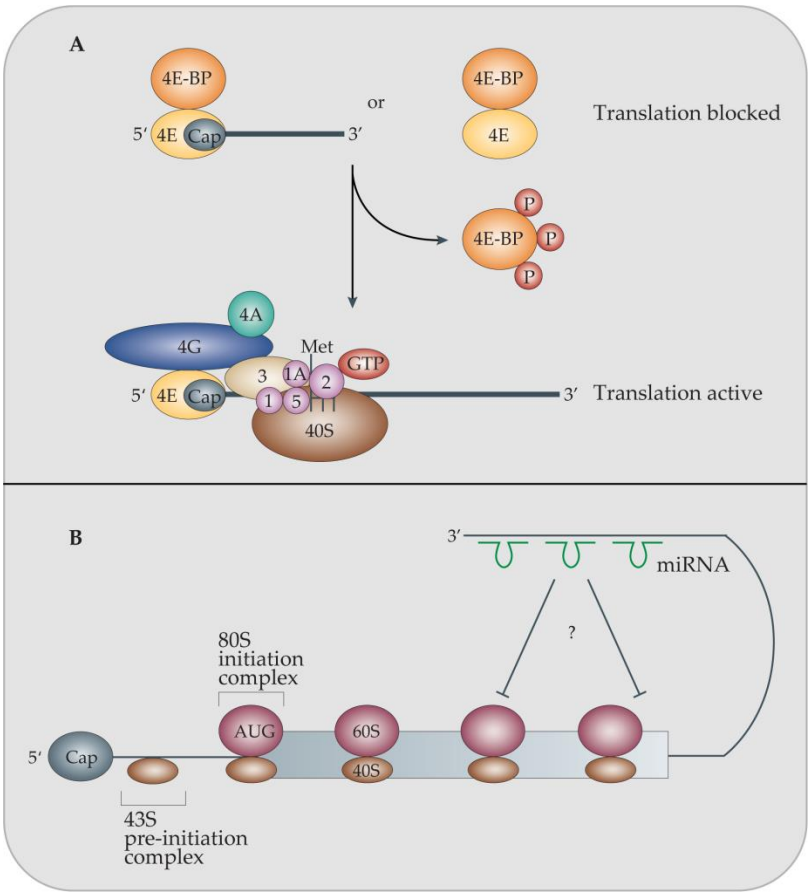

Figure 3| Examples of translational control: A) Global control of protein synthesis: 4E-BP interacts with eIF4E preventing its binding to eIF4G and thereby inhibiting translation. When 4E-BP is phosphorylated, it releases eIF4E allowing its interaction with 4F and thereby allowing translation activation. **B)** Translational control by miRNAs: microRNAs (showed in green) base-pair within the 3′-Untranslated Region (3′-UTR) of mRNAs causing either translational arrest or mRNA degradation. *(Adapted from Gebauer et al., Mol. Cell. Bio., 2004).*

1.3 Post-transcriptional control of gene expression

Following transcription in the nucleus, nascent transcripts undergo a series of coupled nuclear-cytoplasmic processes collectively named post-transcriptional modification.

The processing of transcripts represents the first layer of the post-transcriptional regulation of gene expression and begins during transcription in the nucleus. 3′-end capping, splicing, 5′-end cleavage and polyadenylation are conserved processes required to produce a functional and productive mRNA. Once in the cytoplasm, mRNA can be

translated, stored, degraded or localized in specific cellular compartments (Schoenberg, 2012; Xing, 2013 and Buxbaum, 2015). Many of these processes are mediated by distinct RNA-binding proteins (RBPs) that interpret the information within the mRNA and profoundly influence its function and fate (Dreyfuss, 2002 and Singh, 2015).

The system containing a transcript and RBPs is called **Ribonucleoprotein complex** (**RNPs**) and represent the functional form in which pre-mRNA and mRNA exist in cells. RNPs are formed co-transcriptionally, and while some of them assemble by virtue of an RNA sequence, some bind because of the process that transcript experiences (e.g. splicing). In all the cases, RNPs are informational-rich packet which influence the subsequent life of an mRNA and can link the nucleus/cytoplasm regulation of gene expression into an only interconnected pathway. In this sense, the EJC (exon junction complex) is an explanatory example: in the nucleus, the EJC proteins can interact with export factors thus enhancing the export of a spliced mRNA (Stutz, 2000; Zhou, 2000) and Le Hir, 2001) and can activate NMD (nonsense-mediated decay) in the cytoplasm (Le Hir, 2001).

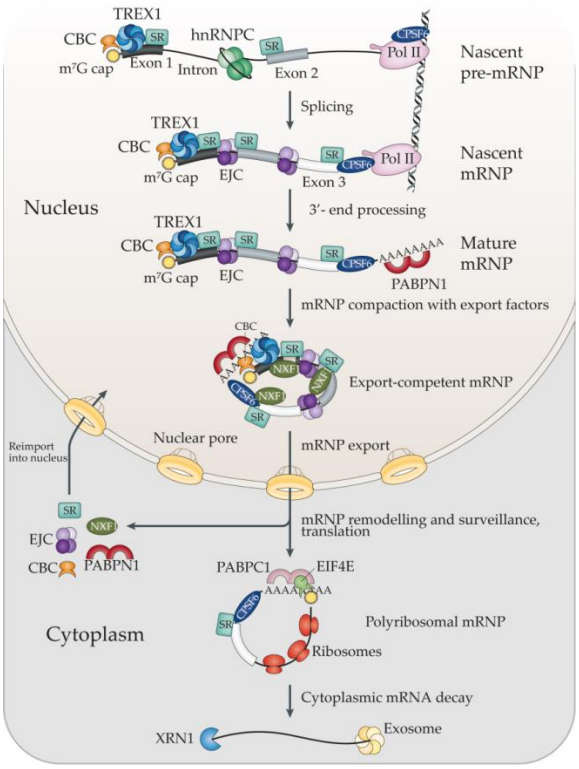

Figure 4| Co-transcriptional assembly and remodelling of mRNPs: mRNPs are co-transcriptionally assembled and modelled. CPSF6, cleavage and polyadenylation specificity factor 6; EJC, exon junction complex; hnRNPC, heterogeneous nuclear ribonucleoprotein C; NXF1, nuclear export factor 1; PABPC1, cytoplasmic poly(A) binding protein 1; PABPN1, nuclear poly(A)-binding protein 1; Pol II, RNA polymerase II; pre-mRNP, precursor mRNP; TREX1,transcription export complex 1; XRN1, 5′–3′ exoribonuclease 1. *(Adapted from Muller-McNicoll and Neugebauer, Nat. Rev. Genet., 2013).*

1.3.1 RNA modifications and the newly concept of the Epitranscriptomic code

The sequence of an mRNA is not sufficient to drive the binding of specific RBPs, as RBPs consensus motives are overrepresented compared with the incidence of actual binding (Hafner, 2010 and Taliaferro, 2016). An emerging body of evidence shows that post-transcriptional gene regulation also relies on the secondary structures and chemical modification of the RNA bases, that are able to expand the information within the sequence and therefore facilitating the binding of RBPs and affecting mRNAs fate.

Recent technological advancements and the development of high-throughput detection methods have allowed the discovery of more than 160 different post-transcriptional modifications. Although some of them were already well known and studied (such as pseudo-uridylation), recent studies have revealed their presence in every class of RNAs, both non-coding (tRNAs and rRNAs) and coding (as internal modification in mRNAs). Chemical modification in RNAs can affect transcripts by altering base-pairing potential, secondary structure and protein-RNA interactions that in turn, can shape the outcome of gene expression by altering processing, localization, translation and decay (in mRNAs) or biogenesis, structure and function (in tRNA and rRNA).

Analogously to the epigenetic marks on DNA, the complete set of RNA post-transcriptional modification represents the ‘Epitranscriptomic Code’, which is widely recognized as a new layer in the regulation of gene expression and opened a new wave of prolific scientific work.

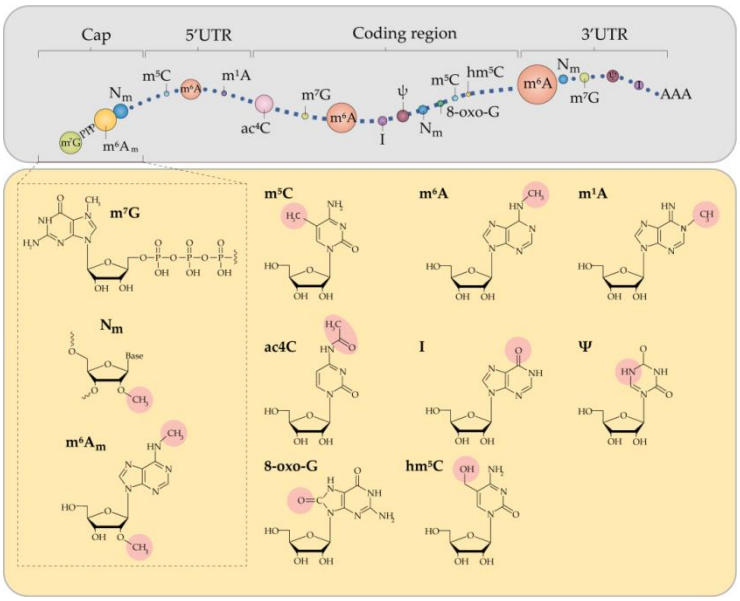

Figure 5| Position and biological outcome of the Epitranscriptomic Code: Post-transcriptional modifications are present either in the 5′-UTR, CDS and 3′-UTR of mRNAs. In the 5′-UTR, the levels of m^1A and m^6A are dynamically altered in response to stress. M^1A promotes cap-dependent translation via an unknown reader and is altered by nutrient deprivation. M^6A promotes cap-independent translation via the activity of eIF3 and YTHDF2 in response to UV damage and heat shock. In the coding sequence, hm^5C improves translational efficiency via an unknown mechanism and its level are higher in the brain where it seems to be involved in brain development. M^6A affects mRNAs processing such as splicing and polyadenylation by the recognition of different reader proteins. In the 3′-UTR, m^6A promotes cap-dependent translation and RNA degradation via two different readers of the same family, YTHDF1 and YTHDF2 respectively. Precise regulation of mRNA stability by m6A is essential for proper stem cell differentiation and circadian clock control. M^5C is linked to the translational efficiency of senescence-related genes, and Ψ increases the stability of modified transcripts during heath shock. *(Adapted from Zaccara, Nat. Rev. Mol. Cell. Bio, 2019).*

2. M^{6}A: one modification to rule them all

Among more than 160 post-transcriptional modifications, the N6-methyladenosine (commonly known as m6A) is the most abundant and pervasive one. Discovered in the 1970s, the interest in m6A resurfaced later on when the technological advancement allowed the single nucleotide-precise mapping of its distribution within the transcriptome and upon the breakthrough discovery that the modification is reversible. Soon after, a flurry of evidence has shed light on the role of the m6A, dissecting both its molecular functions and its contribution in several biological processes.

2.1 Serendipitous discovery of m^{6}A

"Shallow men believe in luck or in circumstances.

Strong men believe in cause and effect."

Ralph Waldo Emerson

The presence of the m^{6}A modification in polyadenylated RNAs was serendipitously discovered in 1974 by several groups, while studying the newly described methylated cap structure at the 5'-end (Perry, 1974 and Desrosiers, 1974). The use of radioactive [^{3}H]-methionine, the methyl source of most biological processes, showed that the radioactive signal was not confined to the cap but also came from other regions of the digested transcript, providing the first evidence the m^{6}A was also present in poly(A) RNAs and mRNAs (Perry, 1974 and Desrosiers, 1974). Nevertheless, the scientific community had reluctances to accept the biological relevance of the modification. In essence, the signal could have arisen from contamination of known m^{6}A sources (such as rRNAs and snoRNAs), and mutation of specific m^{6}A sites did not result in changing RNA fate, suggesting that m^{6}A had a minimal impact on mRNAs.

2.2 m⁶A RNA methylation in eukaryotes

One breakthrough in the field was the development of novel tools and techniques to precisely map the m⁶A at the transcriptome-wide level. Mostly, these are techniques that rely on the immunoprecipitation of anti-m⁶A antibodies followed by next-generation sequencing of m⁶A-containing fragments (Dominissini, 2012 and Meyer 2012). Several other methods have been developed in the following years.

One of the main finding of the MeRIP-seq and the m⁶A-Seq was that the m⁶A is not randomly distributed within the transcript but is enriched in specific sequences. The majority of m⁶A is located near the stop codon but can also be found in the CDS corresponding to long exon and, as a minor part, in the 3'UTR. A subset of mRNAs shows m⁶A residues in their 5'-UTR and importantly, no tissue completely lacks m⁶A (Meyer, 2012). The asymmetric distribution of m⁶A immediately suggested a functional role in the life and fate of methylated transcripts and raised the question of how cells achieved this specificity. The m⁶A is installed in a precise consensus motif RRACH (R = A or G; H = A, C, or U) (Liu, J., 2014) that, if mutated, is sufficient to block methylation (Kane and Beemon, 1987).

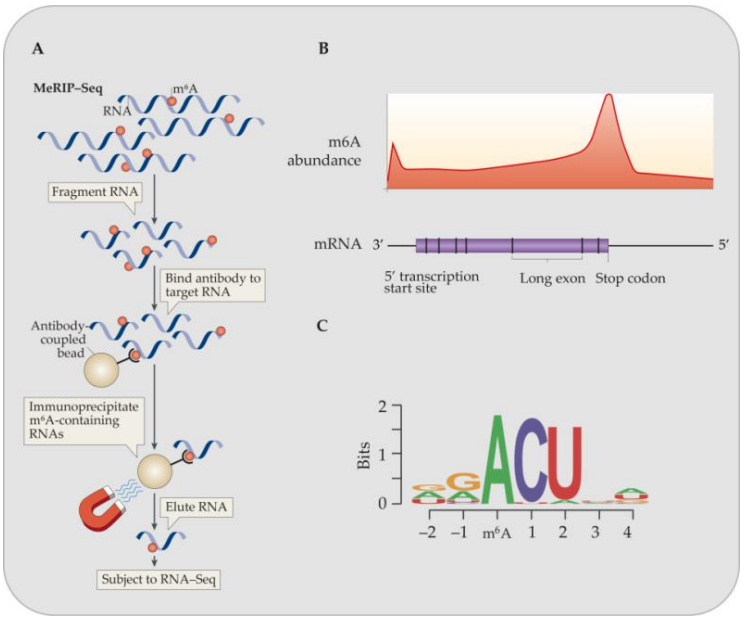

Figure 6| m⁶A mRNA methylation distribution in eukaryotes: A) In MeRIP-Seq RNAs are fragmented in ~100 nucleotide-long fragments and incubated with an anti-m⁶A antibody.

Methylated-RNAs are then immunoprecipitated and subjected to sequencing. After sequencing, the reads are mapped on the genome to identify m^{6}A peaks. **B)** Representative distribution of m^{6}A within a transcript. M^{6}A peaks are specifically enriched near the stop codon and the 5'UTR, with a minor distribution in the CDS and the 3'UTR. **C)** Sequence logo representing the deduced consensus motif for m6A deposition following clustering of all enriched motifs.
(Adapted from Meyer and Jaffrey, Nat. Rev. Mol. Cell. Bio, 2014 and Fu et al., Nat Rev Gen, 2014).

The consensus sequence GAC is found approximately every 64 nucleotides in RNA, suggesting an even distribution along the length of the transcript therefore but the particular localization of m^{6}A suggests the involvement of not only of *cis*-acting features (the ribonucleotide sequence) but also *trans*-acting factors. Moreover, post-translational modification (PTMs) could affect the stability, catalytic activity, localization and the interactome of several m^{6}A-related proteins, therefore influencing m^{6}A deposition in specific region of the transcript. (Wang, 2016). The transcript-specificity of m^{6}A could be due to the methyltransferase tethering induced by specific TFs (Knuckles, 2017 and Bertero, 2018) or epigenetic marks: for example, Huang and colleagues demonstrated that the H3 trimethylation at lysine 36 (H3K36me3) could recruit the methyltransferase complex (Huang, 2019). These and other evidence reinforce early speculations that m^{6}A might be the result of transcripts biogenesis and processing and that could be a co-transcriptional process.

2.3 Being an m^{6}A modification: writing, erasing and reading.

A large number of crucial regulators determine the effects of the m6A. In analogy to epigenetic effectors, they are collectively known as 'writers', 'erasers' and 'readers'. The m6A modification is deposited by a multiprotein methyltransferase complex whose components have been described and characterized before the renewed interest in the modification (Bokar, 1997; Zhong, 2008 and Agarwala, 2012). A significant milestone in the field was the discovery of two demethylating enzymes; although one shows specificity to another modification (Mauer, 2017) and the target specificity of the other remains unclear (Zheng, 2013), they supported the intriguing idea that the m6A might have been a reversible and dynamic modification. Finally, the primary mechanism by which m6A exerts its biological effect is the recruitment of m6A-specific RBPs.

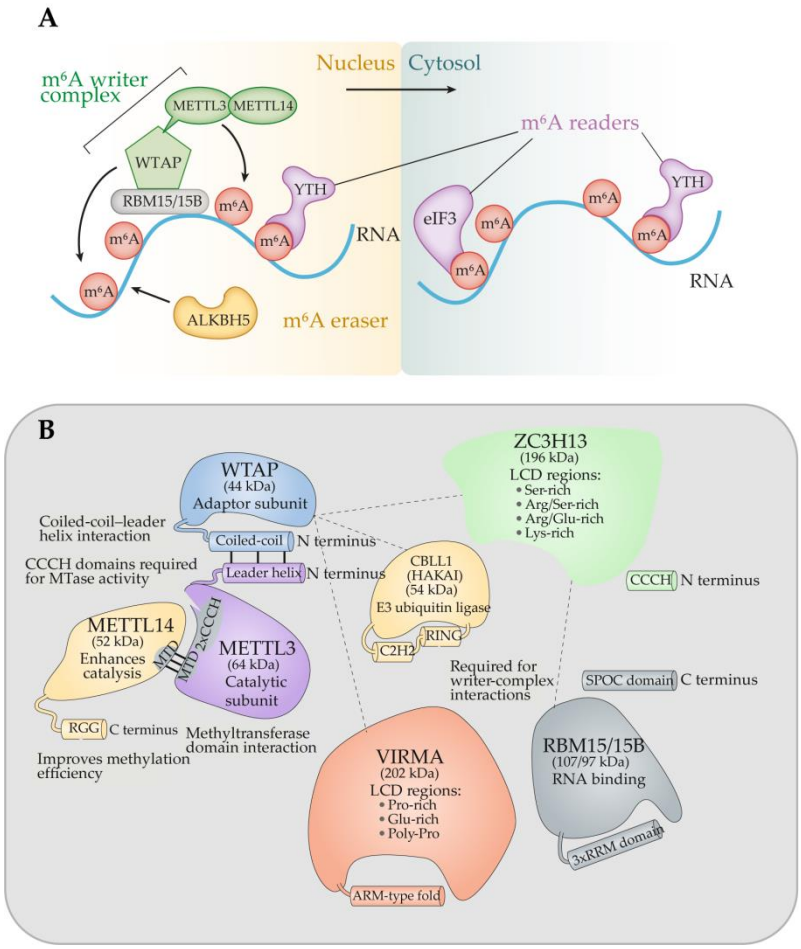

Figure 7| m6A writers, erasers and readers. A) An overview of all the effectors involved in the metabolism of m6A. In the nucleus, the methyltransferase complex co-transcriptionally deposit the modification, while the eraser (ALKBH5 in the figure) demethylate targeted transcripts. In the cytoplasm, reader proteins recognize and bind the modification generating a biological outcome. **B)** Focus on the methyltransferase complex and the interactions between its components. *(Adapted from Meyer and Jaffrey, Ann, Rev. Cell, Dev. Bio, 2017, and Zaccara et al., Nat Rev Mol, Cell. Bio., 2019).*

2.3.1 m⁶A Writers

The mammalian genome encodes four different methyltransferases, that deposit m⁶A in various types of RNA. mRNAs and other PolII-transcribed RNAs are m⁶A-methylated by the METTL3-METTL14 heterodimer (Sledz and Jinek, 2016; Wang, P., 2016 and Wang, X., 2016). Indeed, METTL3 or METTL14 knockout show a 99% reduction of m⁶A sites in poly(A) RNAs (Geula, 2015). The methyltransferase ZCCH4 deposits the single m⁶A in the 28S rRNA (Ma, 2019), whereas the METTL5-TRMT112 deposits the single m⁶A in the 18S

rRNA (van Tran, 2019). Finally, the methyltransferase METTL16 catalyzes the single m^6A in the U6 snRNA and the formation of the m6A in the MAT2A mRNA in a specific secondary structure that closely resembles the U6 RNA (Pendleton, 2017 and Shima, 2017).

For the purpose of this thesis, only the METTL3-METTL14 complex will be discussed in detail.

METTL3: The first *in vitro* methylation assay on HeLa cells showed that the methyltransferase activity was mediated by a ~70-kDa nuclear fraction with an S-adenosylmethionine (SAM)-binding activity (Bokar, 1994). The cloned enzyme that was initially named MT-A70 (Bokar, 1997) is now known as METTL3, and it is the catalytically active subunit of the complex.

METTL14: In 2014, proteomics analyses of METTL3-interacting partners pointed to METTL14 as main interactor (Liu J., 2014; Ping, 2014; and Wang, 2016). While early studies showed that METTL14 had a methyltransferase activity as well (Liu, J., 2014), suggesting that METTL14 and METTL3 could methylate different targets, later bioinformatic analysis ultimately excluded a catalytically active role for METTL14 (Iyer, 2016). Indeed, METTL14 has a degenerate SAM-binding domain, it most likely plays a critical role in the recognition and binding of target RNAs and is an allosteric activator of METTL3 (Sledz & Jinek, 2016; and Wang, X., 2016).

WTAP: The second major component of the methyltransferase complex is WTAP**.** The interaction between WTAP and METTL3 was initially demonstrated in *Arabidopsis* (Zhong, 2008) and yeast (Agarwala, 2012) and confirmed later on in several mammalian cells (Liu, J., 2014; Ping, 2014 and Schwartz, 2014b). The principal role of WTAP is to accurately localize the METTL3-METTL14 complex to nuclear speckles, allowing a correct m^6A deposition on mRNAs.

KIAA1429: KIAA1429 (also known as VIRMA) is one of the WTAP top interactor (Horiuchi, 2013). Its depletion causes loss of m^6A, suggesting an essential role in the maintenance of the methyltransferase complex (Schwartz, 2014)**.**

RBM15/RBM15B: RBM and its paralog RBM15B are the last described components of the methyltransferase complex. RBM15/RBM15B bind to METTL3 in a WTAP-dependent manner (Patil, 2016) and their knockout causes a significant loss of m^6A. Importantly, RBM15/RBM15B recognize and bind U-rich sequences adjacent to RRACH motives (Patil, 2016) recruiting the methyltransferase complex and partially explaining the specificity of the m^6A distribution within transcripts.

2.3.2 m^6A Erasers

m^6A erasers are demethylases that convert m^6A in A. Although at the dawn of the epitranscriptomic era the discovery of erasers suggested that the m^6A could have been a reversible modification, able to respond dynamically and rapidly to specific stimuli, their role in the physiological context is still unclear. Two m^6A demethylases have been described so far: FTO and ALKBH5.

FTO: The Fat mass and obesity-associated protein (FTO) was the first enzyme to be associated with m^6A demethylation (Jia, 2011). A lot of debate exists around the demethylating activity of FTO towards m^6A.Recently, the group of Samie Jaffrey found that FTO shows nearly 100-times higher catalytic activity against m^6A_m when present in its natural context next to the m^7G cap structure (Mauer, 2017). m^6A_m is very similar to m^6A except for the presence of a 2'-O-methyl modification in the ribose moiety of the nucleotide (Wei, C., 1975). The following year Chuan He and colleagues reaffirmed the role of FTO in demethylating both m^6A_m and internal m^6A in different RNA species (mRNAs and snRNAs) (Wei, J., 2018). Therefore, work is still needed to clarify FTO physiological role.

ALKBH5: The AlkB Homolog 5 (ALKBH5) is the second m^6A eraser enzyme discovered. Unless FTO, ALKBH5 doesn't show specificity toward the m^6A_m modification (Mauer, 2017). ALKBH5 localizes in the nuclear speckles, thus it more likely exerts its activity co-transcriptionally (Zheng, 2013). In 2014, the crystal structure of ALKBH5 revealed unique structural features compared to other AlkB family proteins (Feng, 2014 and Aik, 2014).

Among these, the disulphide bond between residues Cys-230 and Cys-267 that allows the distinction of single-stranded from double-stranded oligos potentially conferring ssRNA selectivity (Feng, 2014 and Aik, 2014). Interestingly, ALKBH5 can also demethylate RNA-RNA hybrid suggesting structure-specificity of binding (Zhan, 2017); indeed Chen and colleagues suggested that partially double-stranded mRNAs can disrupt the bond expanding the substrate selectivity of ALKBH5 (Feng, 2014).

2.3.1 m6A Readers

The m6A methylation exerts its molecular and biological effects by recruiting RNA-binding proteins (RBPs). Historically, YT521-B homology (YTH) domain-containing proteins were the first m6a 'readers' discovered (Dominissini, 2012). The YTH domain is extremely conserved amongst eukaryotes, and it falls into two evolutionary subclades consisting in the YTH Domain Family (YTHDF1-2-3) and the YTH Domain Containing proteins (YTHDC1-2) (Zhang, 2010; Scutenaire, 2018). Structurally, all YTH domains include three α-helices and six β-strands: together, this conserved conformation forms a hydrophobic core composed of three tryptophans in mammals (the WWW type), two tryptophans and one tyrosine in yeast (the WWY type) and two tryptophans and one leucine in most YTHDCs (the WWL type) (Luo, 2014; Theler, 2014 and Xu, 2015). Although the nucleoside surrounding the m^6A (in position -2, -1, +1 and +2) are important to define binding intensity, no base-specific interactions have been observed in these studies except for a different selectivity in YTHDC1 binding favouring a G over an A in -1 position (Theler, 2014 and Xu, 2015).

The YTH domain-containing proteins are well-established readers, but accumulating evidence reports the existence of other types of non-YTH-readers, such as HuR (ELAVL1) (Dominissini, 2012), IGF2BP1/2 (Huang, 2018b) and FMR1 (Arguello 2017). How these non-YTH readers can bind m^6A as well as their role as direct -or more likely indirect - readers remains to be elucidated.

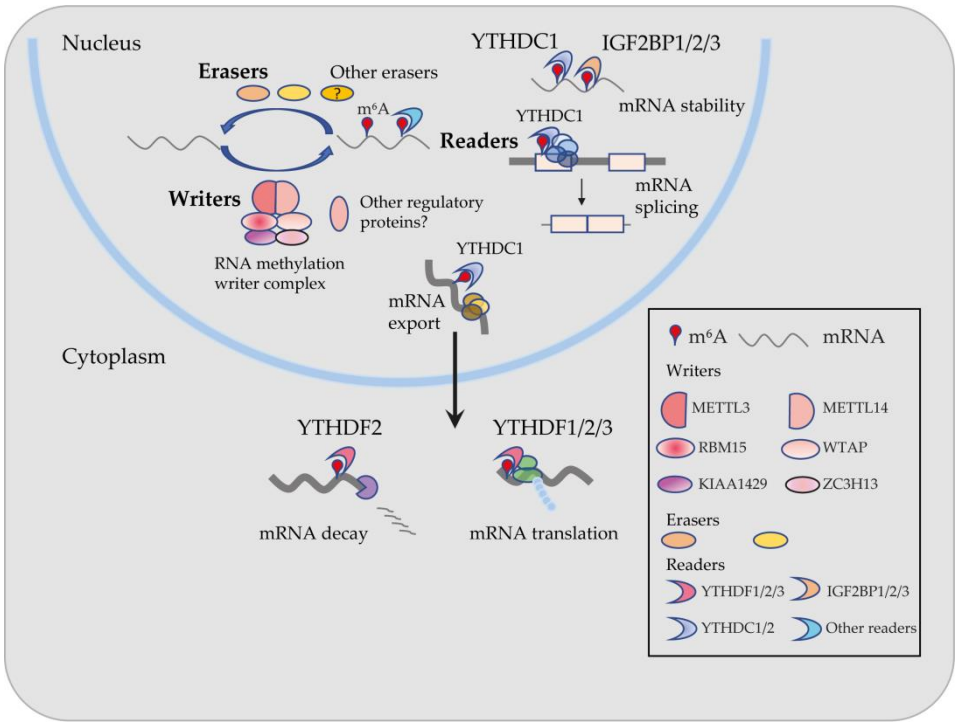

Figure 8| m⁶A readers activity in the cell. Readers include a diverse group of proteins, such as the YTH domain family (YTHDFs and YTHDCs), IGF2BP1/2/3 family, and other factors, i.e., eIF3, HNRNP2AB1, HNRNPC, and HNRNPG. These readers can directly bind to m⁶A or are indirectly recruited to the sites to mediate downstream processes including mRNA export, mRNA stability, mRNA splicing, mRNA translation, and mRNA decay. *(Adapted from Vu et al., Cancer Discovery, 2018)*

YTHDC1: YTHDC1 is enriched in nuclear speckles and acts as a splicing regulator: its depletion causes splicing abnormalities that can be rescued by a YTH-containing protein, suggesting that the m6A recognition can mediate YTHDC1 effect (Zhang, 2010). YTHDC1 appears to mediate its function especially in lncRNAs such as *MALAT1* and *NEAT1*, although its function has only been proved in the case of *XIST*. YTHDC1 mediates the epigenetic effect of *XIST* since its depletion prevents *XIST* from inducing gene repression on the X chromosome (Lee, 2009 and Patil, 2016).

YTHDC2: The function of YTHDC2 is poorly understood. Differently from the other YTH domain-containing proteins that are ubiquitously expressed, YTHDC2 is confined to testes. Indeed, *Ythdc2* knockout mice show spermatogenesis defects (Wojtas, 2017). Interestingly, YTHDC2 shows a weaker binding to m⁶A RNAs compared to the other

readers and, even though it maintains the tryptophan cage, the YTH domain shows divergence in the region designated to recognized m^{6}A-adjacent areas (Xu, 2015 and Wojtas, 2017).

YTHDF PROTEINS: The YTHDF protein family comprises three paralogs, YTHDF1, YTHDF2 and YTHDF3. There have been conflicting results about the function of individual YTHDF proteins. YTHDF2 was the first member to be characterized (Wang, X., 2014) with a role in destabilizing m^{6}A-containing targets: this effect seems to be due to YTHDF2 direct interaction with the CCR4-NOT deadenylation complex (Du, 2016). On the contrary, YTHDF1 promotes translation by binding eIF3 and other translation initiation factors (Wang, 2015). YTHDF3 seems to show both activities. The main question that remained unanswered is how these almost identical proteins (DFs share a higher degree of sequence similarity and almost identically m^{6}A-binding site) can mediate opposite functions. Recent studies proved that the YTHDF proteins have all similar roles (Kennedy, 2016). In particular, the fact that *Drosophila melanogaster* contains a single DF-like YTH protein, CG6422 (Kan, 2017), reinforces the model that the YTHDF proteins are functionally redundant in mammals.

2.4 Molecular effects of the m^{6}A modification.

Being the most pervasive modification, m^{6}A controls almost every aspect of the life cycle of mRNA throughout its journey from transcription in the nucleus to decay in the cytoplasm.

The first effects of m^{6}A are observed in the nucleus, since m^{6}A deposition occurs co-transcriptionally. From the first observation that the m^{6}A modification is present in intronic regions, it has been speculated that the modification could have a role in splicing regulation (Carrol, 1990). Some of the most substantial evidence of this comes from studies in *Drosophila melanogaster*. In *Drosophila*, the intronic m^{6}A affects the splicing of the *Sex-lethal* gene, which has a pivotal role in sex determination. When it comes to mammals everything became airy, with several studies reaching conflicting results: some groups have shown that m^{6}A is enriched near the exonic 5′ splice site (Liu, N., 2015), while others have found no enrichment (Ke, 2015). Recently, Zhou and colleagues have demonstrated

that the simultaneous binding of the RNA-binding protein hnRNPG with the CTD of RNA PolII and the m6A near the splice site of regulated exons can increase RNA PolII occupancy and exon inclusion (Zhou, K., 2019).

The m^{6}A modification plays a role in controlling mRNA nuclear export. Specifically, ALKBH5 depletion causes a significant switch in the ratio of nuclear to cytoplasmic mRNAs, by affecting the function of the ASF/SF2 splicing factor/export effector in a demethylation-dependent manner (Zheng, 2013).

The final steps of mRNA life are translation and decay in the cytoplasm: these processes have been historically ascribed to YTHDF1 (Jackson, 2010; Meyer, 2015 and Wang, X., 2015) and YTHDF2 respectively (Du, 2016). The question on how these two almost identical proteins can mediate opposite effects is still under debate. DF proteins contain a large glutamine/proline/glycine-rich low-complexity domain that phase-separated and partition in endogenous liquid droplets such as stress granules or p-bodies, thus targeting mRNAs to different fates (Ries, 2019). Moreover, it is essential to take into consideration the context in which the m^{6}A effectors act, such as cell types, external stimuli, subcellular localization and protein-protein interactions (Shi, 2019).

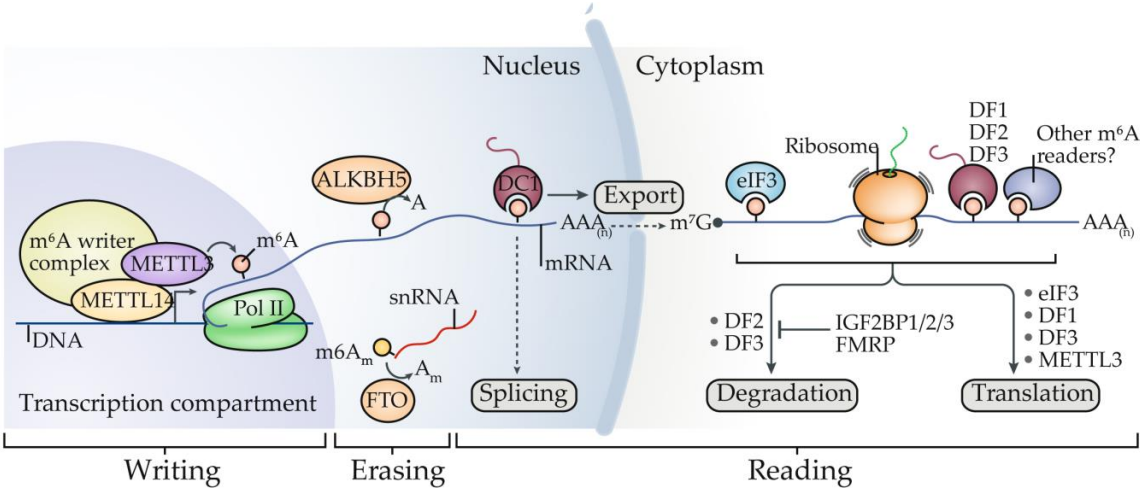

Figure 9| Molecular effects of the m^{6}A modification: The m6A methylation occurs dynamically and co.-transcriptionally in the nucleus where the methyltransferase complex localize. The m6A erasers primarly localized in the nucleus as well. Reader proteins bind m6A-methylated transcripts both in the nucleus, where they mainly affect splicing and export and in the cytoplasm where they

affect the stability, translation and decay of mRNAs. *(Adapted from Zaccara et al., Nat Rev Mol, Cell. Bio., 2019).*

2.5 Regulation of m6A modifications in cancer

Consistent with its central role in fine-tuning mRNAs gene expression, aberrations of m^{6}A methylation levels can affect many cellular processes, several of which related to tumour development and progression. Different mechanisms can contribute to m6A alteration: deregulations of the machinery, gain or loss of m^{6}A sites in mRNA due to mutations, or change of m^{6}A epitranscriptome by environmental factors.

Numerous cancers exhibit alteration in m6A abundance and, interestingly, both elevated and reduced level of m6A methylation has been associated with carcinogenesis. In the past few years, a growing body of literature has reported aberrant expression levels of the m6A machinery both in solid and liquid tumours. **TABLE 1** summarizes the roles of m6A key regulators in human cancer with the relative references (from Huang *et al.*, *Cancer Cell Review*, 2020).

It is noteworthy to mention, that different studies have obtained opposite results regarding the contribution of m^{6}A methylation to tumour progression, even on the same tumour type. In Acute Myeloid Leukemia (AML) elevated levels of METTL3 or METTL14 and therefore, high m6A levels, are associated with increased tumour aggressiveness (Vu, 2017 and Weng, 2018) while in an AML subtype elevated FTO expression, which leads to the downregulation of m^{6}A levels, contributes to cell transformation and leukemogenesis (Li, 2017). It has to be taken into account the importance of the context: what m6A readers and general RBPs are involved and which is the extent of modified sites in methylated transcripts? Are the effects direct, or indirect?

Table 1. Roles of m ^{6}A Writers, Erasers, and Readers in Human Cancers

m^{6}A Regulator	Role in Cancer	Cancer Type	Target Genes	References
Writer				
METTL3	oncogene	acute myeloid leukemia	MYC , BCL2 , PTEN , SP1 , SP2	Barbieri et al., 2017; Vu et al., 2017
		glioblastoma	SRSFs , SOX2	Li et al., 2019a; Visvanathan et al., 2018
		hepatocellular carcinoma	SOCS2 , SNAIL , LINC00958	Chen et al., 2018; Lin et al., 2019b; Zuo et al., 2020
		hepatoblastoma	CTNNB1	Liu et al., 2019
		bladder cancer	AFF4 , IKBKB , RELA , MYC , CDCP1 , miR-221/222 , ITGA6	Cheng et al., 2019a; Han et al., 2019b; Jin et al., 2019b; Yang et al., 2019a
		breast cancer	HBXIP , BCL2	Cai et al., 2018; Wang et al., 2020
		gastric cancer	ZMYM1 , HDGF , SEC62 , ARHGAP5-AS1	He et al., 2019; Lin et al., 2019a; Liu et al., 2020b; Wang et al., 2019b; Yue et al., 2019; Zhu et al., 2019b
		pancreatic cancer	pri-miR-25	Taketo et al., 2018; Xia et al., 2019; Zhang et al., 2019b
		colorectal cancer	SOX2 , pri-miR-1246	Li et al., 2019c; Peng et al., 2019
		colon cancer	TP53 (R273H ,G>A)	Uddin et al., 2019
		melanoma		Dahal et al., 2019
		osteosarcoma	LEF1	Miao et al., 2019
		prostate	GLI1	Cai et al., 2019
		non-small cell lung cancer	YAP , MALAT1	Jin et al., 2019a
	tumor suppressor	glioblastoma	ADAM19	Cui et al., 2017
		endometrial cancer	PHLPP2 , MTORC2	Liu et al., 2018a
		renal cell carcinoma		Li et al., 2017c
METTL14	oncogene	acute myeloid leukemia	MYB , MYC	Weng et al., 2018
		breast cancer	transforming growth factor b signaling pathway genes	Panneerdoss et al., 2018
	tumor suppressor	endometrial cancer	PHLPP2 , MTORC2	Liu et al., 2018a
		glioblastomas	ADAM19	Cui et al., 2017
		hepatocellular carcinoma	pri-miR-126	Ma et al., 2017
		bladder cancer	NOTCH1	Gu et al., 2019
		renal cell carcinoma	P2RX6	Gong et al., 2019
		gastric cancer		Zhang et al., 2019a
		colorectal cancer	pri-miR-375	Chen et al., 2019a
WTAP	oncogene	hepatocellular carcinoma	ETS1	Chen et al., 2019b
VIRMA (KIAA1429)	oncogene	hepatocellular carcinoma	ID2, GATA3	Cheng et al., 2019b; Lan et al., 2019

Table 1. Continued

m^{6}A Regulator	Role in Cancer	Cancer Type	Target Genes	References
Eraser				
FTO	oncogene	acute myeloid leukemia	ASB2 , RARA , MYC , CEBPA	Li et al., 2017d; Su et al., 2018
		glioblastomas		Cui et al., 2017
		non-small cell lung cancer	MZF1 , USP7	Li et al., 2019b; Liu et al., 2018b
		pancreatic cancer	MYC	Tang et al., 2019
		cervical squamous cell carcinoma	b-catenin , E2F1 , MYC	Zhou et al., 2018; Zou et al., 2019
		breast cancer	BNIP3	Niu et al., 2019
		melanoma	PDCD1 , CXCR4 , SOX10	Yang et al., 2019b
		gastric cancer		Zhang et al., 2019a
ALKBH5	oncogene	glioblastomas	FOXM1	Zhang et al., 2017c
		breast cancer	NANOG	Fry et al., 2018; Wu et al., 2019; Zhang et al., 2016a, 2016b
		non-small cell lung cancer	UBE2C , FOXM1	Chao et al., 2020; Guo et al., 2018
		gastric cancer	NEAT1	Zhang et al., 2019c
		ovarian carcinoma	BCL2	Zhu et al., 2019a
		oral squamous cell carcinoma	FOXM1 , NANOG	Shriwas et al., 2020
	tumor suppressor	bladder cancer	ITGA6	Jin et al., 2019b
		pancreatic cancer	KCNK15-AS1 , WIF1	He et al., 2018; Tang et al., 2020
Readers				
YTHDF2	oncogene	acute myeloid leukemia	TNFRSF2	Paris et al., 2019
		hepatocellular carcinoma		Yang et al., 2017b
		prostate cancer		Li et al., 2018
		pancreatic cancer	YAP	Chen et al., 2017
		gastric cancer		Zhang et al., 2017b
		non-small cell lung cancer	6PGD	Sheng et al., 2019
		cervical cancer	GAS5	Wang et al., 2019c
	tumor suppressor	hepatocellular carcinoma	EGFR , IL11 , SRPINE2	Hou et al., 2019; Zhong et al., 2019
YTHDF1	oncogene	colorectal cancer		Bai et al., 2019; Nishizawa et al., 2018
		hepatocellular carcinoma		Lin et al., 2019b; Zhao et al., 2018
		non-small cell lung cancer	KEAP1	Shi et al., 2019
		Markel cell carcinoma		Orouji et al., 2020
YTHDF3	oncogene	colorectal cancer	GAS5 lncRNA	Ni et al., 2019
YTHDC2	oncogene	colon cancer	HIF1A	Tanabe et al., 2016
IGF2BP1/2/3	oncogene	hepatocellular carcinoma and cervical cancer	MYC , FSCN1 , TK1 , MARCRSL1	Huang et al., 2018

Table 1. Continued

m^{6}A Regulator	Role in Cancer	Cancer Type	Target Genes	References
IGF2BP1	oncogene	hepatocellular carcinoma and ovarian cancer	SRF	Muller et al., 2019
IGF2BP2	oncogene	colorectal cancer	SOX2	Li et al., 2019c
		pancreatic cancer	DANCR	Hu et al., 2019
IGF2BP3	oncogene	gastric cancer	HDGF	Wang et al., 2019b
METTL3	oncogene	non-small cell lung cancer	EGFR , TAZ , BRD4	Choe et al., 2018; Lin et al., 2016
		ovarian carcinoma	AXL	Hua et al., 2018

It is reasonable to speculate that mutations of m^{6}A sites in critical transcripts may disturb m^{6}A deposition, thus playing a role in cancer. In *TP53* pre-mRNA, the adenosine resulting from the G>A transition in codon 273 (R273H mutation) is m6A-methylated by METTL3. This additional methylation results in the preferential p53 R273H splicing variation that confers drug resistance to colon cancer cells (Uddin, 2019).

A large-scale population analysis has revealed a missense variant located in the exon of *ANKLE1* gene with a G>A change in colon-rectal cancer. In contrast to the [G] allele, the recognition of the methylated [A] allele by YTHDC1 increases protein expression of the tumour suppressor ANKLE1 , thus inhibiting cell proliferation (Tian, 2019).

In addition to the intracellular deregulation of m^{6}A machinery and mutations on m^{6}A sites, environmental factors modulate m^{6}A modification and contribute to cancer development. Recent studies have demonstrated that chemical carcinogens can dramatically change m^{6}A abundance in epithelial cells, (Gu, 2018 and Yang, 2019) as well as the exposure to cigarette smoke condensate in immortalized human pancreatic duct epithelial cells (Zhang, 2019).

Given the roles of m6A modification and its associated machinery in several types of cancer, it is not surprising that numerous efforts are being made in cancer therapy to target different m6A regulators pharmacologically. Few examples of this expanding fields are the discovery of the FTO inhibitor R-2-hydroxyglutarate (R-2HG), that exhibits antitumor activity in AML cells (Su, 2018), and the piperidine and piperazine rings of small ligands, that activate and enhance the METTL3-14-WTAP complex and produce phenotypic effects on HEK293T cells (Selberg, 2019). Moreover, there is growing interest toward the idea of using the m^{6}A signature of some particular transcripts or loci as biomarkers for early cancer diagnosis and classification, outcome prediction and risk stratification as well as co-adjuvant and sensitizer to chemotherapy, radiotherapy and immunotherapy.

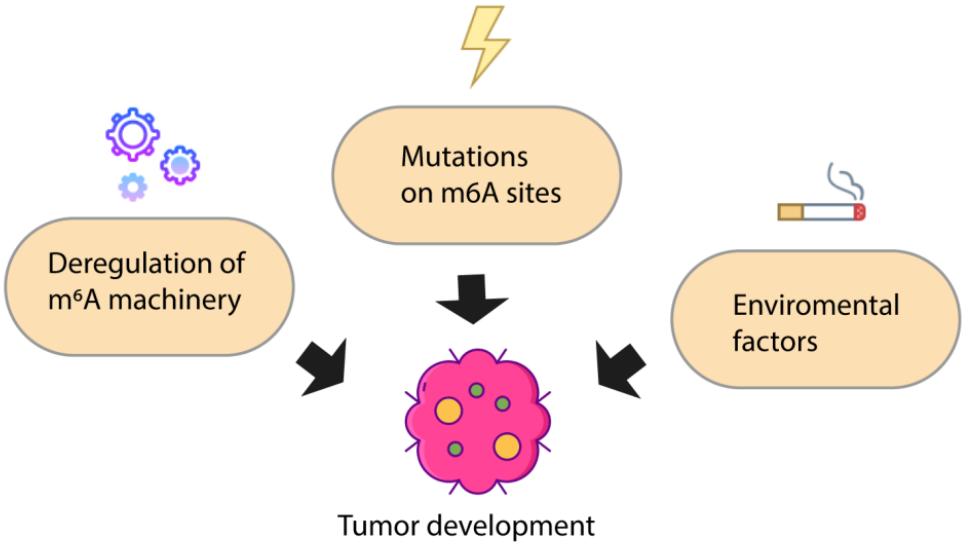

Figure 10| m6A alterations are linked to cancer. Other than deregulation of m6A machinery, mutations on m6A sites and environmental factors (such as carcinogens, the smoke of cigarettes and oncogenic viruses) have been shown to cause tumour development.

3. Neuroblastoma

3.1 Epidemiology and genetic risk factors

Neuroblastoma (NB) is the most common extra-cranial solid tumour in early childhood. 40% of the patients are diagnosed at infancy and 90% of patients at < 10 years of age (London, 2005). Age and race profoundly influence the phenotype of the disease. The median age of diagnosis is 18 months, as patients less than 18 months have a better prognosis compared to older patients (London, 2005 and Cohn, 2009). Adolescents and adults rarely develop neuroblastoma and the tumour seems to be more indolent, albeit, still lethal (Mosse, 2013). Besides, individual with African ancestry are more prone to have a malignant disease compared to individuals with European descendent (Gamazon, 2013). NB is also more common in boys than in girls, but the genetic and epigenetic basis of this predisposition is still unknown.

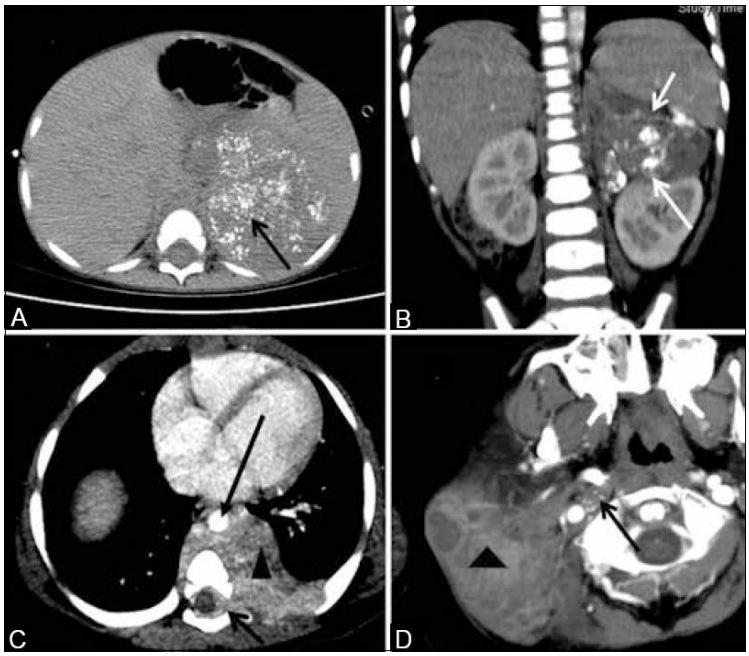

Figure 11| CT imaging of Neuroblastoma (A-D): Common locations of NBs. Image **(A and B)** show adrenal NBs- a left supra-renal mass with typical stippled calcifications (arrow in A) and a mass with calcifications (arrow in B) displacing the left kidney inferiorly. A posterior mediastinal mass that crosses the midline and encases the descending aorta (long arrow) is seen in image **(C)**. The short arrow points towards the intraspinal extension through a neural foramen, which is often seen in NB arising from paravertebral sympathetic chain. Image **D** reveals a tiny mass with calcific foci postero-medial to the carotid sheath (arrow), corresponding to the location of superior cervical ganglion. Associated large nodal mass is seen lateral to the carotid sheath (arrow head). (Figure and caption are from Kembhavi *et al., Indian J. Radiol. Imaging*, 2015)

NB can be divided into familial and sporadic. Familial NB development was initially explained with the 'two-hit' model, with the first hit being a germline mutation and the second hit a later acquired somatic mutation (Knudson, 1972). Familial cases of NB are extremely rare, accounting for only 1-2% of the total cases, and only two germline mutations have been identified so far: a germline gain-of-function mutation in *ALK*, as the main predisposing factor (Mosse, 2008 and Knudson, 1972), and a loss-of-function mutation in *PHOX2B* (Trochet, 2004). Genome-wide association studies (GWAS) have revealed that polymorphic alleles associate with NB (Manolio, 2009).Several of them (such

as BARD1 and LMO1) have a modest effect individually, but multiple association can cooperate to promote malignant transformation (Manolio, 2009 and Bosse, 2016).

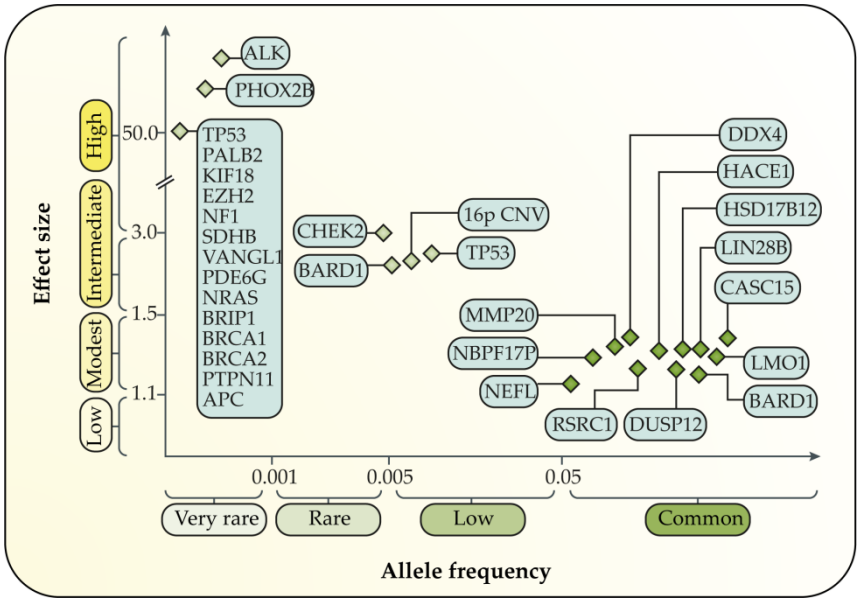

Figure 12| Neuroblastoma genetic risk factors. *ALK* and *PHOX2B* germline mutation are associated with the development of familial neuroblastoma with a high penetrance even though their mutations are sporadic and are inherited as autosomal dominant. Other genes can be mutated in the germline (such as *TP53*, *EZH2*, *NRAS*, *BRCA1* and *BRCA2*) but their contribution to the disease is still unknown. Several polymorphisms (i.e. LMO1 and BARD1) have small effects individually on tumour initiation but can cooperate and increase disease penetrance. *(Adapted from Matthay et al., Nat Rev Dis, Primers, 2016).*

Different genetic alterations have been observed in NB, other than *ALK* and *PHOX2B* germline mutation. These include genes amplification and dramatic chromosomal aberrations. *MYCN* has been identified as one of the primary drivers of NB development. Its product, N-MYC, is a master regulator of transcription that activates gene associated with several hallmarks of cancer. For example, some of the transcriptional targets of *MYCN* activate cell cycle progression, translation, ribosome biogenesis, and metabolic processes and repress genes that drive differentiation (Huang & Weiss, 2013). *MYCN* associates with tumour progression and is used as a marker for risk-stratification (Brodeur, 1984 and Seeger, 1985). Although *ALK* germline mutations are

associated with familial NB, *ALK* somatic mutations have also been identified in approximately 14% of NB cases other than its co-amplification with *MYCN* due to their same location on 2p chromosome (Bresler, 2014).

Polymorphic alleles within the *LIN28B* locus are highly associated with the development of high-risk NB (Diskin, 2012) and both loss-of-function alteration in *ATRX* (in 10% of patients) and promoter rearrangements in *TERT* (approximately in 25% of patients) (Peifer, 2015 and Valentijn).

In general, NB has a shallow rate of somatic mutation, but almost all high-risk NB show recurrent patterns of dramatic chromosomal alteration. The gain of 17q and loss of 1p correlate with MYCN amplification and poor prognosis, while the loss of 11q inversely correlates with MYCN amplification (Bown, 1999 and Attiyeh, 2005). The loss of 1p and 11q suggest the presence of tumour suppressor on these chromosomes, although no such gene has been identified yet. Other relatively common genetic alterations include gains of 1q and 2p (where MYCN localizes) and loss of 3p, 4p and 14q (Huang & Weiss, 2013 and Pugh, 2013).

NB manifests as a very heterogeneous disease, from rapid progression to spontaneous regression. Peculiarly, some patients that are less than 1 year old and that show metastasis limited to the skin, liver or bone-marrow (Strother, 2012 and De Bernardi, 2009), undergo spontaneous regression without any treatment. The molecular mechanisms underlying this process are not fully understood, but the immune system seems to play a role in developing antibodies against the tumour. Moreover, the depletion of the nerve growth factor (NGF) induces many pro-apoptotic genes that are also expressed at a high level in favourable NB. (Brodeur & Bagatell, 2014).

Box 1|**International Neuroblastoma Staging System**

Stage 1
Localized tumour with complete gross surgical excision and no metastasis to the representative ipsilateral lymph nodes that were not attached to tumour.
Stage 2A
Localized tumour with incomplete gross surgical excision and no metastasis to the lymph nodes.
Stage 2B
Localized tumour with or without complete gross surgical excision, with tumour metastasis to the ipsilateral lymph nodes but no tumour metastasis noted in any enlarged contralateral lymph nodes.
Stage 3
Unresectable, unilateral tumour infiltrating across the midline, with or without regional lymph node metastasis, or localized unilateral tumour with contralateral regional lymph node metastasis, or midline tumour with bilateral infiltration or lymph node involvement.
Stage 4
Any primary tumour with metastasis to distant lymph nodes and/or other organs, except as defined for stage 4S.
Stage 4S
Localized primary tumour (stages 1, 2A or 2B) in patients <1 year of age, with metastasis limited to the skin, liver or bone marrow (<10% tumour involvement).

3.2 Neuroblastoma staging, risk stratification and management

The evaluation of the disease spreading is called staging. The most widely accepted system is the International Neuroblastoma Staging System (INSS) (Brodeur, 1997). The INSS identifies 5 stages that are described in **BOX1** (from Brodeur, 1997). The staging system also enables the classification of patients into very-low-risk, low-risk, intermediate-risk and high-risk groups and helps to assess treatment management. Very-low-risk represents nearly 50% of all newly diagnosed diseases. The observational approach is used in patients below 1 year of age with localized adrenal masses (<5cm in diameter), and it consists in monitoring urine catecholamine and tumour imaging (Nuchtern, 2012). For patients > 1 year with localized diseases, the tumour can be resected. In the absence of MYCN amplification, the overall-survival and the disease-free survival is around 99-100% and 90% respectively (Strother, 2012 and Iehara, 2013). Chemotherapy begins to be used in low-risk patients (only in the presence of clinical symptoms) (Baker, 2010 and Strother, 2012) and in intermediate-risk NB other than tumour resection when possible. High-risk patients are usually >18 months old and show unfavourable prognosis (i.e. *MYCN* amplification). The 5-years overall survival probability is very low and has been estimated at 29% (Pinto, 2015). The current approach for high-risk NB comprises an intense treatment that consists in induction chemotherapy to reduce the tumor, followed by resection, chemotherapy and radiotherapy regimen and myeloablative chemotherapy. Myeloablative therapy is then followed by the use of anti-GD2 monoclonal antibody and cytokine immunotherapy, in addition to differentiation therapy with isotretinoin (Park, 2013).

3.3 Neural crest cell and NB development

NB is a tumour of the neural crest cells (NCC), a transient cell population that arise from the dorsal region of the closing neural tube, beneath the ectoderm (Le Dourin and Kalcheim, 1999). During normal mammalian embryonic development, NCC induction and delamination happens along the entire length of the neuro-axis; based on their axial level of origin, NCC can be divided into cranial, cardiac, vagal, trunk and sacral. The different type of NCC are characterized by specific migratory pathway and differentiation capability specified by extrinsic signals coming from the surrounding tissue. Given the variety of lineages generated, the neural crest has been described as the fourth germ layer (Hall, 1999). Among others, NCC can differentiate into the peripheral nervous system, the enteric system, Schwann cells, melanocytes, pigment cells, cells of the craniofacial skeleton and adrenal medullary cells (Dourin and Kalcheim, 1999). This variety could partially explain the heterogeneity of the tumour. NB can develop from the transformation of any neural crest element however, the majority of cases arise in the abdomen and the adrenal medulla while are less represented in the paraspinal sympathetic ganglia of the neck, chest and pelvis (Maris, 2007).

Shortly after the delamination from the neural tube, neural crest cells undergo an Epithelial-to-Mesenchymal transition (EMT) which allows the NCC to leave the dorsal neural tube (Le Dourin and Kalcheim, 1999). The same EMT might likely play a role in the development of NB. Early post-migratory NCC is characterized by high levels of N-MYC that are important for NCC migration and expansion (Zimmerman, 1986). N-MYCN levels progressively decrease during the sympathoadrenal lineage differentiation into neural or chromaffin cells so, persistent *MYCN* expression during this maturation stage could result in the acquisition of paraneoplastic lesions (Zimmerman, 1986 and Marshall, 2014) and eventually NB development as being demonstrated in zebrafish (Zhu, 2012). LIN28B can contribute to sustaining N-MYC expression by downregulation of let-7 pre-miRNA, thus playing a crucial role in maintaining an undifferentiated (stemness) phenotype throughout embryonic development (Ju, 2007 and Molenaar, 2012).

3.3.1 The sympathetic neuron differentiation

The sympathetic nervous system derives from the trunk NCCs, that are thought to generate a sympatho-adrenal (SA) progenitor. Under local environmental cues, the SA progenitor can differentiate into three related cell types: sympathetic neurons, chromaffin cells and small intensely fluorescent (SIF) cell all of which showing catecholaminergic traits (Unsicker, 1973; Vogel and Weston, 1990). The earliest cell of origin of NB seems to be the SA progenitor which had not received or had not appropriately responded to signals that determine its terminal differentiation (Glenn, 2014).

Truck crest cells can be identified by the expression of SOX10 (Huber, 2008 and Betters, 2010). While migrating along the ventral pathway, they receive BMP signals that activate MASH1 (Huber, 2006). PHOX2B sustains the expression of MASH1 and the temporal expression of these two factors seem to produce an early separation between the sympathetic and the adrenal lineages (Huber, 2006). PHOX2B is also crucial for NB development, since germline mutation in the *PHOX2B* gene is associated with familial NB. Finally, MASH1 induces the expression of PHOX2A, which is required for the production of the biosynthetic enzymes beta-hydroxylase (DBH) and tyrosine-hydroxylase (TH) in the last differentiation step of noradrenergic cells (Huber, 2006).

3.3.2 The prenatal origin of NB

The idea of a prenatal origin of NB is sustained by expression profile analysis, showing that human foetal adrenal neuroblasts are very similar to those of NB. Moreover, a unique feature of childhood cancer is the initial hyperplasia of precursor cells that then undergo to programmed cell death, a process that mirrors the physiological organogenesis in which many more cells than required are produced. Indeed, in NB a portion of patients undergo spontaneous disease regression without any treatment, and the incidence of NB precancerous lesions are 40-fold higher than the incidence of the clinical disease (Beckwith & Perrin, 1963).

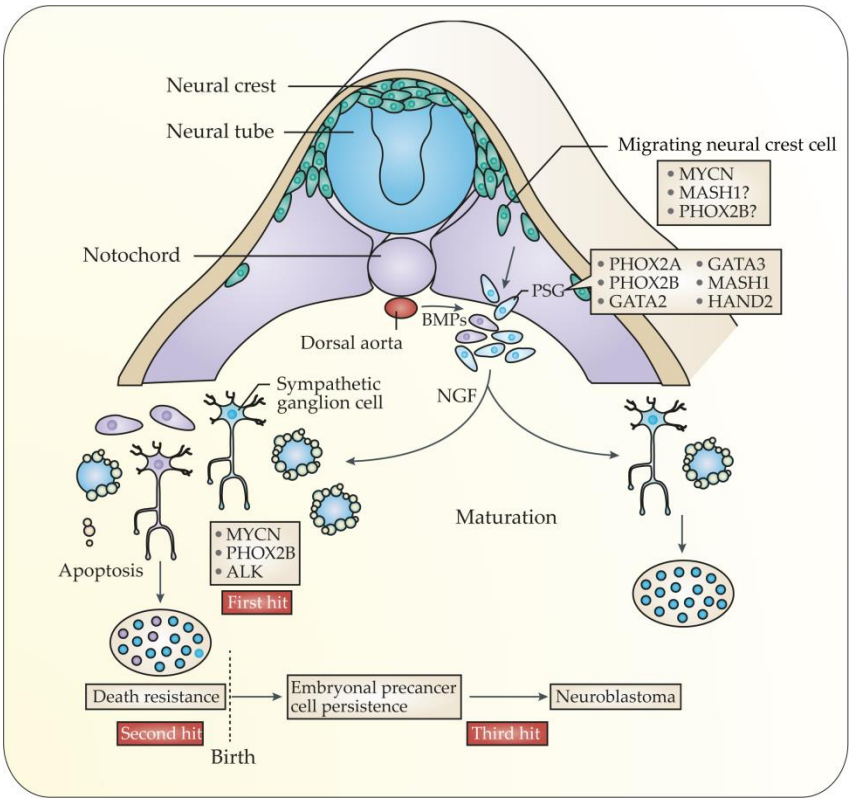

Figure 13| Neural Crest Cell development. Under the influence of MYCN and bone morphogenetic proteins (BMPs), neuroblast progenitors migrate from the neural crest and around the neural tube to a region that is immediately lateral to the notochord and dorsal aorta. At this site, the cells undergo specification as the primary sympathetic ganglia (PSG) before divergence into neural cells of the mature sympathetic ganglia or chromaffin cells (not shown). *MYCN* is a 'first hit' by virtue of the observations from a tyrosine hydroxylase (*Th*)–*MYCN*-transgenic mouse model, whereas mutations in anaplastic lymphoma kinase (*ALK*) and paired-like homeobox 2B (*PHOX2B*) are germline mutations. Local access to nerve growth factor (NGF) determines whether a normal sympathetic ganglion cell (blue) matures into a terminal ganglion cell or undergoes apoptotic cell death. A relatively common pathological state is postnatal survival of neuroblast precancer cells (purple), which requires the cell that is destined to become malignant to be resistant to trophic factor withdrawal before these persistent precancer cells undergo a third change to induce transformation, which presents as neuroblastoma in early childhood. HAND2, heart and neural crest derivatives expressed 2; MASH1, murine achaete-scute homologue 1. (*Figure and caption are from Marshall et al., Nat. Rev. Cancers, 2014).*

HYPOTHESIS AND AIM OF THE PROJECT

Neuroblastoma is the most common extra-cranial solid tumour in early childhood and accounts for 15% of all paediatric deaths. NB is a very heterogeneous disease and, according to its spreading in the body, it is classified in five different stages by the International Neuroblastoma Staging System (INSS) corresponding to different risk groups. Although very-low-risk and low-risk patients show localized masses and overall survival of 90-100% without any –or modest- treatment, high-risk patients survival with unfavourable biology (i.e. MYCN amplification) has been estimated as 29% despite an aggressive therapeutic approach, consisting in tumour resection, chemo-and radiotherapy, and myeloablative therapy. Therefore, novel and less invasive therapeutic approaches are urgently needed.

NB lacks somatic mutation and is mainly a copy number variation-driven tumour. The quantitative rather than qualitative imbalance in the transcriptome coupled with the ability of some metastatic NB at diagnosis to undergo spontaneous regression suggest the involvement of reversible epitranscriptomic alteration.

Based on this premise, this project aims at identifying m6A alteration in NB tumour to demonstrate that m6A might play a role in neuroblastoma development and progression.

Considering the pressing in finding innovative therapeutic approaches, the ultimate scope of this study is to point the m6A regulators as pharmacological targets for NB treatment.

RESULTS

1. METTL14 and ALKBH5 are aberrantly expressed in NB tumour

1.1 Expression of m6A regulators in NB patients

To corroborate the hypothesis that the m6A modification might be relevant in the development and progression of NB, we first correlated the expression of m6A-related genes with different clinical variables, using public available RNA-seq data from 409 NB patients. We classified m6A-related gene expression according to disease stage, MYCN amplification, overall survival (OS) and disease-free survival (DFS) probability. Our discoveries are summarized in **Figure 14** (writers), **Figure 15** (erasers) and **Figure 16** (readers). We found that METTL14, a member of the methyltransferase complex, showed a significantly higher expression ($p<0,0001$) in the aggressive stage 4 also correlating with MYCN amplification (one of the major tumorigenic driver in NB), reduced survival and worst prognosis. In the eraser group, the demethylase ALKBH5 associated oppositely with the same clinical features, showing poor survival and prognosis when its expression is low in stage 4 NB. Intriguingly, METTL3 and FTO – respectively METTL14 and ALKBH5 counterpart- did not show any significant alteration over the progression of NB patients along with the other m6A regulators, except for the reader YTHDF1 that showed a significant increase in stage 4 patients.

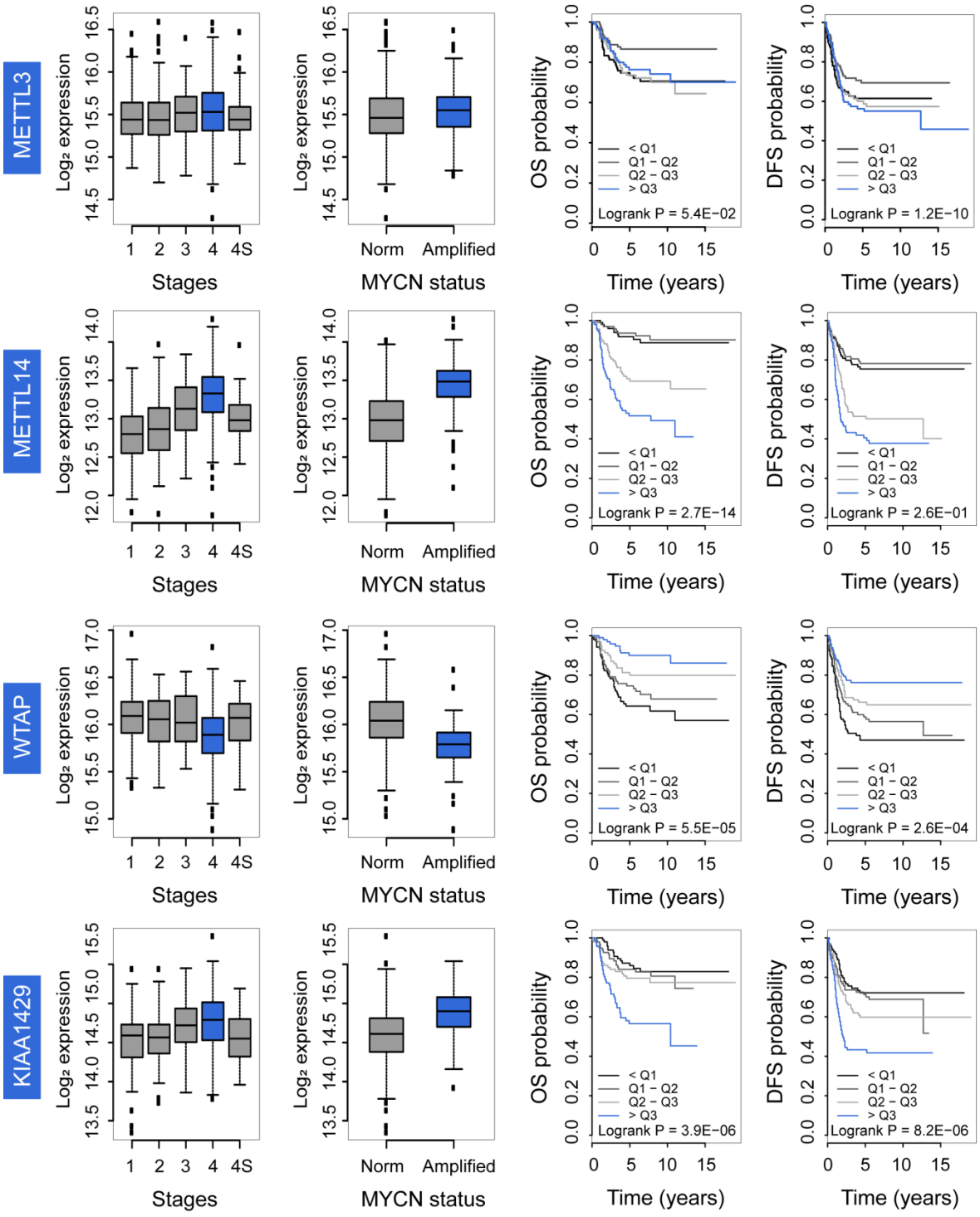

Figure 14| Writers expression in NB patients. RNA-seq expression of genes involved in the methyltransferase complex in tumour samples from NB patients (n=409), according to disease stage. The expression values were log2-transformed and median centred. The box-and-whisker plots indicate where 50% of the data points are located, with the upper border at 75% and the lower border to 25%. Error bars indicate the range of expression; circles represent outlier values. ****p<0.0001. Kaplan-Meyer curves showing overall survival (OS) and disease-free survival (DFS)

of neuroblastoma patients with high expression of METTL3, METTL14, WTAP or KIAA1429. Sample were sorted according to mRNA expression and stratified in four groups on the basis of a cut-off expression value, from the lower expression quartile (Q1) to the higher-expression quartile (Q3). Outcome prediction model was calculated as indicated as square correction index (rsq)

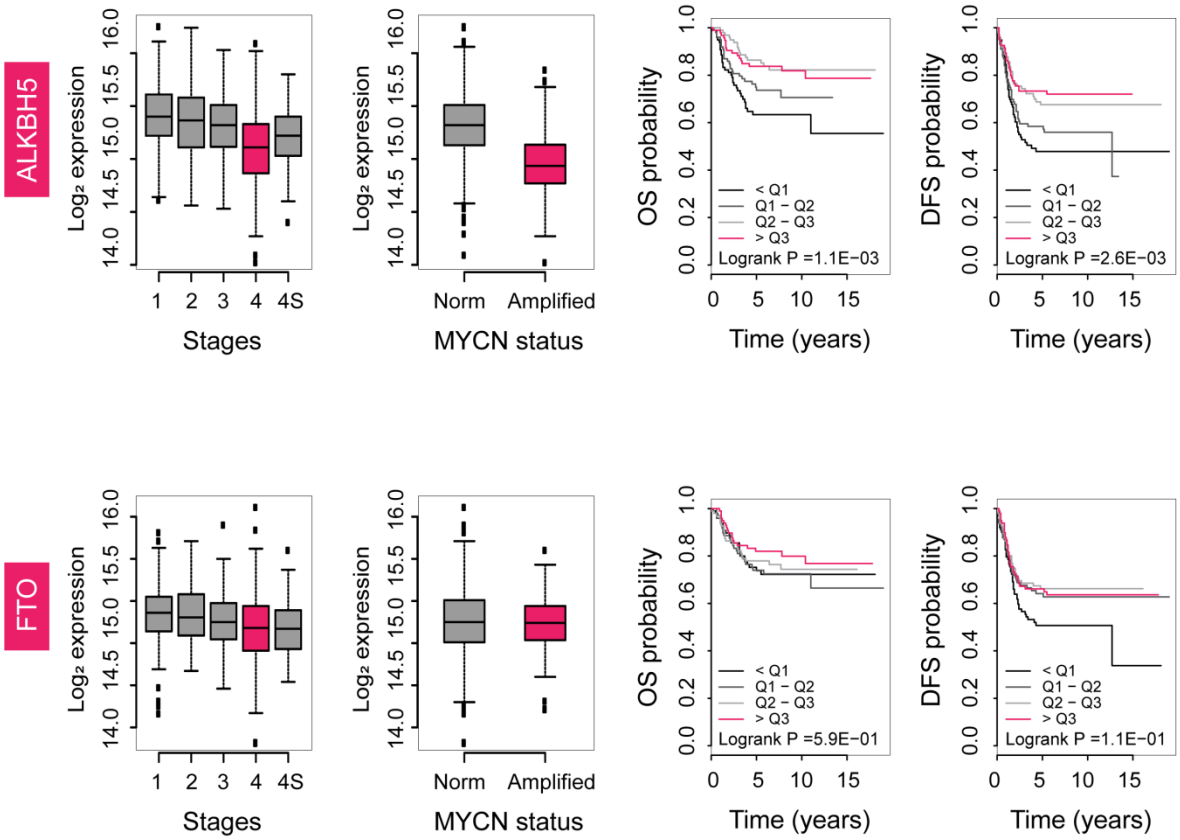

Figure 15| Writers expression in NB patients. RNA-seq expression of demethylase genes in tumour samples from NB patients (n=409), according to disease stage. The expression values were log2-transformed and median centred. The box-and-whisker plots indicate where 50% of the data points are located, with the upper border at 75% and the lower border to 25%. Error bars indicate the range of expression; circles represent outlier values. ****p<0.0001. Kaplan-Meyer curves showing overall survival (OS) and disease-free survival (DFS) of neuroblastoma patients with high expression of ALKBH5 or FTO. Sample were sorted according to mRNA expression and stratified in four groups on the basis of a cut-off expression value, from the lower expression quartile (Q1) to the higher-expression quartile (Q3). Outcome prediction model was calculated as indicated as square correction index (rsq).

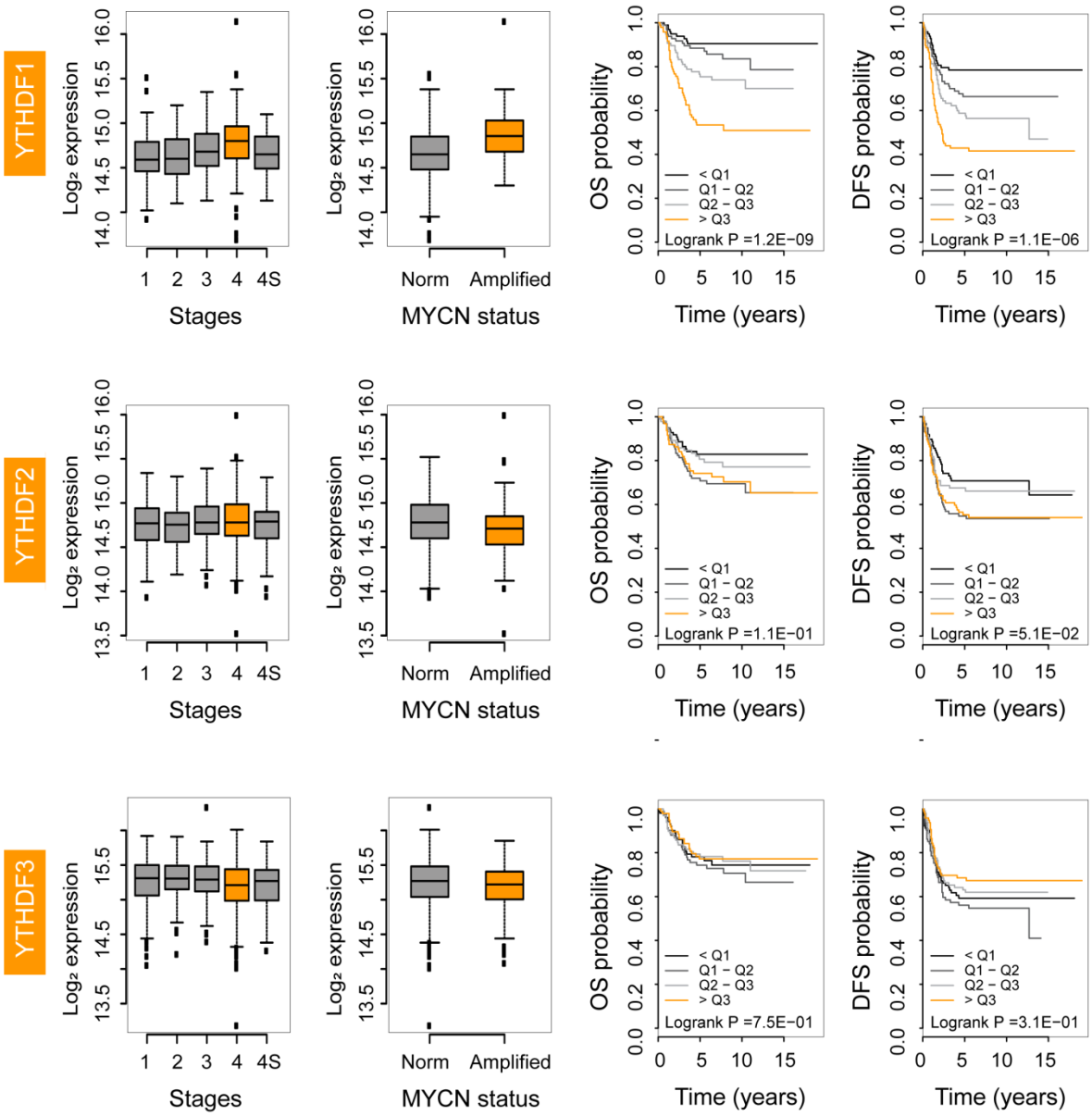

Figure 16| Writers expression in NB patients. RNA-seq expression of reader genes in tumour samples from NB patients (n=409), according to disease stage. The expression values were log2-transformed and median centred. The box-and-whisker plots indicate where 50% of the data points are located, with the upper border at 75% and the lower border to 25%. Error bars indicate the range of expression; circles represent outlier values. ****p<0.0001. Kaplan-Meyer curves showing overall survival (OS) and disease-free survival (DFS) of neuroblastoma patients with high expression of YTHDF1, YTHDF2 or YTHDF3. Sample were sorted according to mRNA expression and stratified in four groups on the basis of a cut-off expression value, from the lower expression quartile (Q1) to the higher-expression quartile (Q3). Outcome prediction model was calculated as indicated as square correction index (rsq).

These data are consistent with the analysis of the Broad Institute Cancer Cell Line Encyclopedia (CCLE) showing that NB has one of the highest and lowest levels of *METTL14* and *ALKBH5* expression, respectively, compared to the majority of other solid and liquid tumours (**Figure 17A-B**).

These early observations suggested a role of the m6A (specifically, its abundance) in NB progression with a conceivable effect on particular transcripts, as METTL14 and ALKBH5 mainly have a specific, rather than a broad impact on mRNAs.

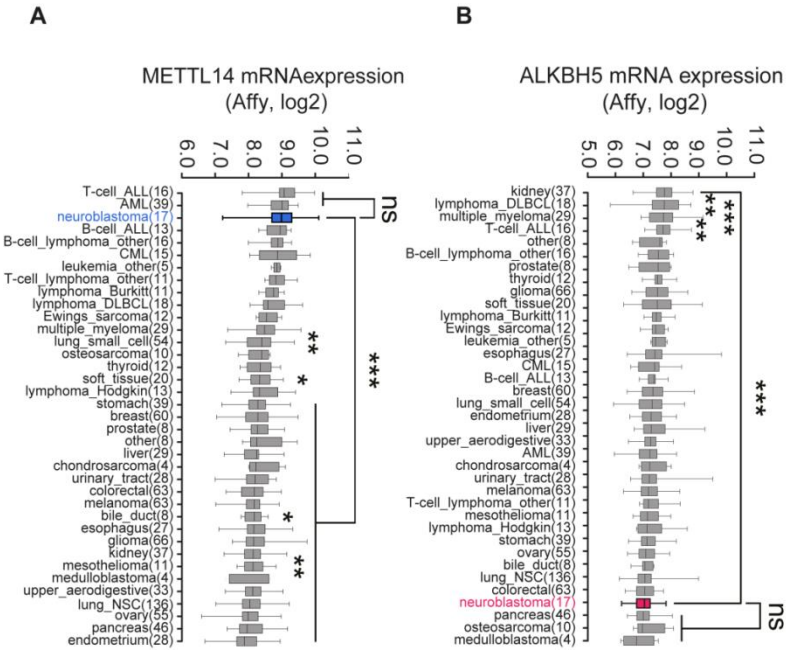

Figure 17| METTL14 and ALKBH5 expression in solid and liquid tumours. Gene expression levels (Affymetrix) of METTL14 and ALKBH5 in neuroblastoma cells compared to other human cancer cell lines. Data extracted from the CCLE Expression Database, RMA-normalized mRNA expression data (http://www.broadinstitute.org/ccle/home), and presented as log2 expression, median centred with ranges at 75% and 25% data point distribution. The number of tumor cell lines are indicated in parenthesis. The dark blue (METTL14) and pink (ALKBH5) boxes highlight neuroblastoma cells. *p<0.05, **p<0.01, ***p<0.001, ns not significant; one-way ANOVA test followed by Tukey's post-test.

2. M6A is required to sustain the aggressiveness of NB cells

2.1 Expression of m6A regulators in NB cell lines

To validate our preliminary observation, we decided to examined m6A regulators expression in a panel of commercially available NB cell lines, both at the RNA and protein level. We selected 14 different cell lines, all purchased either at ATCC (CHP-212), ECACC (CHP-134, SK-N-AS, SK-N-BE(2), SK-N-DZ, KELLY, LAN1, IMR-32, SK-N-SH and NB69) or DSMZ (MHH-NB-11 and SIMA). STA-NB-7 and STA-NB-11 cell lines were a kind gift of Dr Peter F. Ambros of the Children's Cancer Research Institute CCRI, St. Anna Kinderspital.

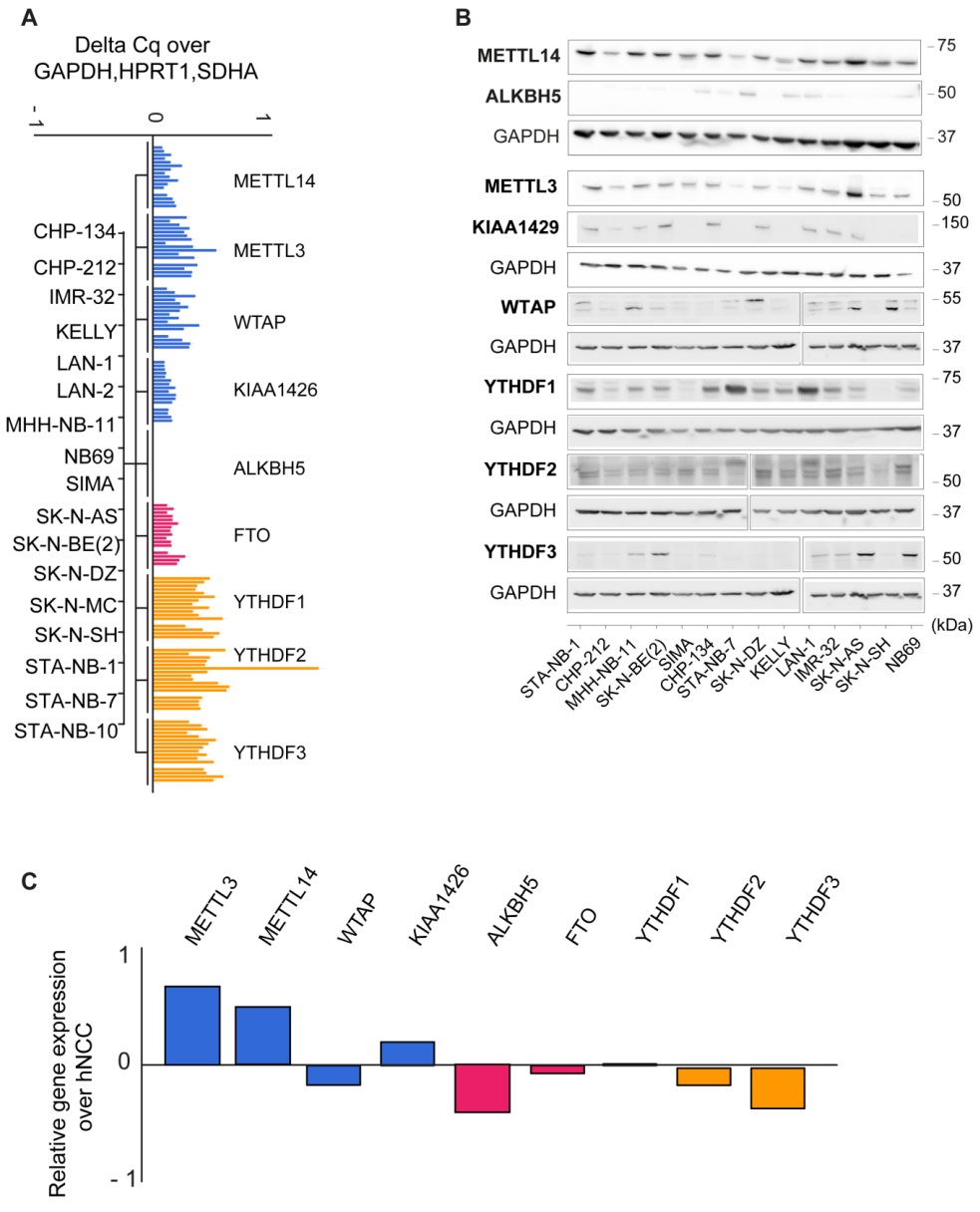

Figure 18| m6A regulators expression in NB cell lines. (A) Endogenous mRNA expression of m6A "writers", "erasers" and "readers", and m6A-methylation complex associated factors, by qPCR and normalized on housekeeping control genes in 18 neuroblastoma cell lines. **(B)** Endogenous protein expression of m6a "writers", "erasers", "readers" and m6A-methylation complex associated factors, along with GAPDH (loading control) in neuroblastoma cell lines. Representative images of n=3 independent experiments.

Endogenous RNA and protein levels of m6A regulators, evaluated by a quantitative Real-Time PCR and Western Blot, respectively, resulted to be quite homogeneous among all the NB cell lines. Remarkably, ALKBH5 expression seems to be almost null (**Figure 18A,B**).

2.2 Generation of engineered NB cell line

To investigate the contribution of *METTL14* and *ALKBH5* on NB tumour progression, we selected two out of fourteen NB cell lines to modulate their expression. The two cell lines were selected based on *METTL14* and *ALKBH5* endogenous protein expression, MYCN status (amplified and not amplified) and their cultured properties (growth in fully adherence condition and easily-transduced). We finally selected CHP-212 and SK-N-AS cell lines. CHP-212 is a MYCN-amplified neuroblastoma cell line with low expression of both *METTL14* and *ALKBH5*, while SK-N-AS is a MYCN non-amplified NB cell line with low expression of *ALKBH5* and an endogenous amplification of *METTL14*.
I decided to overexpress either *METTL14* or *ALKBH5* in CHP-212 cells using lentiviral transduction. I sub-cloned the human *METTL14* (NC_000004.12) or *ALKBH5* gene (NC_000017.11) into a pENTR1A vector, recombined it into a Destination Vector with antibiotic resistance, infected and selected the cells with 1µg Puromycin for five days. Before starting with various tumorigenic assays, I checked METTL14 and ALKBH5 expression after the selection. As shown in **Figure 19A**, both METTL14 and ALKBH5 were correctly overexpressed compared to Control cells, infected with an empty lentiviral backbone. I also decided to verify the activity of *METTL14* and *ALKBH5*, with a colorimetric quantification of the m6A, in the engineered CHP-212 cells. Total RNA was extracted from *METTL14*- and *ALKBH5*-overexpressing cells and enriched for the poly(A)-fraction. mRNAs were spotted onto an

8-well Assay strips and treated with a detection antibody. Samples were finally incubated with a developer and enhancer solution, and the absorbance was read at the spectrophotometer at 450 nm. After demonstrating that the overexpression of *METTL14* and *ALKBH5* had led to a coherent increase and decrease of m6A levels (**Figure 19B**), I moved to a detailed phenotypic characterization of the engineered CHP-212 cells.

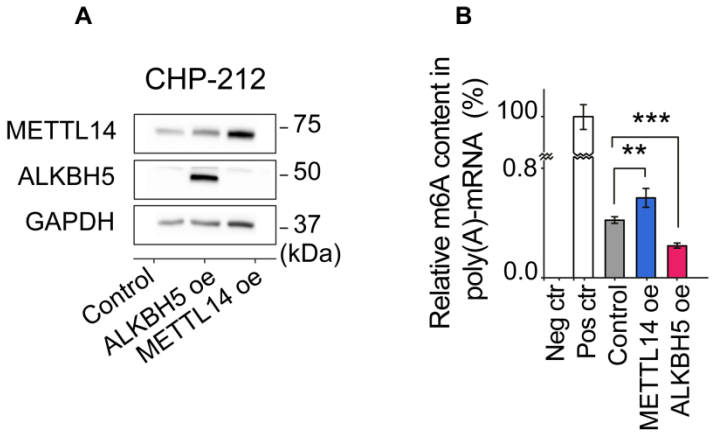

Figure 19| Characterization of genetically engineered CHP-212 cell line. A) Representative western blotting of METTL14, ALKBH5 and GAPDH (loading control) of CHP-212 cells, transduced with either control (empty vector), METTL14-overexpressing (METTL14 oe) or ALKBH5-overexpressing (ALKBH5 oe) lentiviral vectors. **(B)** Quantification of m6A levels of poly(A)-purified mRNA, in CHP-212 cells overexpressing either METTL14 or ALKBH5 as assessed by colorimetric assay; negative (Neg ctr) and positive (Pos ctr) controls were used as internal references; means ± SD of n = 4 technical replicates, normalized and expressed as a percentage of global m6A, on the basis of negative and positive controls. **P < 0.01, ***P < 0.001, two-tailed Student's t test.

2.3 *In vitro* characterization of METTL14- and ALKBH5 overexpressed NB cells

To test the impact of the m6A on NB aggressiveness, we decided to evaluate several tumorigenic features, such as cellular proliferation, apoptosis and invasion ability of either METTL14 or ALKBH5-overexpressing cells. Proliferation ability was assessed using a non-invasive electrical impedance monitoring, named Real-Time Cell Analyzer. This technology is based on gold microelectrodes fused with the bottom surface of a plate well. The presence of adherent cells at the electrode-solution interface impede electron flow,

and the magnitude of this impedance depends on the number of cells, their size and shape. I seeded 5000 cells per well and acquired cells impedance every 15 minutes for 144 h. Each Cell Index value was normalized at 11 h post-seeding, when the cells had wholly adhered to the surface of the plate, to obtain the graph represented in Figure **20A**. METTL14 overexpressing cells (light blue line) exhibit a rapid growth rate compared to control cells. To address the requirement of the catalytic activity of METTL14, I also overexpressed a catalytically mutant form of METTL14 (here referred as ΔMETTL14) observing no differences in the proliferation rate compared to control cells (**Figure 23A**). On the other hand, ALKBH5 overexpressing cells (pink line) behave oppositely, showing a robust decrease in proliferation. This drop might be partially explained by a slight, still significant, increase in apoptosis (**Figure 20B**) which, on the contrary, doesn't affect METTL14 cells. Invasion is one of the main characteristics of human tumours and has important implications for diagnosis and disease progression. To evaluate whether the m6A might influence the invasion ability of NB cells, I assessed their capacity to invade a matrix over time. METTL14, ALKBH5 or control CHP-212 were completely embedded in Matrigel® and the area of invasion was calculated at day 2 and 3 post-seeding. At the endpoint, cells were treated with Hoechst to highlight the area. As shown in **Figure 20C** and by its quantification in **Figure 20D**, METTL14 overexpression increases NB cells invasivity, enhancing their aggressiveness once again, while ALKBH5 almost completely abrogate this ability.

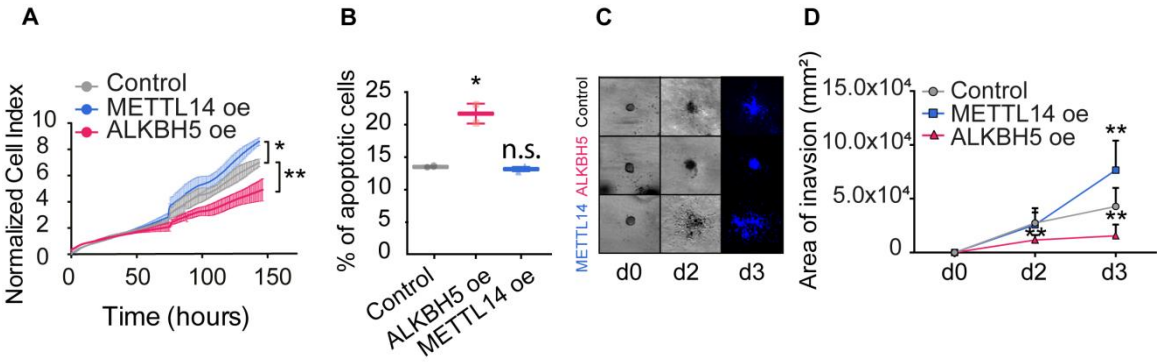

Figure 20| In vitro phenotypic assays of engineered CHP-212 cells. (A) Proliferation of CHP-212 cells transduced with either control, METTL14-overexpressing, or ALKBH5-overexpressing lentiviral vectors monitored real-time by the RTCA (xCELLigence) and reported as normalized cell index; means ± SD of n=3 independent experiments consisting of n=4 technical replicates. *p<0.05,

p<0.01, ***p<0.00, two-tailed Student's t test. **(D) Percentage of apoptotic cells in CHP-212 cells either transduced with METTL14-overexpressing or ALKBH5-overexpressing lentiviral vectors. Cells were stained for Annexin V and quantified by flow cytometry. mean ± SD of n=2 independent experiments. *p<0.05, ns not significant, two-tailed Student's t test. **(E)** Invasion ability of CHP-212 transduced with either control (empty vector), METTL14-overexpressing (METTL14 oe) or ALKBH5-overexpressing (ALKBH5 oe) lentiviral vectors. Left panel indicates representative images. Right panel, quantification of the area of invasiveness over the course of 3 days; means ± SD of n = 3 independent experiments. **p<0.01, two-tailed Student's t test.

The SK-N-AS cell line is a *MYCN* non-amplified NB cell line with an endogenous amplification of *METTL1*; we exploit this characteristic to investigate the effect of a reduction in the m6A content due to an alteration of the methyltransferase. We designed four inducible short hairpin RNA against *METTL14* (sh1387, sh616, sh583 and sh213) and a control shRNA against *GFP* (called, shGFP#1) and we examined *METTL14* expression with and without Doxycycline treatment. Short hairpins sh616 and sh583 resulted in an efficient decrease of METTL14 mRNA (**Figure 21A**) and protein (**Figure 21B**) upon Doxycycline supplement; therefore, the two were chosen to investigate the impact of *METTL14* knockdown on cell proliferation. We observed a trend toward a reduction in proliferation, although not significant (**Figure 21C**).

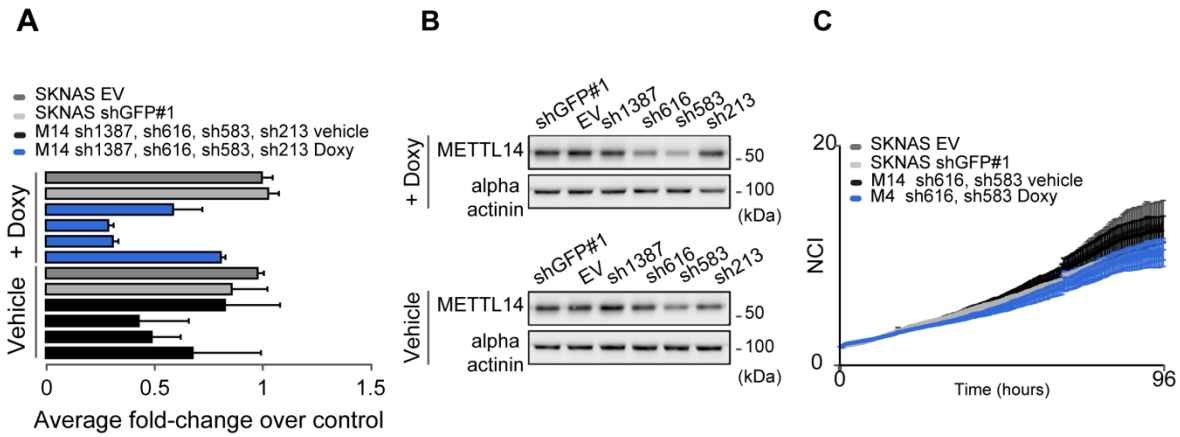

Figure 21| Knockdown of METTL14 with shRNAs. (A) quantitative-PCR of METTL14 mRNA expression in SK-N-AS neuroblastoma cell line transfected with either an inducible control short hairpin (shGFP#1) or four different inducible shRNAs (sh1387, sh616, sh583 and sh213). Cells were grown in normal or Doxycycline-enriched medium. Means ± SD of n=3 independent experiment.

(B) Representative western blotting of METTL14 and alpha-ACTININ (loading control) protein expression in SK-N-AS neuroblastoma cell line transfected with either an inducible control short hairpin (shGFP#1) or four different inducible shRNAs (sh1387, sh616, sh583 and sh213), with and without Doxycycline treatment. **(C)** Proliferation of SK-N-AS cells transduced with either an inducible control short hairpin (shGFP#1) or four different inducible shRNAs (sh1387, sh616, sh583 and sh213) monitored real-time by the RTCA (xCELLigence) and reported as normalized cell index (NCI); means ± SD of n=3 independent experiments consisting of n=4 technical replicates.

To test if the mildness of the phenotype was due to an inefficient downregulation of METTL14, I moved to exploit the CRISPR/Cas9 knockout system and designed three independent sgRNAs (#1a, #1b, #2 collectively named as sgRNAs). I then perform the same panel of experiment starting from validating METTL14 knockdown at the protein level and m6A abundance. All three sgRNAs resulted in a substantial depletion of METTL14 (**Figure 22A**) and a significant reduction in m6a content (**Figure 22B**). In contrast with the short hairpin system, the *METTL14* CRISPR/Cas9 knockout generate a severe phenotype characterized by a dramatic reduction in proliferation and invasion ability, and increasing apoptosis (**Figure 22C-E**).

As expected, *METTL14* cause opposite phenotypic effects when overexpressed or knockout in NB cell lines and its knockout produce comparable results as *ALKBH5*overexpression since the biological outcome is the same, a reduction in m6A content in the transcriptome.

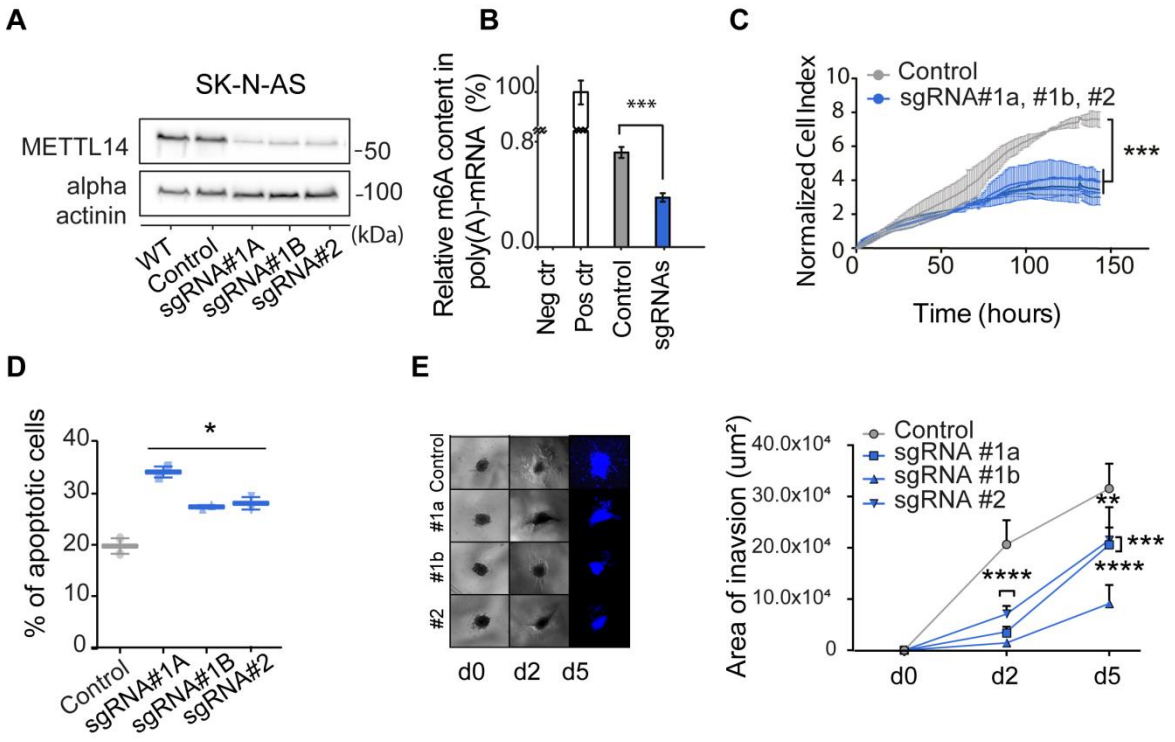

Figure 22| In vitro phenotypic assays of engineered SK-N-AS cells. (F) Representative western blotting of METTL14 and alpha-Actinin (loading control) of SK-N-AS cells, transfected with either control (empty vector) or three different RNA guides for CRISPR/Cas9-mediated silencing of METTL14 (gRNA #1A, #1B, #2). **(G)** Quantification of m6A levels inpoly(A)-purified mRNA upon removal of rRNA, in METTL14 knockout SK-N-AS as assessed by colorimetric assay; negative (Neg ctr) and positive (Pos ctr) controls were used as internal references; means ± SD of n = 4 technical replicates, normalized and expressed as a percentage of global m6A, on the basis of negative and positive controls. **P < 0.01, ***P < 0.001, two-tailed Student's t test. **(H)** Proliferation of SK-N-AS cells transfected with either control (empty vector) or three different RNA guides against METTL14 (gRNA #1A, #1B, #2), monitored real-time by the xCELLigence and reported as normalized cell index; means ± SD of n = 3 independent experiments, consisting each of n = 4 technical replicates. ***P < 0.001, one-way ANOVA followed by Tukey's post-test. **(I)** Percentage of apoptotic cells of SK-N-AS cell lines. Cells were stained for Annexin V and quantified by flow cytometry. mean ± SD of n=2 independent experiments. *p<0.05, ns not significant, two-tailed Student's t test. **(J)** Invasion ability of SK-N-AS cells, transfected with CRISPR/Cas9-mediated silencing of METTL14, as measured by the Operetta High Content Imaging System. Cells were stained with DAPI at the end of the experiment. Quantification of the area of invasiveness over the course of 5 days; means ± SD of n = 3 independent experiments. **p<0.01, ***p<0.001, ****p<0.0001 two-tailed Student's t test.

MYCN amplification is one of the major drivers of NB tumorigenesis so, to test whether m6A effects on NB cells were MYCN-dependent, I decided to restore METTL14 or ALKBH5 expression also in others NB cell lines, both MYCN amplified and non-amplified (**Figure 23**) The fact that *METTL14* and *ALKBH5* alteration generates coherent phenotype and that their endogenous expression seems to be not influenced by *MYCN* genetic status (**Figure 18B**), lead us to speculate that m6A effect on NB tumour are MYCN-independent.

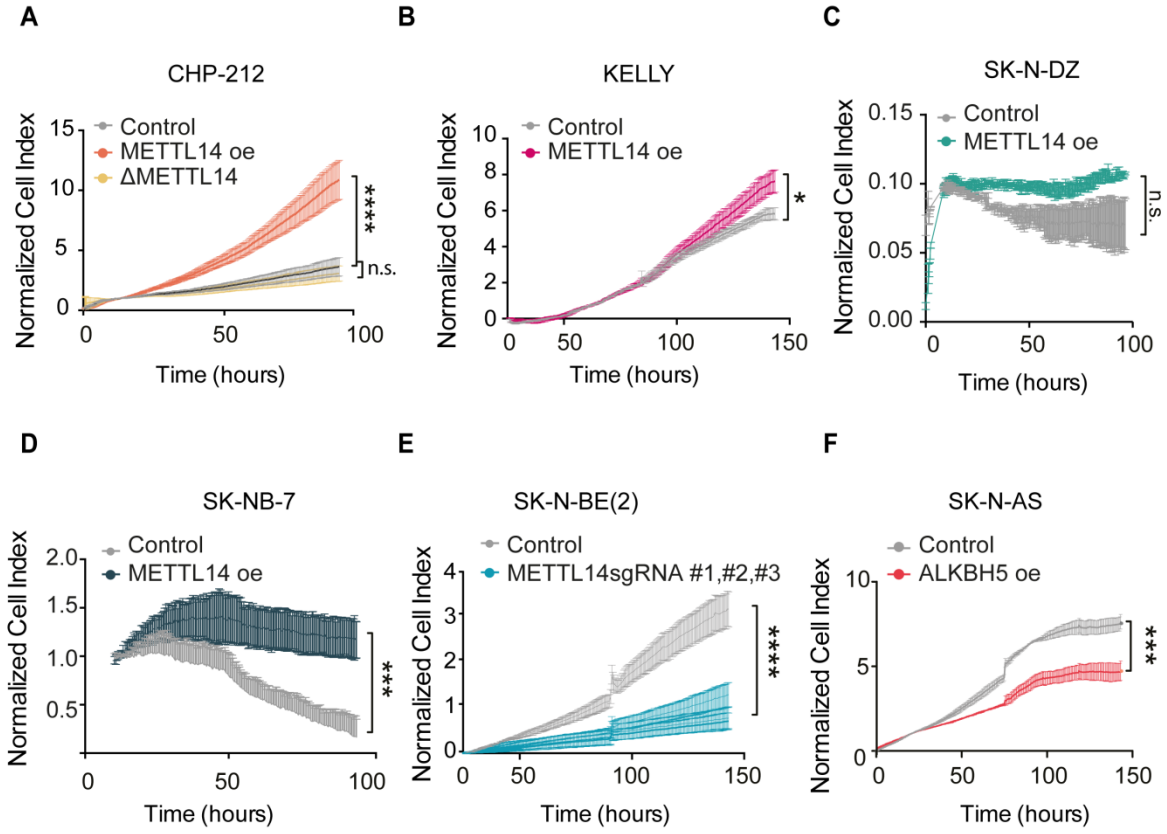

Figure 23| METTL14 and ALKBH5 overexpression in other NB cell lines (A-F) Proliferation of CHP-212, KELLY, SK-N-DZ, SK-NB-7, SK-N-BE(2) and SK-N-AS cells transduced with either control, METTL14- or ALKBH5-overexpressing lentiviral vectors monitored real-time by the RTCA (xCELLigence) and reported as normalized cell index; means ± SD of n=3 independent experiments consisting of n=4 technical replicates. ****p<0.0001, ***p<0.001, *p<0.05, n.s., not significant, two-way ANOVA.

2.4 *In vivo* characterization of METTL14- and ALKBH5 overexpressing NB cells

When it comes to cancer studies, in vitro experiments might be not sufficient, due to the lack of the appropriate microenvironment that enables tumour development and growth. To mimic at least some extent of the clinical situation in a human organism, I decided to move to the in vivo analysis of METTL14 and ALKBH5 by performing xenotransplantation of METTL14- and ALKBH5-overexpressing CHP-212 cells in the Foxn1 nu/nu (nude) mice. Firstly described by Flanagan in 1966, the essential trait of these mice is their lack of thymus and therefore, the lack of T-cells responsible for destroying malignant cells and for the host reaction to grafts.

I tested different cell concentration to be injected in mice, spanning from 1x106 to 15x106 per mouse and choosing 15x106 one, that resulted in being the most efficient in developing visible masses in a suitable time. For evaluating tumour development and progression, I used a preclinical optical/X-ray imaging, called In-Vivo Xtreme I (Bruker). Specifically, I decided to exploit the fluorescence imaging setting; therefore, I co-infected CHP-212 METTL14- and ALKBH5 cells with a GFP-expressing plasmid. I injected the desired number of cells subcutaneously in the right flank of Foxn1 nu/nu mice and evaluated the course of each xenograft every three days for 30 days. The experimental flow is graphically described in **Figure 24**.

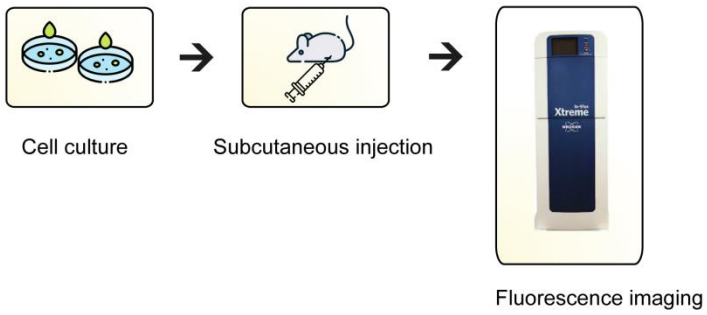

Figure 24|Experimental workflow of tumor progression *in vivo*

Figure 25A shows representative images of control, METTL14- and ALKBH5-overexpressing-tumours acquisition over time. The resulting image is an overlay between a foreground (fluorescence) and a background acquisition (X-ray). CHP-212 NB cells generated visible masses not so efficiently; in this light, the behaviour of METTL14-

overexpressing cells in making huge and fast-growing tumours is even more remarkable. They displayed a significantly more rapid growth rate (**Figure 25B**) and dimension (**Figure 25C**) already at day 6 post-injection, compared to control tumours, and reached the human end-point (1,5 cm^2 of diameter) before the established end of the procedure. Oppositely, *ALKBH5*-overexpressing cells failed to form proper masses, and the fluorescence signal coming from the injected cells remained virtually identical over time and, in 2 out of 6 animals, wholly disappeared (**Figure 25A,C**). This effect might be due to a dramatic growth rate slowing-down and cell death (**Figure 25B**). To verify that the altered level of m6A indeed had impacted tumour progression, I quantified it in METTL14-overexpressing tumours demonstrating that higher levels of m6A are retained *in vivo*, compared to control tumours (**Figure 25D**).

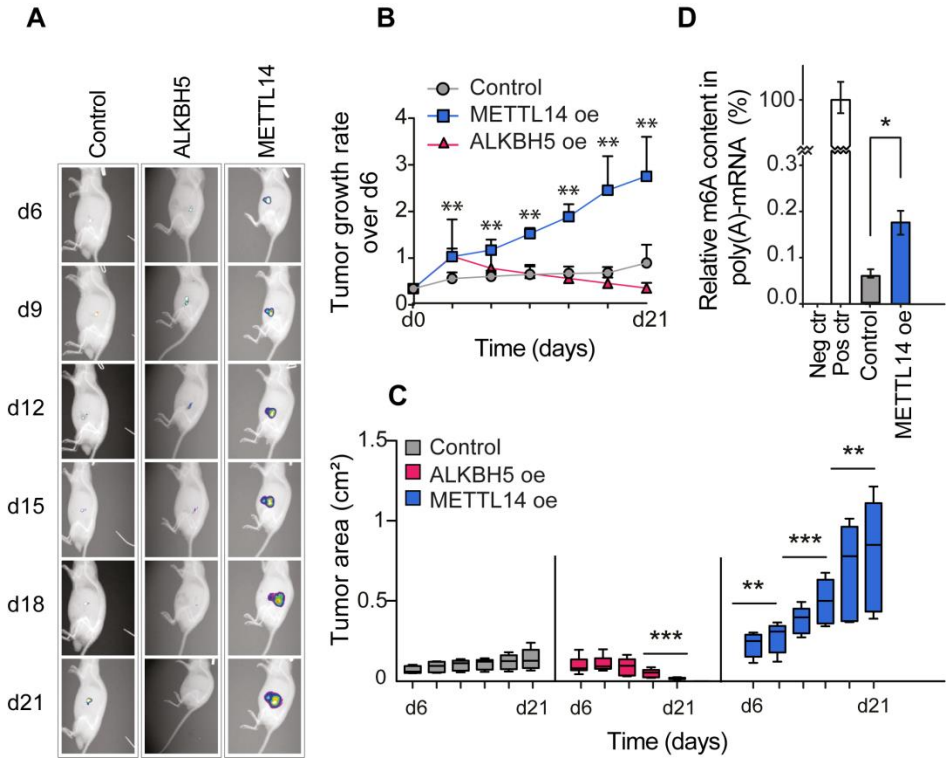

Fig. 25| METTL14 promotes tumour progression and aggressiveness *in vivo*. (**A**) Representative xenograft tumours of GFP-expressing CHP-212 cells, transduced with either control (empty vector, EV), METTL14-overexpressing, or ALKBH5-overexpressing lentiviral vectors. The GFP signal was measured every three days. (**B**) Tumor growth rate of control, METTL14-overexpressing, and ALKBH5-overexpressing cells, normalized at T0 of n=6 individual for each condition; means ± SD.

P < 0,01, two-tailed Student's t test, relative to d0. (C**) Quantification of tumours area, as assessed by GFP signal; means ± SD. **p<0,01, ***p< 0,001, two-tailed Student's t test, relative to d6. (**D**) Quantification of m6A levels of total poly(A)-purified mRNA in resected xenograft tumors derived from METTL14-overexpressing cells, compared to control tumours, as assessed by colorimetric assay; negative (Neg ctr) and positive (Pos ctr) controls were used as internal references; means ± SD of n = 3 replicates, normalized and expressed as a percentage of global m6A, on the basis of negative and positive controls. *p<0.05, two-tailed Student's t test.

The constitutive expression of *ALKBH5* seems to prevent NB tumour growth *in vivo*. Therefore to evaluate *ALKBH5* effect and to simulate its modulation during tumour progression in patients, I develop a TetOn doxycycline-inducible system using an all-in-one system; This system is represented by a plasmid both containing the tetracycline-responsive promoter element (TRE) and TET repressor (rTetR) that enable more controlled expression of the gene of interest and avoid a double infection that could compromise cells viability and thus the results. A graphical schematization of the pcw57.1 all-in-one plasmid is represented in **Figure 26A**. Since CHP-212 cells do not efficiently generate tumour masses when xenografted, I decided to use SK-N-AS cells. 48 h of treatment with 1 µg/mL doxycycline produced a strong induction of *ALKBH5* at the protein level (**Figure 26B**) and, coherently with the above-mentioned phenotypic effects, *ALKBH5* induction cause a slowing-down in proliferation (**Figure 26C**).

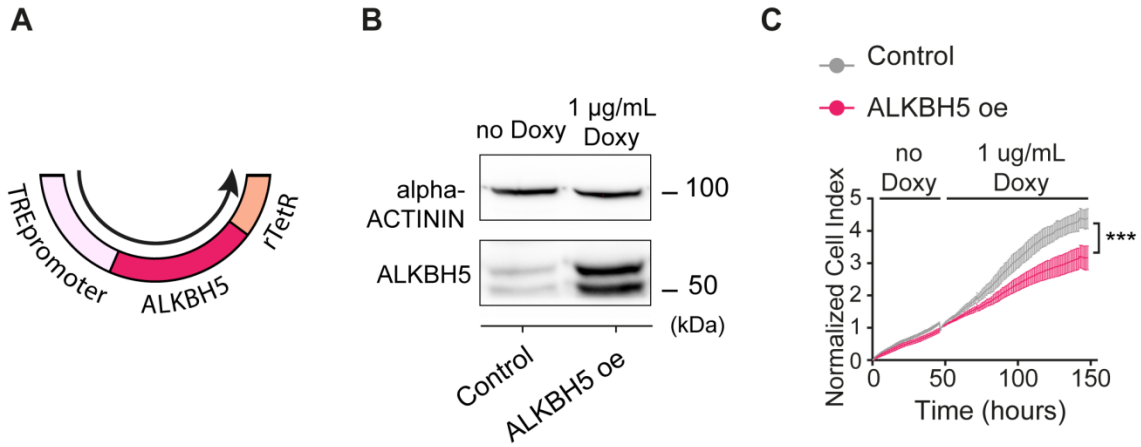

Fig. 26| Validation of the inducible system. (A) Schematic representation of the pcw57.1 "all-in-one" system (Addgene). In the same backbone, the tetracyclin-responsive promoter element (TRE) and the Tet Repressor (rTetR), are present. **(B)** Representative western blotting of *ALKBH5*

expression with or without doxycycline treatment and alpha-*ACTININ* (loading control) of SK-N-AS cells, transduced with either control (empty vector), or *ALKBH5*-inducible lentiviral vectors. **(C)** Proliferation of SK-N-AS cells transduced with either control or *ALKBH5*-inducible lentiviral vectors monitored real-time by the RTCA (xCELLigence) and reported as normalized cell index; means ± SD of n=3 independent experiments consisting of n=4 technical replicates. ***p<0.001, two-tailed Student's t test.

Several methods are described to deliver doxycycline *in vivo*: by gavage, in drinking water or standard feed but, to reduce animals stress, I immediately excluded gavage administration. Doxycycline is known to be very bitter, and thus it has to be mixed in water with sucrose to increase palatability. Nonetheless, many reports describe substantial dehydration and weight loss associated with this route of doxy administration (Li, 2005; Cawthorne, 2007). Therefore, I opted for using a specific doxycycline-enriched feed that ensures a sure and continuous induction of the gene.

The experimental strategy for the *in vivo* xenotransplantation of inducible *ALKBH5* cells is virtually identical to this mentioned above, and it is described in **Figure 27A**. In essence, tumour progression was evaluated every three days for three weeks and, 9 days post-injection, mice were switched to a doxycycline-enriched diet to evaluate *ALKBH5* impact on established masses. All mice were injected with the same cells, the SK-N-AS all-in-one, and divided into two groups of n=6 individuals nine days post-injection: one group followed a regular diet while the other was shifted to the doxycycline-enriched diet (625 mg/kg). **Figure 27B** shows representative images of the two groups.

As expected, tumours grew at the same rate with slight differences due to individual variability of the animals, but right after doxy induction, the group of induced tumours showed a partial but substantial blockage in growth (**Figure 27C**) and a reduction of mass (**Figure 27D**). This effect is more evident in **Figure 27E,** representing resected tumours belonging to both experimental groups, in which it can be seen how induced tumours (the one with higher expression of *ALKBH5*) are visibly smaller compared to not-induced ones.

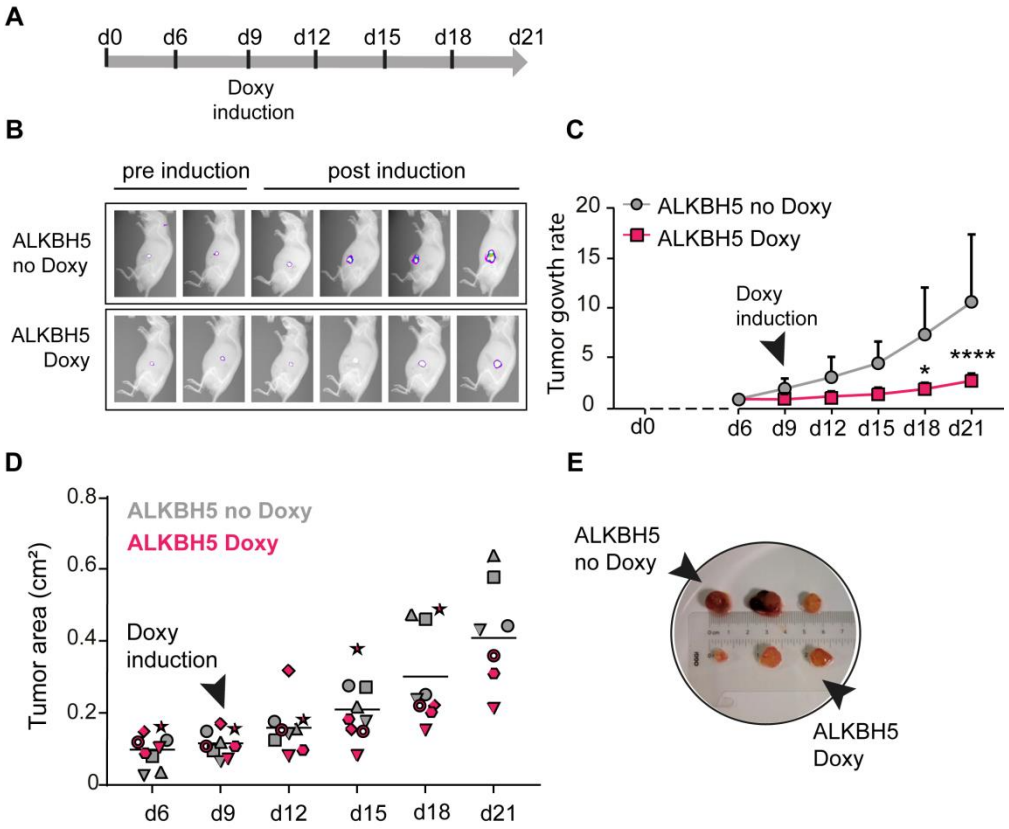

Figure 27| ALKBH5 restoration induces tumour growth arrest *in vivo*. (A) Schematic of the experimental strategy, including xenogenic imaging and doxycycline treatment. **(B)** Representative xenograft tumours of GFP-expressing SK-N-AS cells, transduced with doxycycline-inducible ALKBH5 lentiviral vectors, either feed with normal or doxycycline enriched food. **(C)** Tumour growth rate of either induced and not-induced ALKBH5 tumours; means ± SD. **P < 0,01, two-tailed Student's t-test, relative to T3 (6 days post-injection). **(D)** Tumour area (in cm^2) of single xenograft followed over time of acquisition. Induced tumours are represented in pink, not-induced tumours in grey. **(E)** Representative induced and not-induced tumours resected at T8 (24 days post-injection).

To understand the molecular effect of *ALKBH5* restoration *in vivo*, I perform immunofluorescence on both induced and not-induced tumours. Right after resection, tumours were immersed in 4% formaldehyde/PBS for 24 h, moved in 30% sucrose/PBS for other 24 h, frozen in OCT in an isopropanol-dry ice bath and finally cut up in 40 μm slices at the cryostat (Leica CM 1850 UV cryostat). Anti-annexin V staining shows massive

apoptosis in *ALKBH5* induced tumours and virtually no signal in not-induced one (**Figure 28A**).

Collectively, these data demonstrate that *ALKBH5* plays an essential role in NB progression: its stable expression prevents tumours formation and, importantly, its restoration substantially blocks the progression of established tumours causing the dramatic apoptosis of cancer cells (that might be more relevant in a clinical context).

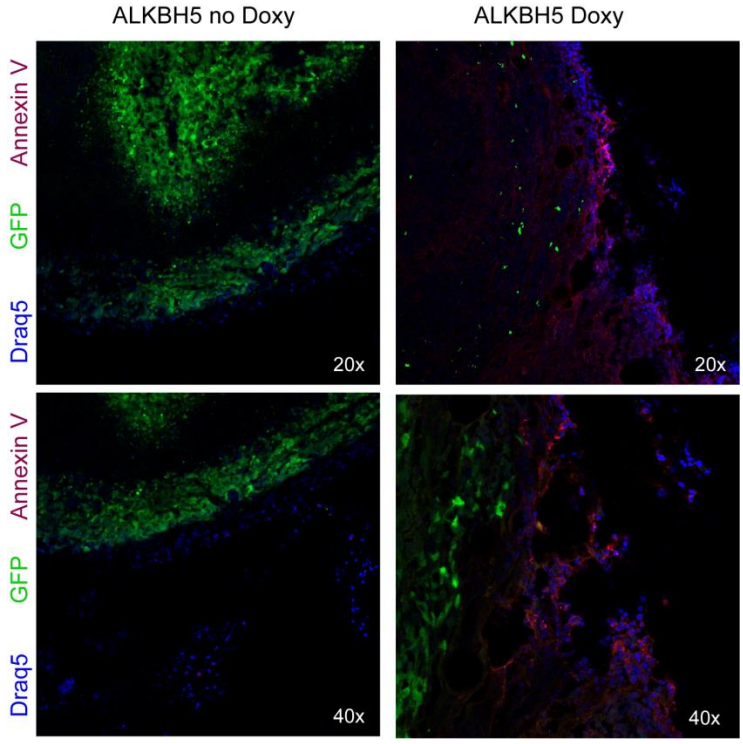

Figure 28| ALKBH5 restoration determined a massive apoptosis *in vivo*. Representative immunofluorescence analysis of ALKBH5 induced and not induced tumours using anti Annexin V (magenta) that highlights apoptotic cells and Draq5 for nuclei (blue). GFP signal (green) is acquired in autofluorescence.

3. ALKBH5 and METTL14 affect the translation and stability of NB transcripts

The m6A modification controls almost every aspect of transcripts life in the cell and can connect the nuclear and cytoplasmic processing of RNAs. In the nucleus, the m6A is mainly involved in the co-transcriptional splicing of transcripts and nuclear export, while in the cytoplasm regulate the latest step of translation and decay, primarily. In this context, we sought to investigate the effect of METTL14 and ALKBH5 alterations, and at a more significant extent those of m6A, on translational efficiency and transcripts stability in NB cells by combining **polysome profiling** followed by RNA-seq and the **Slam-seq** technology, a new metabolic approach capable of differentiating between nascent and existing RNA.

3.1 Polysome profiling of METTL14- and ALKBH5- overexpressing NB cells

Translational control of gene expression has emerged as a principal mechanism in the regulation of protein abundances; therefore, several approaches have been developed for studying the translatome of cellular systems. Polysome profiling is one of the traditional methodology exploited for understanding global or individual changes in mRNAs translation. Polysome profiling consists of polysomes fractionation followed by sucrose density gradient centrifugation and RNA or protein analysis (**Figure 29A**).

To perform the profiling, I set up the seeding condition for control, ALKBH5- or METTL14- overexpressing CHP-212 cells so that each cell line would have reached 75-80% confluence the day of the experiment. Precise seeding is a critical step in the procedure since 100% confluence generates a global slowing down of translation resulting in a lower polysome yield. Before starting with the lysis, I treated cells with cycloheximide to a final concentration of 100 μg/mL and incubated for 5 minutes at 37°C. Cycloheximide immobilizes elongating ribosomes and prevents their disassembling, thus producing a snapshot of the translational state of a cell. Therefore, it is crucial to maintain its presence during all fractionation steps to preserve polysomes structure. Cells were washed with ice-cold PBS supplemented with 10 μg/mL cycloheximide and lysed. After a 5 minutes centrifugation at 16000 g, the supernatant was loaded in the 50-15% sucrose gradient and

ultracentrifuge at 40000 rpm for 1 h 40 min at 4°C. Gradients were prepared in advance in thin-wall polyallomer ultracentrifuge tubes by adding 5.5 mL of 50% sucrose solution and overlaid the 15% solution. The continuous gradient was made using a sucrose gradient former that slowly laid the tubes horizontally (90°C) and straightened them back into the vertical position. After the centrifugation, I analyzed the samples using the Teledyne Isco model 160 gradient analyzer equipped with a UA-6 UV/VIS detector.

Representative profiling of *METTL14*- and *ALKBH5*- overexpressing cells are shown in **Figure 29B**. ALKBH5 (top profile, pink line) seems to have greater effect on NB global translation compared to METTL14 (bottom profile, light blue line). It can be speculated that *ALKBH5* profile is characterized by an increase in free subunits (40S and 60S) and in the 80S monosome and a slight decrease in polysomes, that might be explained with a slowing down in the translation initiation step, although additional data are needed to prove the point.

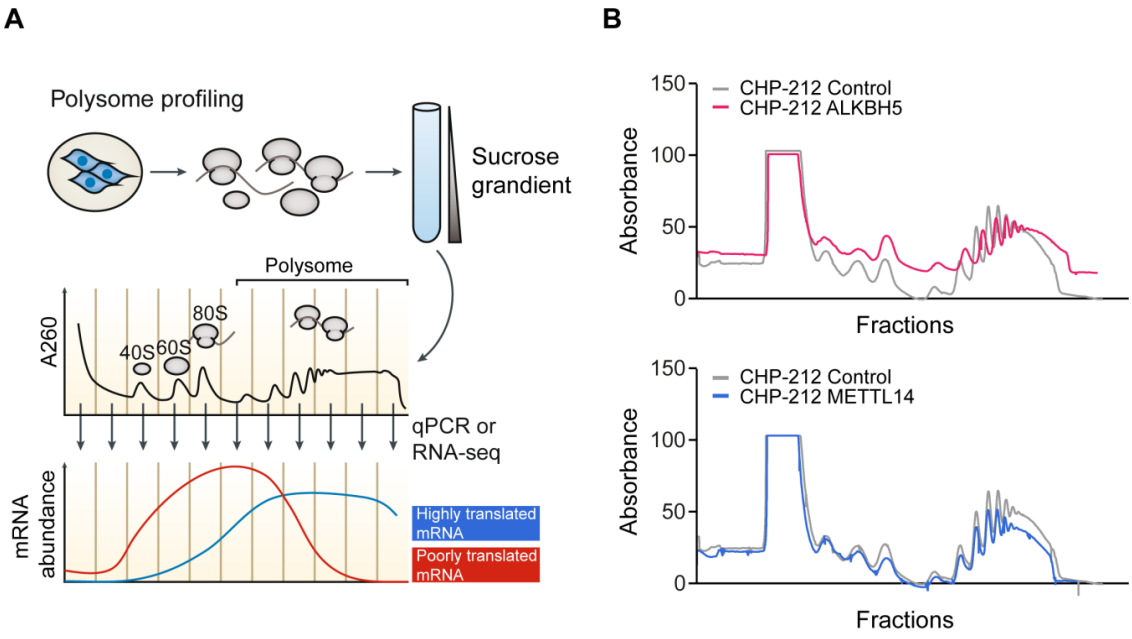

Figure 29| Polysome profiling. (A) Experimental workflow of polysome profiling: lysates from cells are treated with cycloheximide that immobilize elongating ribosomes on mRNAs are loaded onto sucrose gradients and spun in an ultracentrifuge. The free subunits (40S and 60S), 80S ribosome and polysomes are separated into defined fractions in the gradient. RNA is isolated from each individual fraction, and the abundance of genes of interest is determined by quantitative PCR (qPCR) or RNA sequencing (RNA-seq). Highly translated mRNAs are enriched in the heavier

polysome fractions (blue line), while poorly translated mRNAs are enriched in lighter fractions (red line). **(B)** Representative polysome profiling of CHP-212 ALKBH5- or METTL14 overexpressing cells. *(Figure A adapted from Genuth and Barna, Nat. Rev. Gen., 2018)*

To verify the association of specific transcripts with the lighter or heavier polysome fractions, meaning to identify highly and poorly translated mRNAs in *ALKBH5*- and *METTL14*- overexpressing NB cells, I isolated total RNA from all the fraction using phenol/chloroform/isoamyl alcohol solution. Helping with the profiles, I pooled together the RNA extracted from all the fraction defined them as "Total RNA" (Tot RNA) and the RNA extracted from the polysome fractions defined as "Polysomal RNA" (Pol RNA). After checking RNA integrity with a bioanalyzer (**Figure 30**), all the sample were processed for library preparation and sequenced using the Illumina HiSeq2500 platform by the Next-Generation Sequency (NGS) Facility.

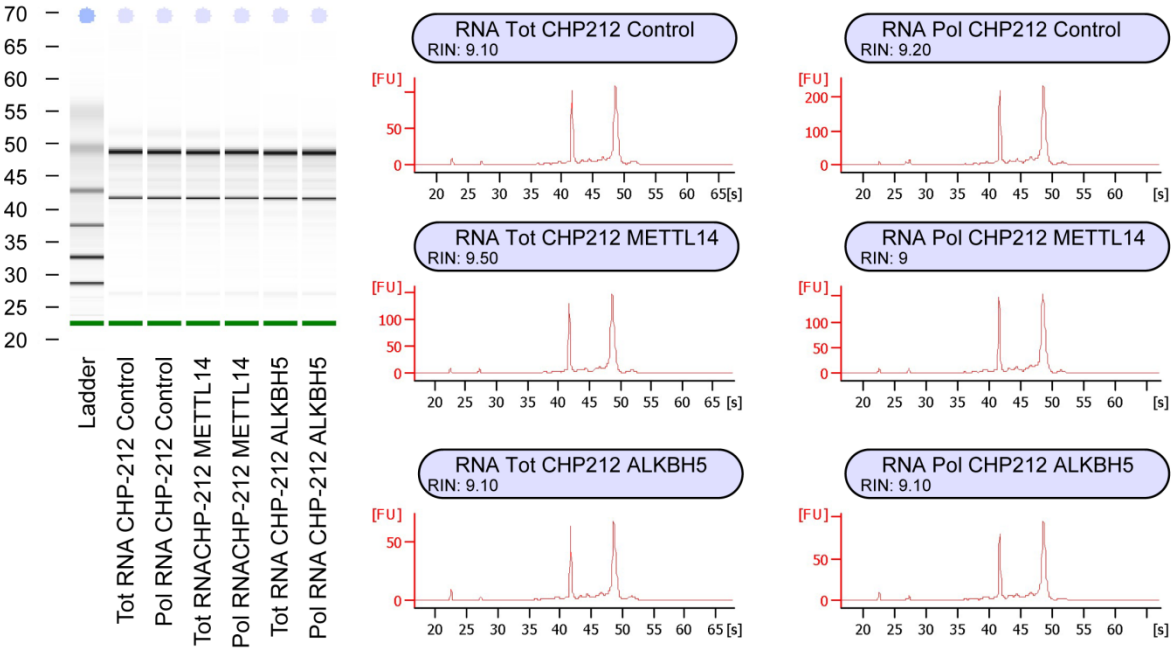

Figure 30 | RNA from polysome profiling fractions. Representative quality control check of Total and Polysomal RNA from CHP-212 cells either METTL14 or ALKBH5-overexpressed using BioAnalyzer.

3.2 Polysome profiling analysis

All the sequencing data were analysed by our collaborators, Dr Erik Dassi and Eliana Destefanis, while I performed the molecular validation.

Polysome profiling data were analysed by using the tRanslatome R package (Tebaldi, 2014). We first analysed all the genes expressed in the "transcriptome" and the "translatome" with the transcriptome represented by the reads coming from "Tot RNA" and the translatome by the reads derived from "Pol RNA". Then, we compared Control and *METTL14* or *ALKBH5* counts polysomal and total data to detect differentially expressed genes applying a 0.05 significance threshold on the adjusted p-value (p-adj).

The Principal Component Analysis (PCA) plot in **Figure 31A** shows that most of the variance (36%) is represented by the differences between the transcriptome ("RNA Tot") and the translatome ("RNA Pol") in all the conditions (Control cells and *METTL14*- or *ALKBH5*-overexpressing cells). The plot also implies that both overexpressed samples are more similar to control expression data at the total level as compared to the polysomal level and that *ALKBH5*-overexpressing cells are significantly more different compared to control cells than *METTL14*-overexpressing cells. This data suggest a more marked involvement of the m6A erasers in influencing the translation processes, coherently with preliminary evidence obtained with the polysomal profiling (**Figure 31B**).

To detect if there were any shifts in relative abundance between mRNAs in active translation and the total pool of mRNAs, we performed a differential gene expression analysis. Particularly, we wanted to identify those groups of genes that move accordingly or with opposite tendencies at the transcriptome and translatome levels between control and *METTL14*- or *ALKBH5*-overexpressing cells. We thus identified eight groups of genes depending on their expression at the transcriptome, translatome, or both levels:

Transcriptome up/translatome unchanged (up/-)

Transcriptome down/translatome unchanged (down/-)

Transcriptome unchanged/translatome up (-/up)

Transcriptome unchanged/translatome down (-/down)

Transcriptome up/translatome up (up/up)

Transcriptome down/translatome down (down/down)

Transcriptome up/translatome down (up/down)

Transcriptome down/translatome up (down/up)

We found only 33 significantly differentially expressed genes (DEGs) in the *METTL14* overexpression condition compared to control

in contrast with 215 DEGs in *ALKBH5* overexpression condition. Most of them showed greater variation at the translatome level (89 DEGs -/up and 90 DEGs -/down) while few moved significantly in the transcriptome (10 DEGs down/-) or both direction (22 DEGs down/down). None moved oppositely (0 DEGs in up/down and down/up groups) (**Figure 31B**). The greater number of DEGs obtained in ALKBH5-overexpressing CHP-212 cells is consistent with the preliminary evidence detected in the exploratory data analysis.

To identify the affected functions, we performed a functional enrichment analysis by looking for annotating pathways and Gene Ontology processes of ALKBH5 DEGs. This analysis revealed the presence of several genes associated with the ribosome machinery and mitochondrial translation (**Figure 31C**). Moreover, several proapoptotic genes come up from the top 20 upregulated DEGs in the translatome dataset of *ALKBH5*-overexpressing cells compared to control, such as PERP, APOL6, TSFM and MTCH1 and one anti-apoptotic gene, STAT6, come up from the top 20 downregulated DEGs.

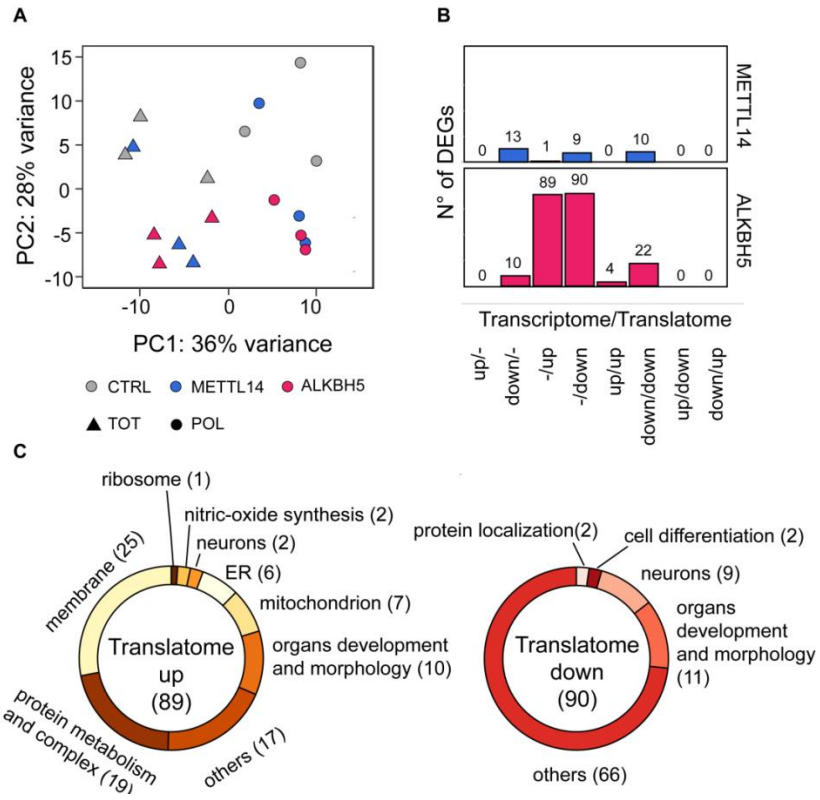

Figure 31| ALKBH5 promotes transcripts translation in CHP-212 NB cell line. (A) PCA on Control CHP-212 Control and *METTL14*- and *ALKBH5*-overexpressing cells. On the x and y axes, the first and second principal components explain 36% and 28% of the gene expression variance, respectively. Color represents cell condition (CTRL/ALKBH5-oe/METTL14-oe), shape represents type (polysomal/total). **(B)** Count of significant differentially expressed genes at the specific gene expression levels (transcriptome and translatome) for METTL14 (up histogram) or ALKBH5 (bottom histogram) overexpressing CHP-212 cells; BH adj p-value < 0.05. **(C)** Macro GO terms which describe the GO annotation results of AKBH5 significantly up-regulated and down-regulated genes at the translatome level. Numbers in brackets referring to the number of DEGs associated to the specific macro GO term.

All the genes resulted coherently up-regulated or down-regulated in the polysomal fraction of ALKBH5 overexpressing cells, compared to Control cells **(Figure 32A, top panel**) and this effect is indeed produced by a reduction in m6A content as assessed by m6A-RIP qPCR on the same transcripts (**Figure 32A, bottom panel**). To make the results more reliable, m6A-RIP was performed on poly(A) RNA and not cells crude extract.

P53 directly activates PERP, thus its induction is linked to p53-dependent apoptosis (Attardi, 2000). Indeed, I observed p53 activation in ALKBH5-overexpressed cells (**Figure 32B**) although a straight link between the two needs further validation. The apolipoprotein l6 (APOL6) is a proapoptotic Bcl-2 homology-3 protein that induces mitochondria-mediated apoptosis in colorectal, liver and breast cancer cell lines (Liu, 2005) as well as MTCH1 which promotes a Bax/Bak independent apoptosis by attaching one or two proapoptotic domain to mitochondria outer membrane (Lamarca, 2008). Coherently, the IL4/STAT6 antiapoptotic signalling (Li, 2008) is maintained low by reducing STAT6 translation.

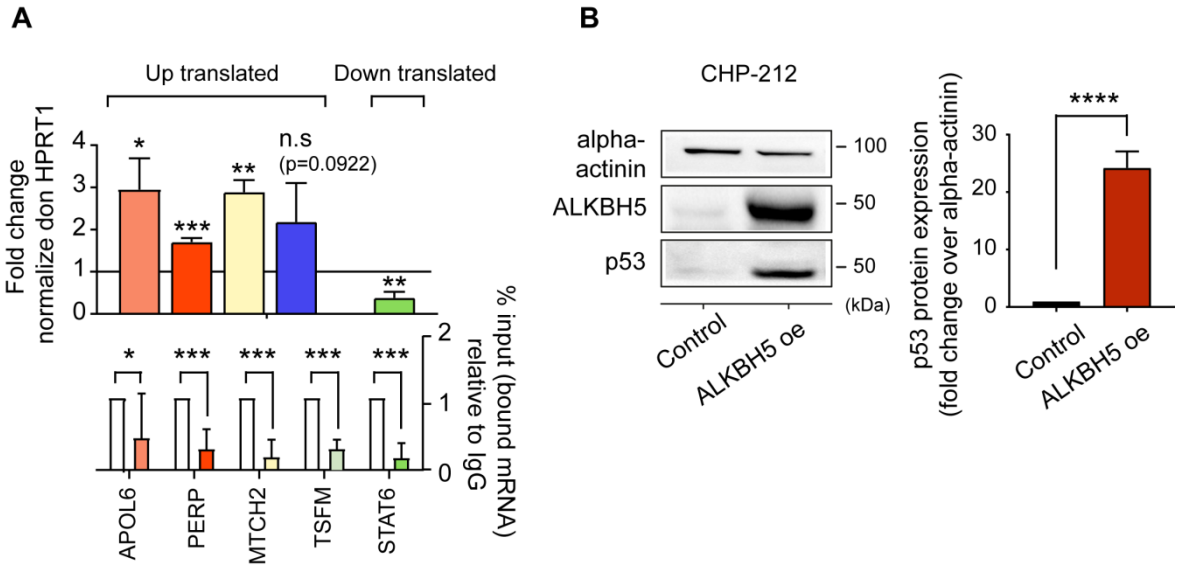

Figure 32| Gene target validation of polysomal profiling. (A) Top panel, APOL6, PERP, MTCH2, TSFM and STAT6 mRNA expression in polysomal fraction of ALKBH5 overexpressing CHP-212 cells compared to control cells, evaluated by qPCR and normalized on housekeeping control genes**.** Bottom panel, m6A-RIP of APOL6, PERP, MTCH2, TSFM and STAT6 in ALKBH5 overexpressing cells, relative to IgG. **(B)** Left panel, representative Western Blot of ALKBH5, p53 and alpha-actinin (loading control) of CHP-212 cells either transduced with control or ALKBH5-overexpressing lentiviral vectors. Right panel, quantification of p53 protein expression in Control and ALKBH5-overexpressing CHP-212 cells. means ± SD of n=3 independent experiments.

3.3 Evaluation of transcripts stability in ALKBH5- and METTL14-overexpressing cells with SLAMseq

To evaluate the contribution of METTL14 and ALKBH5 in regulating NB transcripts stability, we employ the new method of the Thiol (SH)-Linked Alkylation for Metabolic Sequencing (SLAMseq) by Stefan Ameres' group described in Herzog, 2017. The SLAMseq assay involved metabolic labelling with 4-thiouridine (S4U) that is incorporated in newly synthesized RNA transcripts instead of normal Uridine. Following an alkylation step, the Reverse Transcriptase introduces a Guanine instead of an Adenine whenever it encounters a modified S4U. The G is copied as a Cytidine (C) instead of a Thymine (T) during PCR. Therefore, nascent transcripts can be distinguished by existing transcripts identifying T-to-C transition compared to a reference genome (Figure 3.3).

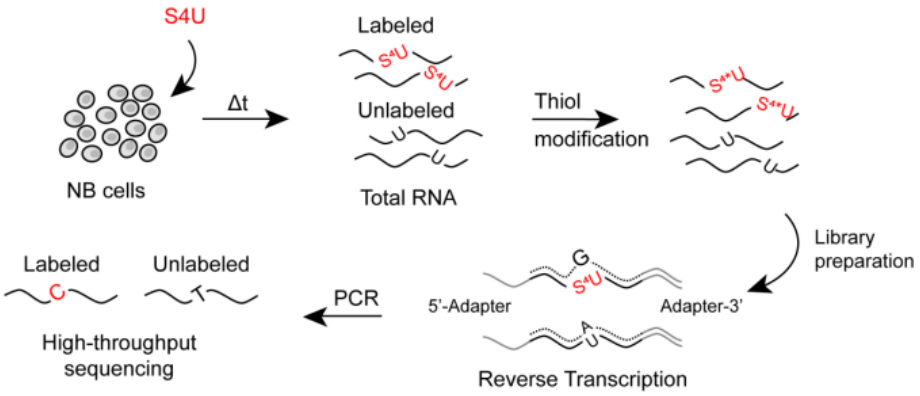

Figure 33 | Schematic of the SLAMseq assay

Before starting the experiment, I carried out an exploratory analysis to determine S4U concentration and uptake using the SLAMseq Explorer Kit - Cell Viability Titration Module (Lexogen, Cat. No. 059.24) and the SLAMseq Explorer Kit - S4U Incorporation Module (Lexogen, Cat. No. 060.24).

The first step was optimizing S4U labelling condition in cultured cells, that is finding the appropriate S4U concentration to avoid cytotoxicity. In a 96-well plate, I seeded 3x104 Control, METTL14- and ALKBH5-overexpressing cells 24 h prior the experiment and treated them with a dilution series of S4U-containing media, ranging from 4 mM to 3.9

μM (11 1:2 dilution plus H2O as control) for 24 h. Since S4U incorporation rate decreases rapidly over time, I supplied fresh S4U-containing medium every three hours for the entire period of the experiment. At the end of the treatment, I evaluated cell viability using the CellTiter-GloTM Luminescent Cell Viability Assay (Promega). The assays quantify the presence of ATP as an indicator of metabolically active cells. For the evaluation of suitable S4U concentration, I plotted the cell viability measure vs concentration to obtain an inhibition vs S4U concentration curve. The curve was used to determine the half-maximal inhibitory concentration (IC50,ti) and experimental working concentration (IC10,ti). The IC10,ti values that is the S4U concentration that would inhibit the 10% of cells in the given time window (ti) were 114 μM for Control, 90 μM for METTL14-overexpressing and 140 μM for ALKBH5-overexpressing cells (**Figure 34A**).

I verified global **S4U uptake** using HPLC. I cultured Control, METTL14- and ALKBH5-overexpressing cells with the optimal IC10 concentration for 24 h refreshing the media every three hours. At the end of the experiment, I isolated and single-nucleoside digested the RNA in reducing condition. HPLC analysis was carried out by Dr Adriano Sterni (University of Trento – Physics Department). S4U incorporation, calculated as the ratio between Thiouridine and Uridine concentration (in μM), was 3,9% for Control cells, 6,1% for METTL14-overexpressing cells and 5,8% for ALKBH5-overexpressing cells (**Figure 34B**).

To finally evaluate RNA degradation rate in my experimental condition, I cultured Control, METTL14- and ALKBH5-overexpressing cells with the appropriate CI10 for 24 h and refreshing the medium every three hours. I exchanged S4U-containing medium with U-containing medium to stop S4U labelling at six different time points (0 h, 1 h, 3 h, 6 h, 12 h, 24 h). In this way, RNAs synthesized during the 24 h pulse phase represents labelled existing transcripts, while RNAs synthesized during the subsequent chase phase represents unlabelled nascent new transcripts. Therefore, the decrease in S4U-labelling over time reveals RNAs degradation rates. After the 24 h chase, I isolated RNA in reducing condition and treated them with Iodoacetamide (IAA) to alkylate the 4-thiol groups presents on transcripts. RNA isolated at 0 h, 1 h, 3 h, 6 h, 12 h, 24 h time points

was used for NGS library preparation using the QuantSeq 3'mRNA-Seq Library Preps (Lexogen, Cat. No. 016).

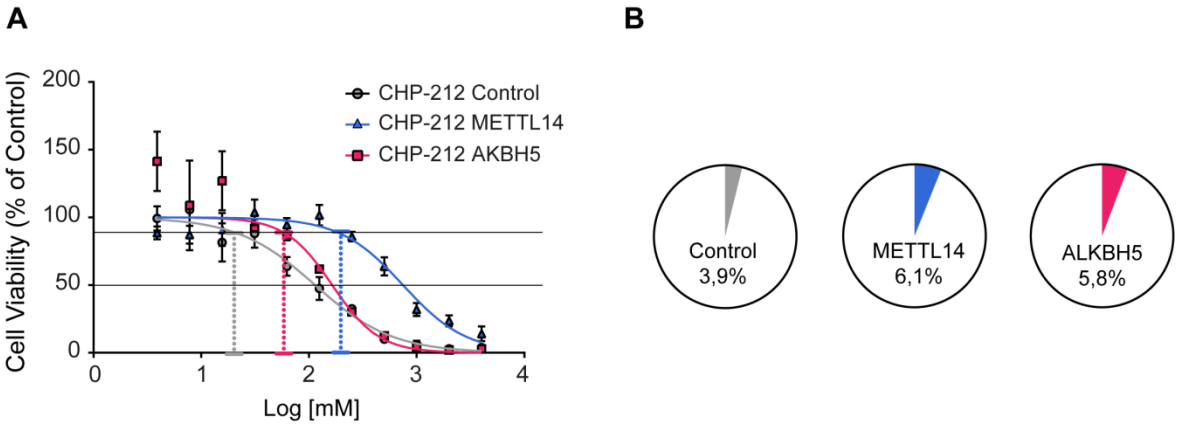

Figure 34| SLAMseq exploratory analysis. (A) Representative curves of Control, METTL14- and ALKBH5 overexpressing CHP-212 cell viability cultured with 12 1:2 dilutions of S4U for 24 h and analyzed using the CellTiter-Glo™ Assay. **(B)** Percentage of S4U uptake in Control, METTL14- and ALKBH5-overexpressing cells assessed with HPLC.

3.4 SLAMseq data analysis

All the sequencing data were again analysed by our collaborators, Dr Erik Dassi and Eliana Destefanis.

For the analysis of SLAMSeq data, we carried out an initial exploratory analysis as well, to identify similarity among the samples. We ran a PCA on Control and METTL14- or ALKBH5-overexpressing cells pulsed for 24h with S4U and collected at six different time points after the pulse (0 h, 1 h, 3 h, 6 h, 12 h, 24 h). The first two principal components (PCA1 on the x-axis and PCA2 on the y-axis) explain 50% of the total data variance and a clustering for the 12 h and 24 h time point is evident, suggesting that more differences in transcripts stability occurs later on (**Figure 35A**). During the 24 h chase phase, RNA collection and sequencing at different time points allows to analysed transcripts degradation time-course. To calculate the T>C conversion rate, we used the SLAMDunk tool (Neumann, 2019), which aligns the reads to the reference genome. Since the

transcripts are assumed to degrade during the 24 hours, the overall amount of T>C conversions-containing reads is also expected to decrease over the six time points. The Spearman correlation coefficients, computed between the total number of reads and the T>C conversion-containing reads, is higher in the earlier time points and starts to decrease in later time points (**Figure 35B**). These results prove that our SLAMseq assay was correct and coherent in detecting the transcripts degradation time course.

To evaluate the differences in transcripts stability between Control and the overexpressed conditions, we performed a Kolmogorov-Smirnov test (KS test) on the mean of all the transcripts half-life, coming from the three replicates, together. The resulted plot in **Figure 35C** indicates that the half-life distribution in the *METTL14*-overexpressing condition is significantly higher compared to Control (p-value=0,007). In contrast, the global half-life in the ALKBH-overexpression condition is less affected (p-value=0,072). This observation suggests that *METTL14* alteration (associated with increased levels of m6A methylation) alters transcripts stability while *ALKBH5* has only marginal effects. Therefore, we analysed the most affected transcripts in METTL14-overexpressing cells condition. Only a few transcripts have a constant alteration over all time points (i.e., increased or decreased stability from 1 h to 24 h compared to 0 h). Particularly, we found eight transcripts with an increase and two with decreased stability (**Table 2**). However, most of the transcripts exhibited a significant stability alteration, especially in the later time points (**Figure 35D)**. We performed functional enrichment analyses on the list of those transcripts showing a more extensive half-life fold change compared to Control cells. The GO and pathway enrichment analyses produced comparable results with the most enriched terms associated with translation initiation, RNA binding, mRNA processing, ribosome assembly and cellular catabolic processes (**Figure 35E**). We confirmed the stability of SRRM1, SNRPD1 (both involved in pre-mRNA splicing) and GPATCH8 transcript (that has already been shown to be an m6A target by Hau and colleagues (Hau, 2016). **Figure 35F** shows the ratios between T>C containing reads and total reads at each time point, for SRRM1, SNRPD1 and GPATCH8 and one transcript with non-significant altered stability (MAPKAPK) in METTL14-overexpressing cells (blue line) and Control (grey line).

.

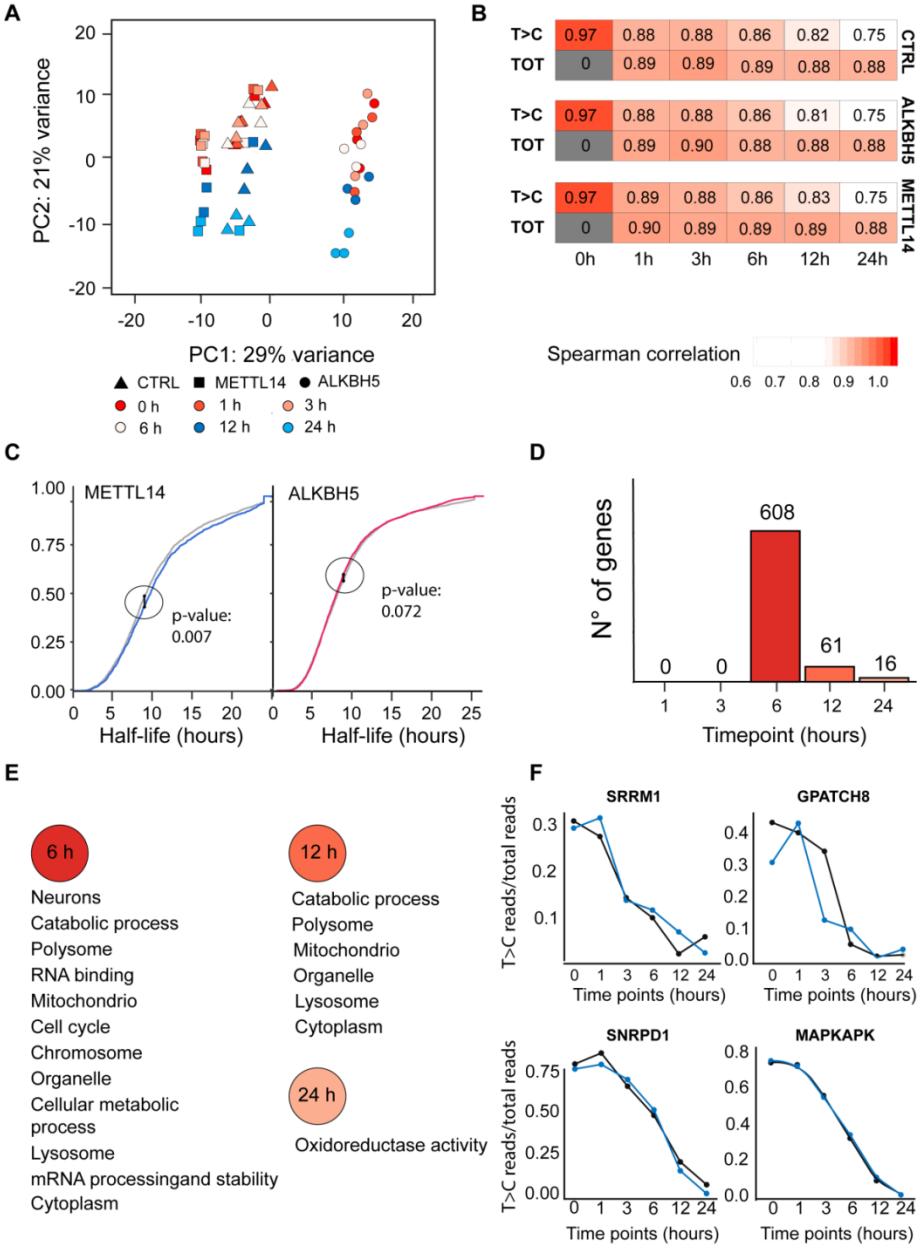

Figure 35 | METTL14 influence transcripts stability in CHP-212 NB cell line. (A) PCA plot of SLAMseq CHP-212 samples; shapes represent conditions (CTRL/METTL14-oe/ALKBH5-oe), and colors represent timepoints. The first and second principal components account for 29% and 21% of the variance, respectively. The first explains the three conditions, while the second explains the 12h and 24h timepoints. **(B)** Spearman correlation coefficients of steady-state expression at the chase onset (0h) vs. steady-state gene expression (all reads, bottom row), or T>C conversion containing reads (top row). Correlations are displayed for control, METTL14 and ALKBH5 replicates mean values, at each time point. **(C)** Empirical cumulative distribution function (ECDF) of control and

overexpressed (METTL14 on the left, ALKBH5 on the right) replicates half-lives mean value distributions. P-values refer to the Kolmogorov Smirnov test between distributions. **(D)** Number of transcripts with a significant stability alteration at a specific time point; BH adj p-value < 0.05, one sample t-tests on METTL14 overexpressed and control normalized T>C conversion rates. **(E)** Macro GO terms which describe the GO enrichment analysis results of METTL14 altered transcripts at each time point. Lines connect the macro terms with the time points where related GO terms are found; black lines connect terms to one single time point and red lines to multiple time points. Numbers refer to the sum of all the genes referable to that specific macro term at the different time points; BH adj p-value < 0.05. **(F)** Ratios between T>C containing reads and total reads at each time point, for three transcripts with significant altered stability (SRRM1, GPATCH8, SNRPD1) and one transcript with a non-significant altered stability (MAPKAPK). Ratios were computed with the means between the three replicates reads counts (CPM). Black and blue lines represent the transcript values in CTRL and METTL14 overexpressing CHP-212 cells, respectively.

Gene ID	Gene symbol	FC 1h	FC 3h	FC 6h	FC 12h	FC 24h
ENSG00000151176.7.3	PLBD2	1.3	1.3	1.3	1.3	1.3
ENSG00000129103.17.6	SUMF2	1.3	1.3	1.3	1.8	1.4
ENSG00000148362.10	PAXX	1.5	1.4	2.0	2.3	3.7
ENSG00000166173.10.1	LARP6	1.6	1.4	1.7	1.6	1.3
ENSG00000148303.16	RPL7A	1.6	1.3	1.4	1.5	1.3
ENSG00000164919.10.4	COX6C	2.4	1.7	1.7	1.4	1.5
ENSG00000163682.16.1	RPL9	4.5	2.0	2.6	2.8	6.5
ENSG00000113296.14	THBS4	10.9	11.8	6.6	5.5	17.5

Table 2| Constant genes. list of transcripts with a constant increased stability at all the time points in METTL14 overexpressed CHP212 cells. Fold-changes were calculated between METTL14 and control normalized T>C conversion rates.

DISCUSSION

Neuroblastoma is a devastating tumour of early childhood that accounts for 15% of all paediatric deaths (Maris, 2010). NB derives from a transient population of embryonic cells, the Neural Crest cells committed to the establishment of the sympathoadrenal lineage, as demonstrated from the anatomical localization of primary tumours (all along the sympathoadrenal chain, specifically in the adrenal medulla or in the paraspinal sympathetic ganglia of the abdomen, chest or pelvis), and the expression of specific markers and developmental pathways (Maris, 2007). However, the exact alterations governing NB initiation are still unclear since the major oncogenic pathways regulating adult tumorigeneses, such as TP53, CDKN2A or *Ras* mutation, are not deregulated in NB except for MYCN in a subset of primary tumours (Maris, 2007). Only a few somatic mutations that contribute to NB development have been added to our knowledge in the past years: *ALK* mutations, polymorphic alleles within the *LIN28B* locus, alteration in *ATRX* or *TERT* promoter rearrangements, all of them accounting only for a small percentage of the disease. Conversely, NB shows a very extreme genetic landscape characterized by genomic rearrangements, copy number alterations (CNAs) and chromosomal gain or losses. This property makes a quantitative rather than a qualitative imbalance in the transcriptome crucial for NB aggressiveness. Neuroblastoma, like all childhood malignancies, has other unique peculiarities. Among them, there is precursor hyperplasia that tends to undergo spontaneous regression and cell death, a characteristic that is expressed in the ability of 4S tumour to revert without any treatment. The embryonic derivation of NB, the lack of somatic mutations and its conceivable reversible nature, led us to hypothesize a role for the N6-methyladenosine (m6A) modification in NB tumorigenesis. In the past decade, a prolific body of literature has been generated regarding the role of the m6A modification in tumour initiation and progression. Controversially associated with both tumour-suppressing and oncogenic function in some tumours (i.e. glioblastoma and hepatocellular carcinoma), the m6A is generally reported to promote tumorigenesis in the majority of adult solid and liquid tumours, despite the absence of studies about the role of the modification in other paediatric tumours (such as rhabdomyosarcoma, medulloblastoma or retinoblastoma). Another growing portion of

the m6A field indicates that the modification modulates both pluripotency and cellular differentiation, although different studies showed discrepant results. In 2014, Wang and colleagues showed that *Mettl3* or *Mettl14* knockout in mouse Embryonic Stem Cells (ESCs) resulted in a decreased expression of pluripotent genes and a reduced self-renewal capability, thus identified the m6A as crucial for keeping ESCs in a pluripotent state. More recent models hypothesize that the m6A is more required for the transition of ESCs to different lineages (Batista *et al*., 2014; Geula *et al*., 2015). In any case, the m6A modification adds a new layer of complexity to our understanding of the molecular events defining the state and identity of ESCs (Aguilo *et al*., 2015).

We first verified the expression of all m6A regulators ("writers", "erasers" and "readers") in a dataset of 409 NB patients, noticing that the methyltransferase *METTL14* and the demethylase *ALKBH5* were aberrantly expressed in stage 4 NB, representing the high-risk group of patients. Specifically, METTL14 expression resulted significantly higher compared to low-risks cases and associated with a poor prognosis, as the lower expression of *ALKBH5*. Interestingly, METTL14 and ALKBH5 counterparts –the catalytically active methyltransferase METTL3 and the other demethylase FTO- did not show significant alteration over the progression of the tumour. NB also shows one of the highest and lowest expression of *METTL14* and *ALKBH5,* respectively, compared to other solid and liquid tumours that also reflected their expression in human Neural Crest. We evaluated how *METTL14* and *ALKBH5* would impact on NB by altering them in cell lines. We screened a panel of 14 commercially available NB cell lines for the expression of *METTL14* and *ALKBH5*, along with others m6A regulators; the almost complete absence of *ALKBH5* mRNA and protein suggested a significant role for reduced levels of methylation in NB. Indeed, when we overexpressed *ALKBH5* in CHP-212 cell line (MYCN-amplified), we witnessed a reduction in proliferation and impairment of cell ability to invade and an increase in apoptosis. The same phenotype was observed upon CRISPR/Cas9-mediated *METTL14* knockdown, suggesting that a global m6A reduction generates an amelioration of the tumorigenic phenotype. Coherently, increasing level of m6A (due to the overexpression of *METTL14*) positively impact on tumour aggressiveness. Subcutaneously injection of *METTL14* or *ALKBH5*-overexpressing CHP-

212 cells in recipient nude mice produced even stronger phenotypes. *METTL14*-overexpressing cells showed a very rapid growth rate that led to large tumours formation, while *ALKBH5* cells failed to form proper masses in all the individuals (n=6); moreover, in 2 out 6 mice the fluorescent signal coming from the cells eventually disappeared. We also verified the effect of *ALKBH5* restoration in SK-N-AS cells. When we induced ALKBH5 expression with doxycycline-enriched food, we observed a dramatic arrest in tumour growth due to massive apoptosis as demonstrated by immunofluorescence in tumour cryo-slices.

These phenotypic assays pointed to *METTL14* and *ALKBH5* as potential new oncogene and tumour suppressor, respectively, in NB tumour. Interestingly, in 2005 Hienonen and colleagues reported a case-study of a Finnish girl diagnosed with neuroblastoma and Smith-Magenis syndrome (SMS), a psychomotor retardation/multiple congenital anomaly; the genetic analysis unveiled a 17p11.2 germline mutation, where *ALKBH5* gene is located.

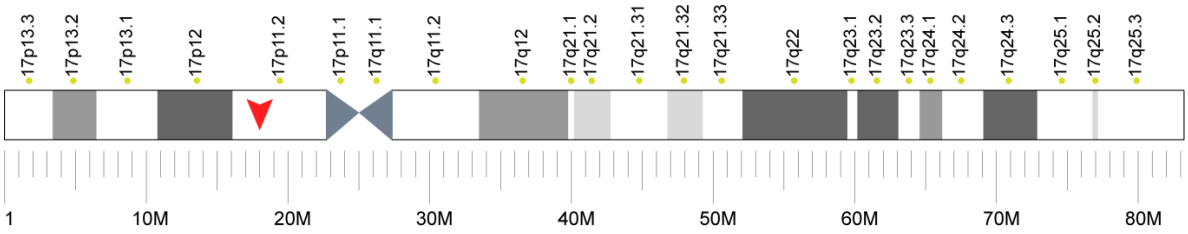

Figure 36| *ALKBH5* locus. ALKBH5 gene is located on the 17p11.2 human chromosome, starting at 18,183,078 bp and finishing at 18,209,954 bp.

Published way before the renewed scientific interest in post-transcriptional modification, the authors identified the ENSG00000091542.1 gene as an alanine-rich/type I antifreeze protein instead of *ALKBH5*. In this light, *ALKBH5* might act as a potent tumour suppressor in neuroblastoma in being not only necessary but also sufficient to tumour initiation. The fact that *ALKBH5* expression is almost null in all NB cell line, regardless of their MYCN status, reinforces this hypothesis. Preliminary data show that *ALKBH5* promoter expression is epigenetically silenced by NB cells (**Figure 37A**).

Treating several NB cell line (SK-N-BE(2), SK-N-AS, CHP-212 and CHP-134) with 5-azacytidine, an inhibitor of DNA methyltransferase (DNMTs) thus an inhibitor of DNA methylation, led to a significant increase in *ALKBH5* RNA and protein expression (**Figure 37B,C**). Whether the effect is specific toward *ALKBH5* promoter or is the product of the aspecific DNA demethylation need however further clarification, for example, using methylation-specific PCR (MS-PCR). Nonetheless, it has been demonstrated that m6A modifiers might be regulated by chromatin state alteration. For instance, during leukemogenesis in AML, KDM4C regulates *ALKBH5* expression via increasing chromatin accessibility of ALKBH5 locus, by reducing H3K9me3 levels and promoting the recruitment of PolII. Therefore, a similar -but the opposite- mechanism it is conceivable in NB tumour for keeping ALKBH5 expression low (Wang, 2020).

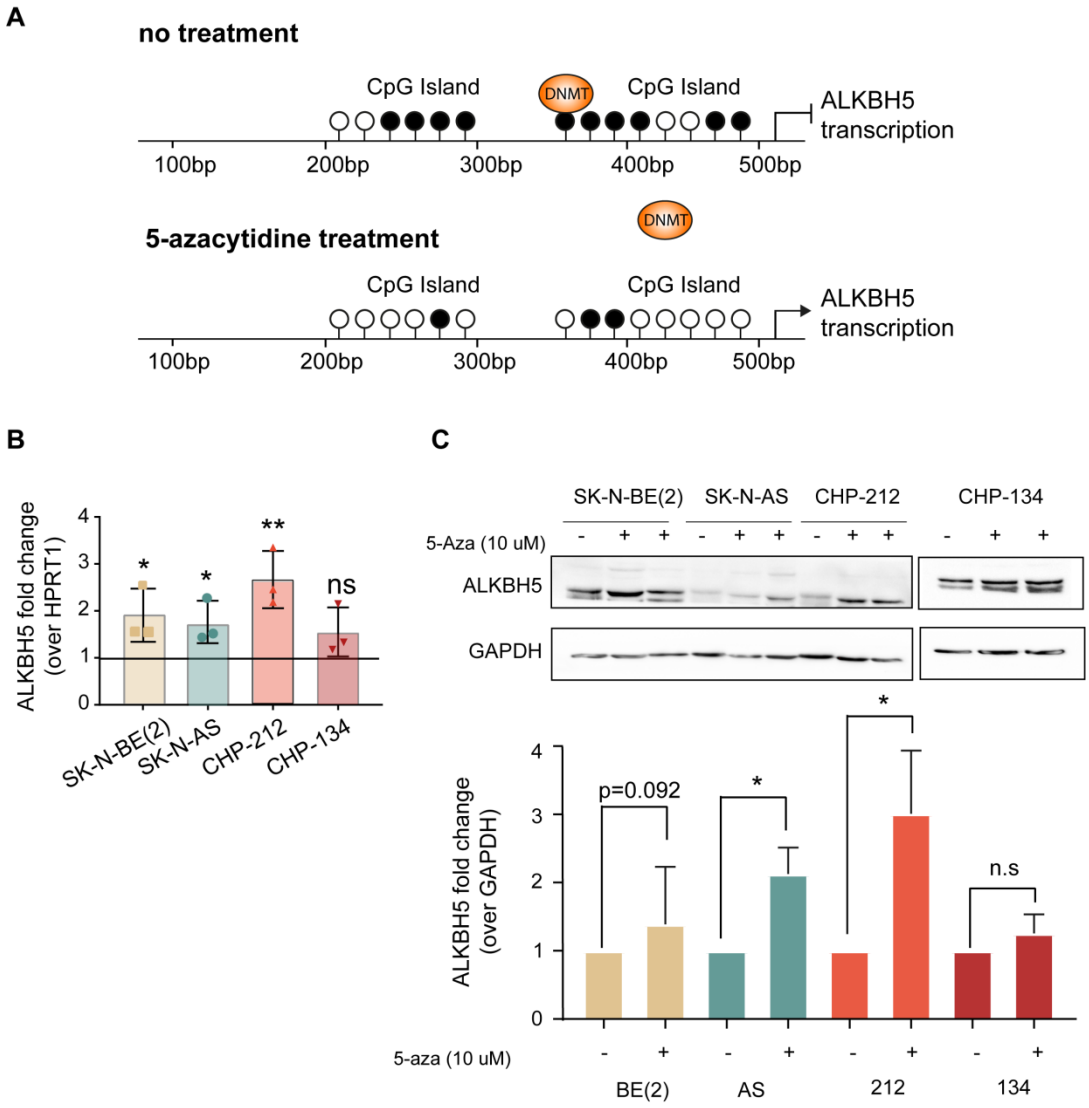

Figure 37|ALKBH5 is epigenetically silenced in NB cell lines. (A) Schematics of ALKBH5 promoter and the effect produced by 5-azacytidine treatment. **(B)** ALKBH5 mRNA expression in SK-N-BE(2), SK-N-AS, CHP-212 and CHP-134 NB cell lines upon 5-azacytidine treatment compared to the respective untreated cells. Fold change normalized on HPRT1. means ± SD of n = 2 independent experiments. **p<0.01. ns, not significant. **(C)** Upper panel, Western Blot of ALKBH5 protein expression in SK-N-BE(2), SK-N-AS, CHP-212 and CHP-134 NB cell lines treated with 10 μM of 5-azacytidine. Bottom panel, ALKBH5 protein quantification upon 5-azacytidine treatment normalized on GAPDH (loading control) and compared to untreated cells.

ALKBH5 and *METTL14* exert their effect on neuroblastoma aggressiveness by affecting NB transcripts at two different levels: translation and stability. *ALKBH5* has significant influences on RNA translation. Among the DEGs in the *ALKBH5*-overexpression condition, we found several genes related to apoptosis, such as *PERP*, *APOL6*, *MTCH1*, *TSFM* and *STAT6*. While *PERP* is associated to p53-induced apoptosis, *APOL6* , *MTCH1* and *TSFM* are related to the mitochondria-induced one, suggesting that *ALKBH5* could initiate cellular apoptosis "whatever it takes". It is also intriguing to speculate that *ALKBH5* might re-activate some programmes regulating cell death throughout embryonic development *in utero* and that are lost during neuroblastoma initiation. The main genetic abnormalities that drive NB formation (such as *MYCN* amplification or *ALK* constitutive activation) are well-known suppressor of apoptosis and differentiation to favour rapid cell proliferation. Indeed, tumour cell elimination via activation of different apoptotic pathway is widely accepted as a successful technique for NB treatment (Patterson, 2011; Bresler, 2014 and Delbridge, 2015) although sometimes associated with a modest efficiency and side effects so as the most common strategies used in NB therapy. The 5-years overall survival probability of high-risk patients has been estimated at 29% (Pinto, 2005) despite an aggressive therapeutic approach that includes radiotherapy and myeloablative chemotherapy. Regardless of the introduction of more effective therapeutic solutions as immunotherapy with a chimeric monoclonal antibody against the GD2 ganglioside in conjunction with cytokine and isotretinoin (Park, 2013; Sait and Modak, 2017) still up to 20% of high-risk patients are refractory to

treatments and 60% experience relapses (Cole and Maris, 2012). In this regard, targeting m6A regulators might be used in combination with other therapies or alone for NB treatment.Conversely, *METTL14* regulates NB transcripts global stability, as assessed by the SLAMseq analysis. Among the most affected transcripts we observed a specific enrichment in mRNA processing-related genes (such as SNRPD1 or SRRM1 both involved in splicing). *METTL14* transcripts stability effect on NB progression appear less obvious, although the importance of alternative splicing is reported to be relevant in neuroblastoma progression. Zhang and colleagues demonstrated that MYCN controls global splicing in MYCN-amplified NB tumours, by binding the promoter regions of the splicing factors *PTBP1* and *HNRNPA1*, while Chen and colleagues identified *de novo* intronic splicing motifs that can be mutated thus influencing the splicing pattern of genes that contribute to NB progression.

CONCLUSION

Collectively, our data identify METTL14 as a novel oncogene and, importantly, ALKBH5 as a potent tumour suppressor in neuroblastoma, and the m6A modification as a crucial regulator of NB progression. Therefore we propose the m6A, and genes belonging to its machinery, as novel candidates for therapeutic intervention. Targeting m6A regulators has become an attractive field, and numerous efforts have been made in cancer therapy, lately. For instance, FTO inhibitors R-2-hydroxyglutarate (R-2HG), MO-I-500 and Meclofenamic Acid (MA) exhibit antitumor activity in AML cells (Su, 2018), triple-negative breast cancer cell line (Singh, 2016) and GBM (Cui, 2017), respectively. Moreover, piperidine and piperazine rings of small ligands can enhance METTL3-14-WTAP complex (Selberg, 2019). Nothing has been done for targeting m6A readers, so far. In collaboration with the Laboratory of Genomic Screening of Professor Alessandro Provenzani, we present an encouraging proof-of-concept of YTHDF1 as a possible pharmacological target. We speculate that YTHDF1 might exacerbate the oncogenic potential of the m6A, since coupled YTHDF1 and METTL14 high expression identify high-risk patients with the worst prognosis, even compared to METTL14 high expression alone (**Figure 38A**). Indeed, YTHDF1 overexpression enhances proliferation, tumour-sphere forming ability and invasiveness of two NB cell lines (SK-N-BE(2) and SK-N-AS) (**Figure 38B-F**). Moreover, we thought that targeting the methyltransferase complex or the demethylase might lead to general and nonspecific demethylation resulting in more severe side effects compared to targeting a reader protein that is the real mediator of the biological effect of the modification. An HTS screening of 2000 FDA-approved drugs allowed the repurposing of the small molecule Ebselen which interacts with the YTH domain through a covalent bond, increasing the occupancy of the domain and thus interfering with the interaction of its natural ligands, the m6A.

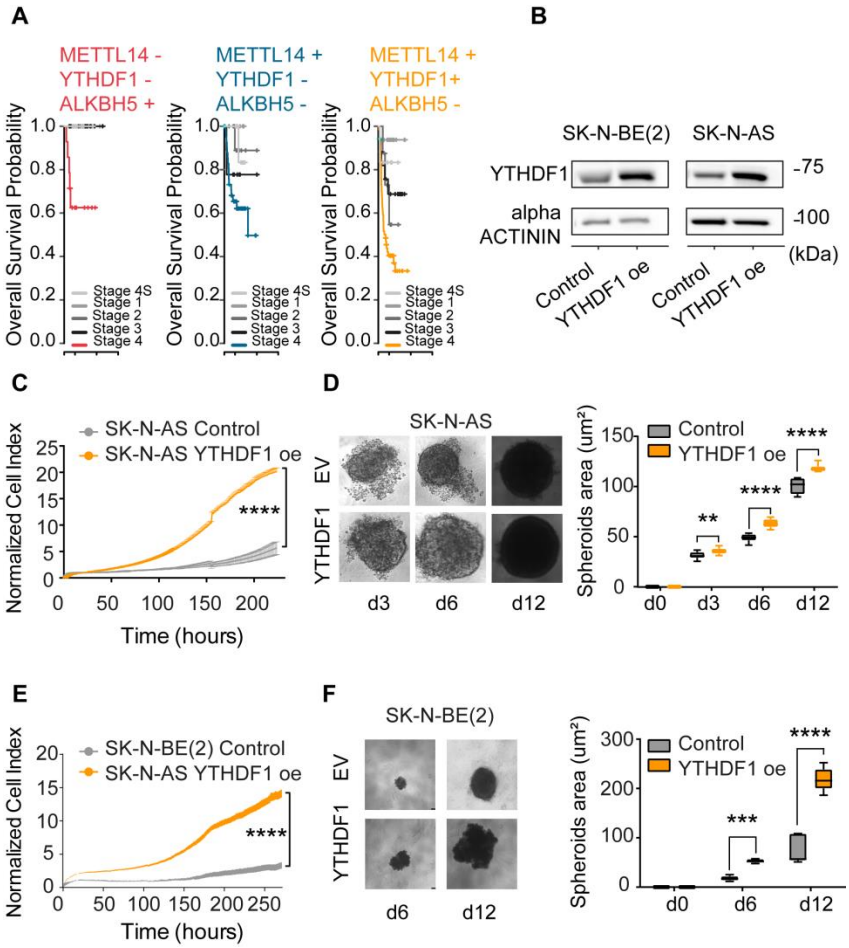

Figure 38| YTHDF1 is a promising pharmacological target for neuroblastoma. (A) Overall survival (OS) probability of neuroblastoma patients with high expression of ALKBH5, METTL14 or METTL14 and YTHDF1 according to disease stage. **(B)** Representative western blotting of YTHDF1 and alpha-ACTININ (loading control) of SK-N-AS and SK-N-BE(2) cells, transduced with either control (empty vector) or YTHDF1 (YTHDF1 oe) lentiviral vectors. **(C)** Proliferation of SK-N-AS cells transduced with either control or YTHDF1 lentiviral vectors monitored real-time by the RTCA (xCELLigence) and reported as normalized cell index; means ± SD of n=3 independent experiments consisting of n=4 technical replicates. ****p<0.0001, two-tailed Student's t test. **(D)** Left, Representative image of SK-N-AS control or YTHDF1-overexpressing spheroids acquired 3, 6 and 12 days post-seeding. Right, quantification of spheroids area at 3, 6 and 12 days post-seeding. means ± SD of n=3 independent experiments consisting of n=20 technical replicates. ***p<0.001, ****p<0.0001, two-tailed Student's t test. **(E)** Proliferation of SK-N-BE(2) cells transduced with either control or YTHDF1 lentiviral vectors monitored real-time by the RTCA (xCELLigence) and reported as normalized cell index; means ± SD of n=3 independent experiments consisting of n=4 technical replicates. ****p<0.0001, two-tailed Student's t test. **(F)** Left, Representative image of SK-N-BE(2) control or YTHDF1-overexpressing spheroids acquired 6 and 12 days post-seeding. Right, quantification of spheroids area at 6 and 12 days post-seeding. means ± SD of n=3 independent experiments consisting of n=20 technical replicates. ***p<0.001, ****p<0.0001, two-tailed Student's t test.

ONGOING WORK & FUTURE PERSPECTIVE

1. Generation of transgenic mice to study NB *in vivo*

In the past decades, several genetically engineered mouse models (GEMMs) have been developed for modelling NB. GEMMs can recapitulate the histopathology of the tumour and thus, they are central for understanding tumour progression and metastasis. The most common GEM models of high-risk neuroblastoma are enlisted in **Table 3.**

GEMM	Aberration	Incidence	Tumour latency	Reference
Th-*MYCN*	*MYCN* amplification	5-100%	4-7 weeks	Weiss, 1997
LSL-*MYCN*;Dbh-iCre	*MYCN* amplification	>75%	80 days	Althoff, 2015
Dbh-iCre/CAG-LSL-*ALK*^{F1174L}	*ALK* mutation	<50%	130-351 days	Heukamp,2012
Dbh-iCre/CAG-LSL-*Lin28b*	*LIN28B* overexpression	25%	56 days	Molenaar, 2012

Table 3 | Genetically engineered mouse models of high-risk neuroblastoma. (*Adapted from Kamili A., Cancer and Metastasis Review, 2020*)

To study the contribution of the m6A modification during tumour initiation and progression *in vivo*, I used four different combinations of genotypes that should cause NB in mice. I crossed Phox2b-Cre or Th-Cre mice with LSL-*MYCN* or LSL-*LIN28B* mice. The paired-like homeobox 2b (Phox2b) and the tyrosine hydroxylase (Th) are promoters that activate during sympathoadrenal lineage commitment and differentiation. LSL-*MYCN* and LSL-*LIN28B* are knockin humanized lox-stop-lox mice, meaning that they harbour the human sequence of *MYCN* and *LIN28B* oncogenes flanked by loxP sequences. Cre transcription and activation cause the elimination of the transcriptional stop sequence of *MYCN* and *LIN28B* oncogenes, thus activating and restricting their expression within the sympathoadrenal lineage (**Figure 39A**).

I crossed either double transgenic Th-Cre;LSL-*MYCN*, Th-Cre;LSL-*LIN28B*, Phox2b-Cre;LSL-*MYCN* or Phox2b-Cre;LSL-*LIN28B* mice with a conditional knockout (cKo) Alkbh5 mouse to generate a triple transgenic strain developing neuroblastoma in the presence of higher level of m6A modification (**Figure 39B**). For creating the Alkbh5 cKo

mouse, the genomic Alkbh5 locus was cloned, and LoxP sites were inserted between intron 1 and exon 1 so that Cre-mediated excision would disrupt the locus (Zheng, 2013).

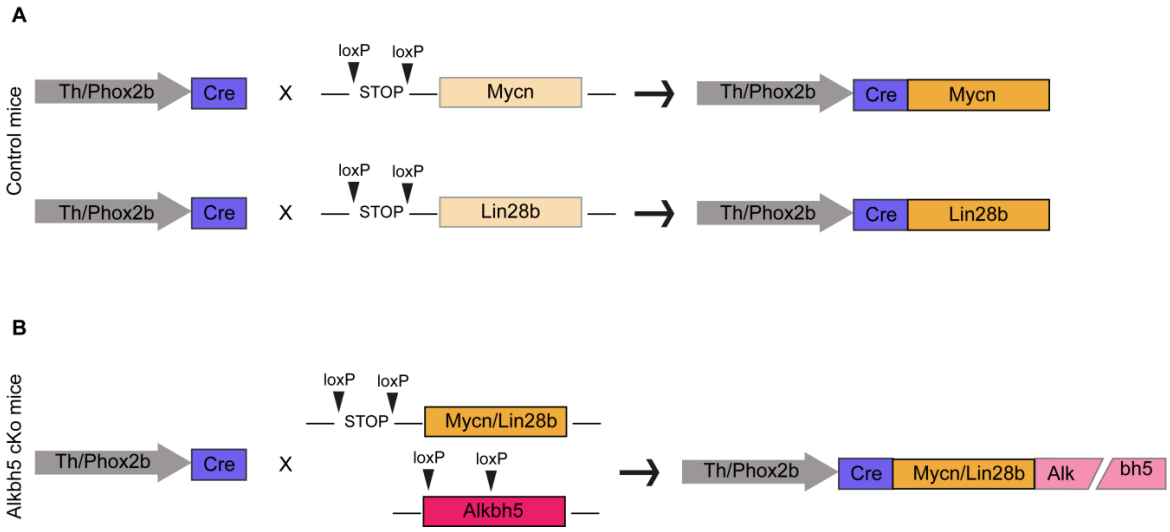

Figure 39| Generation of transgenic mice that develop neuroblastoma. (A) Generation of the double transgenic Control mice by crossing a Th-Cre(Phox2b-Cre) mouse with a LSL-*MYCN*(LSL-*LIN28B*) mouse. **(B)** Generation of the triple transgenic mouse by crossing Th-Cre(Phox2b-Cre) mouse with a double transgenic LSL-*MYCN*(LSL-*LIN28B*);Alkbh5-cKo individual.

Neuroblastoma initiation and progression can be followed thanks to the presence of the IRES-Luciferase sequence in the same transgene vector which produces a bioluminescent signal in the presence of its substrate luciferin (**Figure 4.4**). I intraperitoneally (IP) injected Control or Alkbh5 cKo mice with 200 µl of 15 mg/mL luciferin (pH 7) every two weeks for double transgenic mice and every week for triple transgenic mice.

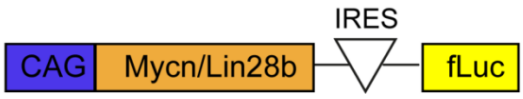

Figure 40| Schematic of the CAG-LSL-MYCN/LIN28B transgene

All the experimental groups will be followed for seven months to calculate tumour incidence and latency for the different combinations of genotype. Moreover, to authenticate the correctness of the genetic models, the expression of the oncogenes *MYCN* and *LIN28b* and the expression of *Alkbh5* will be verify, along with specific NB markers (such as Th and Dbh) in resected tumours. Based on our data, we expected that *Alkbh5*

cKo in the sympathoadrenal lineage, so higher level of m6A would increase tumour incidence and decreased its latency along with mice survival, associating with a more aggressive phenotype.

I followed the first set of individuals for each genotype: 17 for Th-Cre;LSL-MYCN genotype, 13 for the Th-Cre;LSL-LIN288, 4 for the triple transgenic Th-Cre;LSL-MYCN;FloxAlkbh5, 13 for the Phox2b-Cre;MYCN, 22 for the Phox2b-Cre;LIN28B and 14 for the triple transgenic Phox2b-Cre;LSL-MYCN;floxAlkbh5 (as enlisted in **Figure 41A**). Unfortunately, neither of the six genotypes have generated tumours. **Figure 41B** shows a representative necropsy of a mice where the absence of masses in the adrenal glands and the abdomen is indicated (white arrows and dashed lines) when compared to **Figure 41B'** from Molenaar *et al.*, (2012) depicting the proper formation and localization of tumour masses. The fact that the matings have been planned to have all the transgenes in the hemyzygous form might explain the lack of tumour formation. Likely, the monoallelic expression of the oncogene (either MYCN or LIN28B) is not sufficient to trigger the transformation of the cells, since the PCR validating the removal of the transcriptional termination site of the MYCN and LIN28b alleles (black arrows and dashed lines), demonstrates the proper activation of the Cre recombinase (**Figure 41C**). Indeed, LSL-MYCN transgenic mice (lanes 2 and 3) show a ~ 800 bp band that is absent in the adrenal gland of a control mouse (C56BL6 - lane 1), LSL-LIN28B transgenic mice (lanes 4 to 6) and the ear (epithelial tissue) of a second control mouse (lane 7). Conversely, LSL-LIN28B mice (lanes 12 to 14) show a ~300 bp band that is absent in the adrenal gland of MYCN-LSL transgenic mice, control C57BL6 mouse and in the epithelial tissue. To overcome this problem, I'm now mating mice to obtain homozygous individuals for each transgene.

A

Genotype	Total individuals	Tumour
Th-Cre;LSL-MYCN	17	0
Th-Cre;LSL-LIN28B	13	0
Th-Cre;LSL-MYCN;floxAlkbh5	4	0
Phox2b-Cre;LSL-MYCN	13	0
Phox2b-Cre;LSL-LIN28B	22	0
Phox2b-Cre;LSL-MYCN;floxAlkbh5	14	0

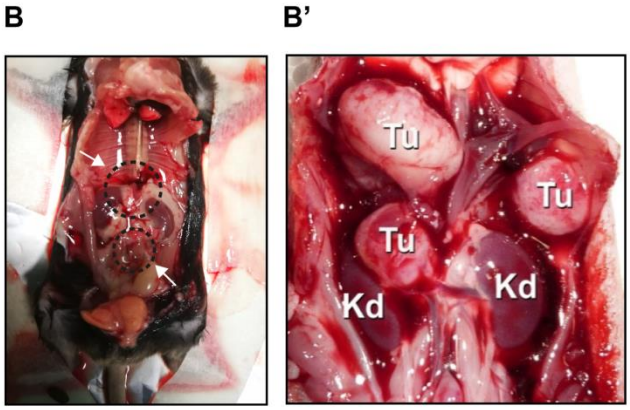

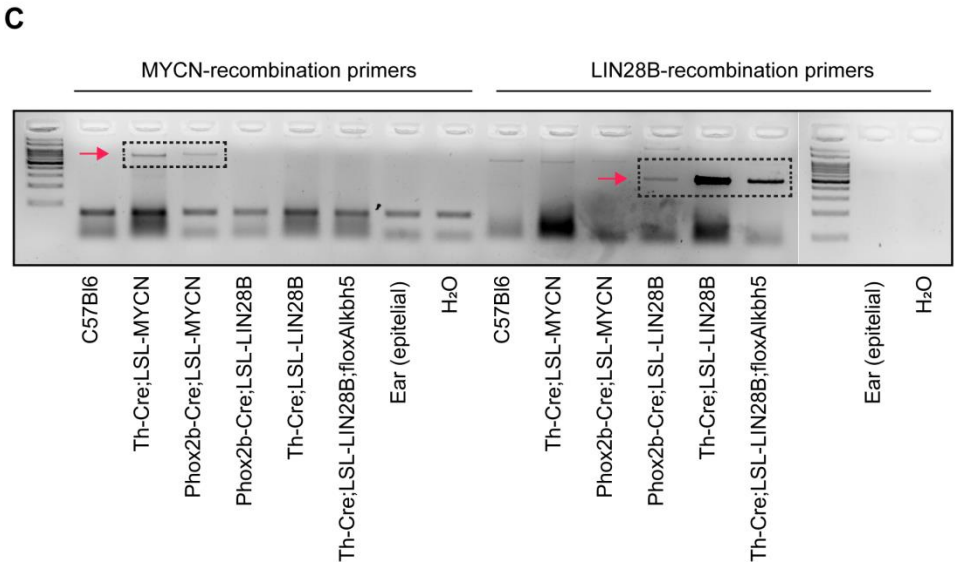

Figure 41| **(A)** Number of individuals and developed tumour in neuroblastoma mice models. **(B)** Representative necropsy of an in-house neuroblastoma mouse models. Arrows and dashed lines indicate the lack of tumour masses in the specific location of the neuroblastoma tumour. **(B')** Representative necropsy of a neuroblastoma mouse models showing the proper formation and localization of masses. (*From Molenaar et al., Nature Genetics, 2012*). **(C)** PCR confirming the removal of the transcriptional termination site of the MYCN and LIN28b alleles.

2. Methylation iCLIP (miCLIP) analysis

To investigate methylated targets that contributed to the phenotype in NB cells, I'm performing an m6A mapping in METTL14- and ALKBH5 overexpressing cells. The current m6A-mapping approaches involve the immunoprecipitation of RNA fragments with anti-m6A antibodies, even though antibody-free methods have been developed in the past few years to avoid several issues, like cross-reactivity to other modifications, high input RNA requirement, reproducibility or batch effect.

The miCLIP technique comprises the RNA-antibody UV-crosslinking that generates truncations or mutations, depending on the antibody that is used. Specifically, I used the Abcam antibody (ab151230) that induces a nucleotide substitution at the invariant cytosine residue adjacent to the m6A as well as at the m6A itself (Linder, 2015).

MiCLIP analysis was performed on CHP-212 Control, ALKBH5- or METTL14-overexpressing cells in biological triplicate. I purified total RNA and enriched for Poly(A) RNA using the Dynabeads Oligo (dT)25 kit (Invitrogen) (**Figure 42A**). Poly(A)+ RNA was fragmented, immunoprecipitated and UV-crosslinked twice with 0.3 J cm-2 UV light at 254 nm in a Stratalinker. After a step of 3'-end RNA dephosphorylation, adaptor ligation and removal, the m6A-RNA complex was run on a 4-12% NuPage Bis-Tris gel and transferred on a nitrocellulose membrane. Antibody-RNA-L3-IR adaptor complexes were visualized at the Li-Cor Odyssey® imaging system (Bioscience) (**Figure 42B**) to allow cutting of the samples. Samples were then purified from the membrane, retrotranscribed, and a test PCR was performed to choose the proper number of cycles. In **Figure 42C,** it is possible to observe the presence of a ~ 150 bp artefact generated by the P3/P5 Solexa primers, while sample 9 represent the excision range for subsequent cDNA purification.

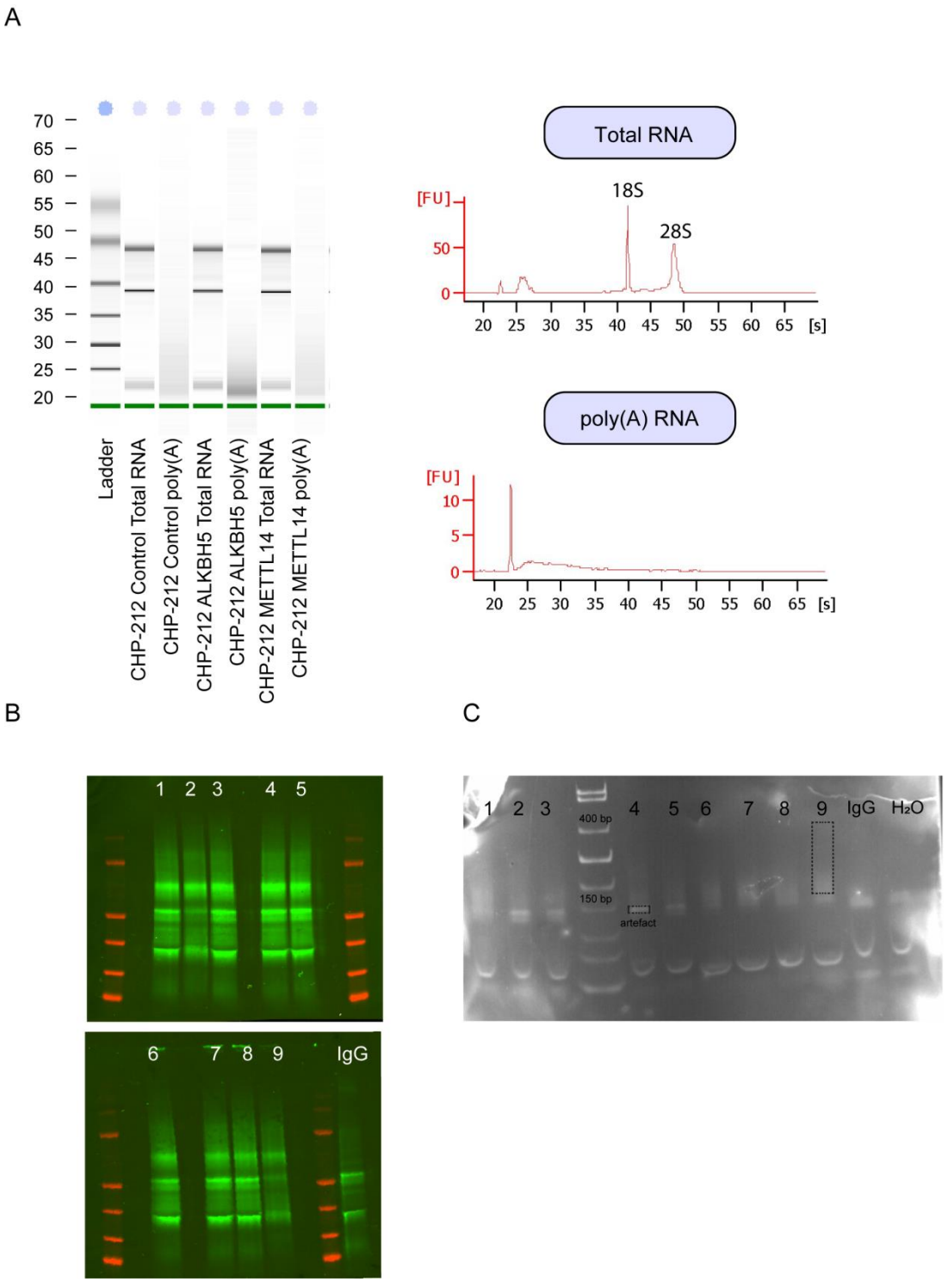

Figure 42| miCLIP analysis. (A) Representative quality control check of Poly(A)+ RNA compared to Total RNA isolated from corresponding samples. **(B)** Li-Cor images of miCLIP samples after nitrocellulose transfer. **(C)** 22 cycles **t**est PCR of miCLIP samples after retro-transcription and cDNA purification.

EXERIMENTAL PROCEDURE

1. Cell culture

Human neuroblastoma cells were cultured as adherent monolayers in cell culture-treated polystyrene surfaces and grown in incubators under standard conditions (37°C, 95% humidity, 5% CO2). All cell lines (listed in **TABLE 2**) were routinely checked for the absence of mycoplasma.

All cell lines were purchased from either ATCC (American Type Culture Collection), ECACC (The European Collection of Authenticated Cell Cultures) or DSMZ (Deutsche Sammlung von Mikroorganismen und Zellkulturen). Human STA-NB-1 and STA-NB-7 neuroblastoma cell lines were a kind gift from Dr. of the Children's Cancer Research Institute of Wien.

TABLE 2 | EXPERIMENTAL MODELS: CELL LINES		
Human: CHP-212 Neuroblastoma cell line	ATCC™	CRL-2273
Human: CHP-134 Neuroblastoma cell line	ECACC	Cat No. 06122002
Human: SK-N-AS Neuroblastoma cell line	ECACC	Cat.No. 94092302
Human: SK-N-BE(2) Neuroblastoma cell line	ECACC	Cat. No. 95011815
Human: STA-NB-1 Neuroblastoma cell line	Children's Cancer Research Institute (Wien)	N/A
Human: MHH-NB-11 Neuroblastoma cell line	DSMZ	ACC 157 LOT3
Human: SIMA Neuroblastoma cell line	DSMZ	ACC 164 LOT4
Human: STA-NB-7 Neuroblastoma cell line	Children's Cancer Research Institute (Wien)	N/A

Human: SK-N-DZ Neuroblastoma cell line	ECACC	Cat. No. 94092305
Human: KELLY Neuroblastoma cell line	ECACC	Cat. No. 92110411
Human: LAN-1 Neuroblastoma cell line	ECACC	Cat. No. 06041201
Human: IMR-32 Neuroblastoma cell line	ECACC	Cat. No. 86041809
Human: SK-N-SH Neuroblastoma cell line	ECACC	Cat. No. 86012802
Human: NB-69 Neuroblastoma cell line	ECACC	Cat. No. 99072802
Human: HEK293T		

Initially, all cell lines were tested for the expression of m^6A crucial regulators. SK-N-AS, SK-N-BE(2), CHP-212 and CHP-134 cell lines were finally chosen for the further experimental procedures.

SK-N-AS (ECACC, 94092302) and SK-N-BE(2) (ECACC, 95011815) were cultured in Dulbecco's Modified Eagle Medium (DMEM, Corning, 15-017-CVR) supplemented with 10% FBS (Corning, 35-079-CV), 1% L-Glutamine (Corning, 25-005-CI), 1% Penicillin/Streptomycin (Gibco, 15140-122).

CHP-212 (ATCC, CRL-2273) cell line was cultured in 1:1 ratio of Minimum Essential Medium (MEM, Gibco,11095-080) and Ham's F12 (Euroclone, ECB7302L) supplemented with 10% FBS (Corning, 35-079-CV), 1% L-Glutamine (Corning, 25-005-CI) 1% Penicillin/Streptomycin (Gibco, 15140-122),1% Non-essential Aminoacids (Euroclone, ECB3064D).

CHP-134 (ECACC 06122002) cell line was cultured in RPMI-1640 (ThermoFisher Scientific, 31870) supplemented with 10% FBS (Corning, 35-079-CV), 1% L-Glutamine (Corning, 25-005-CI) and 1% Penicillin/Streptomycin (Gibco, 15140-122).

2. Plasmid generation

All recombinant plasmids were generated using Gateway™ Technology (ThermoFisher Scientific) according to the manufacturer's instructions.

METTL14 (NC_000004.12), *ALKBH5* (NC_000017.11) and *YTHDF1* (NC_000020.11) human genes were subcloned into a pENTR1A no ccDB entry vector (Addgene, w48-1) and recombined into a third-generation pLenti CMV Puro DEST (w118-1) (Addgene, #17452) to perform overexpression experiments. *ALKBH5* and *YTHDF1* genes were additionally recombined into a third-generation inducible lentiviral pCW57.1 all-in-one plasmid (Addgene, #41393) and into a third-generation lentiCRISPR v2 (Addgene, #52961) to allow the CRISPR/Cas9 mediated knockout, respectively.

sgRNAs were cloned in the respective backbone following Zhang lab general protocol. Briefly, two oligos in the form of

5′ – CACCGNNNNNNNNNNNNNNNNNN – 3′

3′ – CNNNNNNNNNNNNNNNNNNNCAAA – 5′

were designed for ach sgRNA. The oligos were phosphorilated, annealed and cloned into a *BbsI* digested backbone and the final ligated plasmid were transformed into Stbl3 competent cells.

pENTR1A no ccDB (w48-1) and pLenti CMV Puro DEST (w118-1) were a gift from Eric Campeau & Paul Kaufman to Addgene (Campeau, 2009). The px330-U6-Chimeric_BB-CBh-hSpCas9 and the lentiCRISPR v2 were a gift from Feng Zhang.

3. Lentiviral particle production

Lentiviral particles were prepared in HEK293T cells. Briefly, HEK293T cell were transfected with a mix containing the pMD2.G envelope plasmid (Addgene, #12259), the pCMV deltaR8.2 packaging plasmid (Addgene, #12263) and the transfer vector in a 1:2:4 ratio. 48h post-transfection, HEK293T supernatant was collected, filtered in a 0.45 **μ**m filter and ultracentrifuged for 2h at 90′000 g.

4. CRISPR-mediated deletion

For CRISPR-mediated deletion of *METTL14*, SK-N-AS cells were transduced with px330-U6-Chimeric_BB-CBh-hSpCas9 (Addgene, #42230) (Zhang, 2013) expressing either one out of three sgRNAs targeting METTL14 (sgRNA#1, sgRNA#2 and sgRNA#3) or control pSpCas9(BB)-2A-GFP (px458) empty vector (Addgene, #48138) (Zhang, 2013). sgRNAs were chosen for the highest score and fewest predicted off-target sites, designed according to Zhang's website (http://genome-engineering.org). The sequences of sgRNAs were:

#1: CACCGAACATGGATAGCCGCTTGC;

#2: CACCGATAGCCGCTTGCAGGAGATC

#3: CACCGTAACACGGCACCAATGCTGT.

2 days after sgRNAs transfection, cells were selected with 1μg/mL puromycin for 48h.

CHP-212 and CHP-134 cells were transduced with lentiCRISPR v2 expressing sgRNAs targeting YTHDF1 or control lentiCRISPR v2 empty vector. YTHDF1-targeting sgRNAs were designed as previously described. The sequences are:

#2: 5'-CACCGCGCTACCTGGGTGTCCACGC-3'

#3: 5'-CACCGACTTTGAGCCCTACCTTAC-3'.

2 days after transduction, cells were selected with 1μg/mL puromycin for 5 to 7 days according to the cell line

5. Generation of genetically engineered neuroblastoma cell lines

Neuroblastoma cell lines were seeded 24h before transduction. For constitutive infection, the cells were incubated with concentrated lentiviral particle and 5mg/mL polybrene (Hexadimethrine bromide, M&C Gene Technology) in serum-free medium and kept at

37°C with 5% CO2 for 6h. Cultures were then replaced with complete medium and selected 48 h post-infection with 1 μg/mL puromycin.

For the transient knockout of *METTL14*, SK-N-AS cells were transfected with FuGENE® HD Transfection Reagent (Promega, E2311) following manufacturer's instruction. 48 h days after transfection, cells were selected with 1μg/mL puromycin for 2 days.

6. Protein extraction and immunoblot

Cells were lysed on ice in RIPA buffer (ThermoFisher Scientific) containing 25x protease inhibitor cocktail (Sigma-Aldrich). The lysates were incubated on ice for 30 min followed by centrifugation at 4°C for 15 minutes at 12.000 rpm, and the respective protein concentration was quantified with Bradford Reagent (SigmaAldrich, b6916). Proteins were separated through Sodium Dodecyl Sulphate - PolyAcrylamide Gel Electrophoresis (SDS-PAGE) and transferred to a nitrocellulose membrane (GE Healthcare). Membranes were blocked in TBS containing 5% non-fat milk (marca) and 0.1% Tween-20 at room temperature for 1 hour followed by incubation with primary antibodies overnight at 4°C (for the list of antibodies refer to **TABLE 3**). HRP-conjugated secondary antibody diluted in blocking solution was added to the membrane and incubated for 1 hour in agitation. For chemiluminescent signal development, the membrane was incubated in Amersham ECL Select Detection Reagent (Sigma), and images were acquired by high-resolution CCD imaging system Bio-Rad ChemiDoc XRS+ and analyzed through Bio-Rad Image Lab software.

**TABLE 3	LIST OF ANTIBODIES**		
Rabbit polyclonal anti-METTL14	Sigma-Aldrich	HPA038002	1:1000
Rabbit polyclonal anti-ALKBH5	Sigma-Aldrich	HPA007196	1:500
Rabbit polyclonal anti-YTHDF1	Proteintech	Cat.#17479-1-AP	1:1000
Rabbit polyclonal anti-YTHDF2	Proteintech	Cat.#24744-1-AP	1:1000

Mouse monoclonal anti-YTHDF3	Santa Cruz Biotechnology	SC377119	
Rabbit polyclonal anti-METTL3	ThermoFisher Scientific	Cat# 720347	
Mouse monoclonal anti-WTAP	Santa Cruz Biotechnology	SC3774280	
Rabbit polyclonal anti-FTO	CST	Cat# 14386S	
Rabbit polyclonal anti-KIAA1429	Bethyl	A300-648A	
Mouse monoclonal anti-ACTININ	Santa Cruz Biotechnology	SC17829	1:5000
Mouse monoclonal anti-GAPDH	Santa Cruz Biotechnology	SC32233	1:5000
Rabbit polyclonal anti-APOL6	Invitrogen	PA5-83068	1:1000
Rabbit polyclonal anti-PERP	Invitrogen	PA5-19980	1:1000
Rabbit polyclonal anti-MTCH2	Thermofisher	PA5-20696	1:1000
Rabbit monoclonal anti-TSFM	Abcam	Ab173528	1:1000
Mouse monoclonal anti-STAT6	Proteintech	66717-1-Ig	1:1000

7. RNA extraction, reverse transcription and quantitative real-time polymerase chain reaction

Total RNA was extracted using the RNeasy Plus Mini Kit (QIAgen, 74136) following manufacturer's instruction. Reverse transcription was performed on 500 or 1000 ng of starting material using RevertAid First Strand cDNA Synthesis Kit (ThermoFisher Scientific, K1622) on C1000 Thermal Cycler (BioRad). Quantitative real-time PCR was performed on 50 ng of cDNA with KAPA SYBR FAST qPCR Master Mix 2X (Kapa Biosystem) of CFX96™ Real-Time System (BioRad). All assays were performed in technical triplicate and in three independent experiments. Expression values were

analysed using the 2^{-ddCT} methods. All the primers were used at 400 nM concentration and are enlisted in **TABLE 4**.

**TABLE 4	LIST OF PRIMERS**
METTL14_Fw: 5′-AGTGCCGACAGCATTGGTG-3′
METTL14_Rev: 5′-GAGCAGAGGTATCATAGGAAGC-3′
ALKBH5_Fw: 5′-AGGGGAAGCGTGACTGTGC-3'
Primer for qPCR: ALKBH5_Rev: 5′-GGGTGCATCTAATCTTGTCTTCC-3'
Primer for qPCR: YTHDF1_Fw: 5′-
Primer for qPCR: YTHDF1_Rev: 5′-
Primer for qPCR: GAPDH_Fw: 5'-CAACGAATTTGGCTACAGCA-3'
GAPDH_Rev: 5'-GGGGTCTACATGGCAACGT-3'
HPRT1_Fw: 5'-TGACACTGGCAAAACAATGCA-3'
HPRT1_Rev: 5'-GGTCCTTTTCACCAGCAAGCT-3'
PERP_Fw: 5′-TGTGGTGGAAATGCTCCC-3′
PERP_Rev: 5′-TACCCCACGCGTACTCCA-3′
TSFM_Fw: 5′-TGCATACAGTAAAGAAAACTGGGA-3′
TSFM_Rev: 5′-GAACCCAGATGGCACCTTCA-3′
MTCH2_Fw: 5′-CAGTGAAACCGGCGGC-3′
MTCH2_Rev: 5′-AGGCTCATATCCCACCTGGA-3′
GPATCH8_Fw: 5′-CGTCGGGACTTCATTCGTTC-3′

GPATCH8_Rev: 5′-CTTCCTGTGCCAATGTTGCT-3′
STAT6_Fw: 5′-TTGGCAGTGGTTTGATGGTG-3′
STAT6_Rev: 5′-TGAAGCGGAGGAGAAAGGTT-3′
MYCNrecombinant_Fw: 5′-GCCCGCGGTGATGCCTTTGAGG-3′
MYCNrecombinant_Rev: 5′-CGGGGACTGGGCGGTGGAAC-3′
LIN28Brecombinant_Fw: 5′-CCCGCGGTGATGCCTTTGAGG-3′
LIN28Brecombinant_Rev: 5′-GGTTCGTCCTCTGCCAGCCCG-3′

8. M^{6}A quantification

m^{6}A methylation was quantified using Methylation Quantification Kit (Abcam, ab233488). Total RNA was isolated using the RNeasy Plus Universal Mini Kit (Qiagen) and mRNAs were prepared from total RNA using the GenElute Mammalian Genomic DNA Miniprep Kit Protocol (Sigma-Aldrich). mRNAs were spotted onto an 8-well Assay Strips with a binding solution and incubated with a capture and detection antibody. Samples were finally incubated with a developer and enhancer solution and the absorbance was read at the Tecan Infinite M200Pro spectrophotometer at 450 nm.

9. Real Time Cell Analysis proliferation assay

The proliferation ability of neuroblastoma cells was evaluated with the Real-Time Cell Analyzer (xCELLigence® RTCA DP Analyzer, Roche). The RTCA DP instrument uses non-invasive electrical impedance monitoring to quantify cell proliferation. 5000 cells were seeded in an E-16 Plate (Acea Bioscience Inc.) in four technical replicates and at least in three independent experiments. Cells impedance was evaluated every 15 minutes for 144 h with a replacement of culture medium 72 h after seeding. Cell Index values (CI) were acquired by the RTCA Software (V1.2) for subsequently normalization and analysis.

10. Flow cytometric analyses

DNA content of neuroblastoma cell lines was evaluated using the nucleic acid stain Propidium Iodide (Abcam) followed by flow cytometry analysis. Cells were harvested and fixed in 66% ethanol for 2 to 16 hours at 4°C and treated for 30 min at 37°C with 20x PI + 200x RNase. Propidium Iodide fluorescence intensity was collected on a flow cytometer and 488 nM laser excitation and data were analysed by FlowJo™ v10.6.1 software (FlowJo LLC).

Apoptosis was evaluated using the FITC Annexin V Apoptosis Detection Kit I (BD PharmingenTM). Cells were co-stained with FITC and Propidium Iodide in a 1X Binding Buffer and analysed by flow cytometry.

All the flow cytometric experiments were analyzed using FACS (BD FACSCanto II) and all the data were processed by BD FacsDIVA V8.0.1™ software

11. Spheroids formation and invasion assays

Neuroblastoma cells were grown as 3D-spheroids. 1000 cells were seeded in a 96-well Clear Round Bottom Ultra-Low Attachment Microplate (Corning®) in 200 μl of complete medium with 1% Cultrex® Reduced Growth Factor Basement Membrane Matrix, Type 2 (BME 2, Trevigen) and centrifuged at 4°C for 5 minutes at 1600 rpm. Pictures of each spheroid were acquired at four different time points (0, 3, 6 and 12 days post-seeding), and their dimension was evaluated with ImageJ software. Each independent experiment comprised 20 technical replicates for each condition.

At the end of the experiment, at least 7 spheroids were transferred in a standard 96-well plate. All the spheroids were embedded entirely in BME, and complete medium was used as chemoattractant. The invasion ability was evaluated every three days, and the area of invasiveness was calculated as previously described (Berens, 2015) with ImageJ software.

12. Methylation-iCLIP (miCLIP)

The methylation-iCLIP (miCLIP) protocol was used to analyzed m6A abundance and distribution in the transcriptome of engineered neuroblastoma cell lines, as previously described (Linder, 2015). Total RNA of cells was extracted with the RNeasy Plus Mini Kit (QIAgen). Poly(A)$^+$ RNA was purified from 75μg of total RNA using Dynabead Oligo(dT)25 kit (61002) and chemically fragmented with a fragmentation buffer (ThermoFisher Scientific). Poly(A)$^+$ RNA was subjected to m6A-immunoprecipitation using a rabbit polyclonal anti-m6A antibody (Abcam, ab151230) and rabbit IgG as control, and UV crosslinkinked. To isolate proper fragments, RNA was NuPAGE separated and transferred to a nitrocellulose membrane. The isolated RNA was ligated to a barcoded adaptor to enable multiplexing of samples. Reverse transcription was carried out using unique barcoded primers for each sample, and the respective cDNA was amplified and cleaned using AMPure XP beads (Beckman Coulter). QC analysis was carried out using Tapestation (Agilent) and QuantiFluor (Promega).

13. Polysome profile and isolation of total and polysomal RNA from fractions

Neuroblastoma cells were grown in 100 mm dish to 80% confluence and treated with 100 μg/mL cycloheximide (CHX) for 5 minutes before collection. Cells were lysed on ice and pelleted in a refrigerated centrifuge before loading the supernatant (~1 mL) on a 15-50% w/v fresh-prepared sucrose gradient.

The sucrose gradient is prepared in thin-wall, polyallomer ultracentrifuge tubes (Beckman, 331372). 5.5 mL of 50% sucrose solution were added to each tube, and the 15% sucrose solution were carefully overlaid drop-by-drop until the tube were filled. The tubes were finally placed in the gradient former (SEP, 118016).

Sample and gradients were centrifuged at 4°C for 1 h 40 min at 40’000 rpm (Optimal XE-100, rotor SW41Ti). Gradients were fractionated with a 160 gradient analyzer equipped with a UA-6 UV/VIS detector (Teledyne Isco) and, according to the profile, fractions were pooled to isolate in total and polysomal RNA with phenol/chloroform/isoamyl reagent for libraries preparation.

14. SLAMSeq analysis

The SLAMSeq analysis consists of a thiol-linked alkylation of RNA for time-resolving measurement of degradation kinetics. The protocol includes an initial optimization of the 4-thiouridine (S4U) labelling condition and measurement of global S4U uptake under experimental conditions.

Neuroblastoma cells were seeded in a 96-well plate 48 h before the experiment and were incubated with a dilution series of 4-Thiouridine (S4U)-containing media to determine the optimal concentration for kinetics experiments. Cell viability was evaluated at the designated time points (0, 1, 3, 6, 12 and 24 h of treatment) with the CellTiter-Glo® Luminescent Cell Viability Assay (Promega).

Cells were seeded again and treated with the appropriate IC10,ti concentration of 4SU. Total RNA was isolated under reducing condition and digested to single-nucleoside, and S4U uptake was then evaluated using HPLC analysis.

The final analysis of RNA degradation rates was performed as previously described by Herzog *et al*., 2017. Neuroblastoma cells were cultured with the appropriate 4-Thiouridine (S4U)-containing medium for 24h and then treated with a 100x excess of unlabelled Uridine (U). Cells were harvested at the time point of interests (0h, 1h, 3h, 6h, 12h and 24h) for RNA isolation by TRIzol in reducing conditions, followed by Iodoacetamide treatment and libraries preparation.

15. *In vivo* transplantation of neuroblastoma cells and tumor monitoring

All animal-related works were performed under the Ministero della Salute authorization n° 955/2017-PR for the evaluation of xenograft growth in nude mice and under the authorization n° 61/2020-PR for the evaluation of tumour growth in neuroblastoma transgenic mice models.

CHP-212 either METTL14 or ALKBH5 overexpressing- and SK-N-AS ALKBH5-inducible neuroblastoma cell lines were co-transduced with GFP-expressing lentiviral particle and

subcutaneously injected (15x106 for CHP-212 and 4x106 for SK-N-AS) into the right flank of 8-weeks old, age- and gender-matched Foxn1nu$^{-/-}$ mice.

Tumour development and progression were detected by fluorescence imaging using the preclinical optical/X-ray imaging In-Vivo Xtreme I (Bruker) every three days and resected 21 days post-injection or when the tumour has reached 1,5 cm^2 of diameter. Mice were anaesthetized with 2,5% isofluorane to allow the acquisition of a foreground (fluorescence signal) and a background image (X-ray).

Tumour development and progression in genetically engineered neuroblastoma mice model was detected as previously described. Mice were also intraperitoneally injected with 200 μL of 30 mg/mL luciferin and acquired for five minutes to obtain a foreground (bioluminescence signal) and a background signal (reflectance).

16. RNA-seq library preparation and run

RNA from total, polysome profiling (total and polysomal) and SLAMseq samples were subjected to Quant-seq mRNA 3′ end library preparation kit (Lexogen) according to the manufacturer's instructions. Unique Molecular Identifiers (UMIs) were introduced during the library preparation. The libraries were single-read sequenced, generating 100 bp reads, on an Illumina HiSeq 2500 machine.

17. RNA-seq basic data processing

Reads from the polysome profiling (total and polysomal) and SLAMseq RNA-seq were processed in the same way. Reads were quality checked with FASTQC (v0.11.4) (Andrews and Others, 2010). UMI tools (v0.5.5) (Smith, 2017) was used for UMIs removal and the subsequent reads de-duplication, Trim Galore (v0.6.0) (Krueger, 2012) for adapters removal and quality trimming and Cutadapt (v1.18) (Martin, 2011) for polyA trimming. Reads were aligned to the human genome (h38) with STAR (v2.5.2b) (Dobin, 2013) and quantified with HTSeq (v0.11.1) (Anders, 2015).

18. Polysome profiling data analysis

Differential gene expression in the Polysomal profiling dataset was calculated with tRanslatome v1.22.0 software (Tebaldi, 2014) configured to be used with edgeR (v3.28.0) (Robinson, 2010; McCarthy, 2012) allowing the parallel analysis of the transcriptome and translatome of METTL14- and ALKBH5- overexpressing cells compared to control. Gene counts were pre-filtered by keeping only genes with at least one read in each sample, and differentially expressed genes (0.05 BH adjusted p-value cut-off) were retrieved. The list of differentially expressed genes was split depending on whether they were significantly altered in expression in one of the two gene expression levels or both.

19. SLAMseq data analysis

Aligned and deduplicated BAM files were processed with SlamDunk (v0.3.4) (Neumann et al. 2019), recovering T>C conversions. SlamDunk was run with the *all* command. For mapping and SNPs calling, human genome assembly GRCh38.p12 (GENCODE v28) was used. T>C conversions per gene were counted with a 3′ UTR annotation BED file obtained using the extract–transcript–regions tool (Floor). The extracted 3′ UTR positions belonging to the same gene were merged with bedtools (v2.28.0) and mapped to their gene ID with bed map (v2.4.36). Additional SlamDunk parameters were set as *-5 0 -n 100 -rl 100 -t 16 -m -mv 0.2 -mbq 27* (Herzog, 2017; Matsushima, 2018 and Muhar, 2018). As a diagnostic analysis of the data, Spearman correlation coefficients were computed at each time point between the steady-state gene expression (all reads) or the T>C conversion containing reads and the steady-state expression at the chase onset (0h). For calculating RNA half-lives, T>C conversion rates were background subtracted (T>C conversions observed without S4U labelling, from RNAseq data of CHP-212 cells total RNA), and an expression threshold of 3 CPM was applied. Data were normalized to the chase onset (0 h), and transcripts with at least one zero in the time points were discarded. Transcripts half-lives were obtained by fitting an exponential decay curve on the six normalized time points values. Curve fitting was performed with minpack.lm (v1.2-1). Transcripts with half-lives values below zero were discarded and those with values above 24 hours were set to 24. Kolmogorov-Smirnov test was applied on the control, and the overexpressed replicates half-lives mean values and the exact p-value was computed. Two methods were applied to find transcripts with a significant stability alteration. The first method extracted

transcripts with a constant and unidirectional alteration in all the time points. The fold change was calculated between *METTL14* overexpressed, and control normalized T>C conversion rates and only transcripts with a 25% stability increase or decrease were retrieved. Of these, only transcripts with a constant and unidirectional alteration in all the time points were selected. The second method aimed at finding transcripts with a significant stability alteration at specific time points. One sample t-tests were computed on *METTL14* overexpressed and control normalized T>C conversion rates, by comparing each time point and the chase onset. Adjusted p-values between the control and the overexpressed were compared at each timepoint, and only transcripts significant (BH adjusted p-value < 0.05) in overexpressed but not control cells were retained.

20. Functional and regulatory enrichment

Gene Ontology (GO) enrichment was performed on cellular components (CC), molecular function (MF), and biological process domains (BP). Over-represented GO terms were identified with topGO (v2.37.0) (Alexa and Rahnenfuhrer 2010), by running the classical algorithm and Fisher's exact test.

Pathway enrichment was performed with clusterProfiler (v3.14.0) and ReactomePA (v1.30.0) (Yu and He 2016; Yu et al. 2012), using KEGG and Reactome annotations.

Regulatory enrichment analysis was carried out to find post-transcriptional regulators possibly controlling differentially expressed genes or genes with mRNA altered stability. It was performed with tRanslatome (Tebaldi, 2014) by querying the AURA database (http://aura.science.unitn.it, 2014). If not specified, a 0.05 Benjamini-Hochberg adjusted p-value cutoff was applied.

21. Statistical analysis

Data are represented as mean±SD (Standard Deviation), as indicated in figure legends. For the Polysome profiling and the SLAMseq data analysis, statistical tests were performed as described in the respective sections. Unless otherwise specified, a Student's two-tailed *t-test* was performed, a Benjamini-Hochberg (BH) multiple testing correction was applied, and a 0.05 adjusted p-value cutoff was set.

All the statistic (except the analysis of SLAMseq and Polysome profiling datasets) was performed using GraphPad Prism 7 software (GraphPad Software, La Jolla, CA, USA).

In vitro experiments were performed at least in biological triplicate and all the experiments with representative images (i.e. Western Blot) were repeated at least two times.

**TABLE 5	SOFTWARES AND ALGORITHMS**		
Image Lab	BioRad	3.0
ImageJ	NIH	1.51i
GraphPad	Prism	7
RTCA	ACEA Biosciences Inc.	1.2
FlowJo™	FlowJo LLC	v10.6.1
FASTQC	http://www.bioinformatics.babraham.ac.uk/projects/fastqc	v0.11.4
UMI tools	https://github.com/CGATOxford/UMI-tools	v0.5.5
Trim Galore	https://www.bioinformatics.babraham.ac.uk/projects/trim_galore/	v0.6.0
Cutadapt	https://github.com/marcelm/cutadapt	v1.18
STAR	https://github.com/alexdobin/STAR	v2.5.2b
HTSeq	https://github.com/simon-anders/htseq	v0.11.1
tRanslatome	https://bioconductor.org/packages/release/bioc/html/tRanslatome.html	v1.22.0
edgeR	https://bioconductor.org/packages/release/bioc/html/edgeR.html	v3.28.0
extract – transcript – regions	https://github.com/stephenfloor/extract-transcript-regions	

SlamDunk	https://github.com/t-neumann/slamdunk	v0.3.4
topGO	https://bioconductor.org/packages/release/bioc/html/topGO.html	v2.37.0
clusterProfiler	https://bioconductor.org/packages/release/bioc/html/clusterProfiler.html	v3.14.0
ReactomePA	https://bioconductor.org/packages/release/bioc/html/ReactomePA.html	v1.30.0
MEME	http://meme-suite.org/	v5.1.0

REFERENCES

Adelman, K., & Lis, J. (2012). Promoter-proximal pausing of RNA polymerase II: emerging role in metazoans. *Nature Reviews Genetics*, 13, 720-731.

Agarwala, S., Blitzblau, H., Hochwagen, A., & Fink, G. (2012). RNA methylation by the MIS complex regulates a cell fate decision in yeast. *PLOS Genetics*, 8:e1002732.

Aguilo, F., Zhang, F., Sancho, A., Fidalgo, M., Di Cecilia, S., Vashisht, A., et al. (2015). Coordination of m6A mRNA methylation and gene transcription by ZFP217 regulates pluripotency and reprogramming. *Cell Stem Cell*, 17(6): 689–704.

Aik, W., Scotti, J. S., Choi, H., Gong, L., Demetriades, M., Schofield, C., et al. (2014). Structure of human RNA N6-methyladenine demethylase ALKBH5 provides insights into its mechanisms of nucleic acid recognition and demethylation. *Nucleic Acid Research*, 42(7):4741-4754.

Alexa, A., & Rahnenfuhrer, J. (2010). *R Package Documentation*. Retrieved from topGO: enrichment analysis for gene ontology.

Anders, S., Pyl, P., & Huber, W. (2015). HTSeq--a Python framework to work with high-throughput sequencing data. *Bioinformatics*, 31(2):166–169.

Andrews, S. (2011, October 6). *FastQC: A quality control tool for high throughput sequence data*. Retrieved from http://www.bioinformatics.babraham.ac.uk ? /projects/fastqc/

Arguello, A., DeLiberto, A., & Kleiner, R. (2017). RNA chemical proteomics reveals the N(6)-methyladenosine (m(6)A)-regulated protein-RNA interactome . *Journal of the American Chemistry Society* , 139:17249-17252.

Atkins, J., & Gesteland, R. (2002). The 22nd amino acid. *Science*, 296, 1409-1410.

Attardi, L., Reczek, E., Cosmas, C., Demicco, E., McCurrach, M., Lowe, S., et al. (2000). PERP, an Apoptosis-Associated Target of p53, Is a Novel Member of the PMP-22/gas3 Family . *Genes Development*, 14(6):704-718.

Attiyeh, E., London, W., Mossé, Y., Wang, Q., Winter, C., Khazi, D., et al. (2005). Chromosome 1p and 11q Deletions and Outcome in Neuroblastoma. *New England Journal of Medicine*, 353(21):2243-2253.

Backer, D., Schmidt, M., Cohn, S., Maris, J., London, W., Buxton, A., et al. (2010). Outcome after Reduced Chemotherapy for Intermediate-Risk Neuroblastoma. *The New England Journal of Medicine*, 363:1313-1323.

Bannister, A., & Kouzarides, T. (2011). Regulation of chromatin by histone modifications. *Cell Research*, 21, 381-395.

Beckwith, J., & Perrin, E. (1963). In situ neuroblastomas: a contribution to the natural history of neural crest tumors. *The American Journal of Pathology*, 43:1089–1104.

Berens, E., Holy, J., Riegel, A., & Wellstein, A. (2015). A Cancer Cell Spheroid Assay to Assess Invasion in a 3D Setting. *Journal of Visualized Experiments*, 105.

Bertero, A., Brown, S., Madrigal, P., Osnato A, Ortmann, D., Yiangou, L., et al. (2018). The SMAD2/3 interactome reveals that TGFb controls m6A mRNA methylation in pluripotency. *Nature*, 555: 256-259.

Betters, E., Liu, Y., Kjaeldgaard, A., Sundstrom, E., & Garcia-Castro, M. (2010). Analysis of early human neural crest development. *Developmental Biology*, 344 (2):578-92.

Bokar, J., Rath-Shambaugh, M., Ludwiczak, R., Narayan, P., & Rottman, F. (1994). Characterization and partial purification of mRNA N6-adenosine methyltransferase from HeLa cell nuclei. Internal mRNA methylation requires a multisubunit complex. *Journal of Biological Chemistry*, 69,17697-17704.

Bokar, J., Shambaugh, M., Polayes, D., Matera, A., & Rottman , F. (1997). Purification and cDNA cloning of the AdoMet-binding subunit of the human mRNA (N6-adenosine)-methyltransferase. *RNA*, 3:1233-1247.

Bosse, K., & Maris, J. (2016). Advances in the Translational Genomics of Neuroblastoma: From Improving Risk Stratification and Revealing Novel Biology to Identifying Actionable Genomic Alterations. *Cancer*, 122(1): 20-33.

Bourdeaut, F., Trochet, D., Janoueix-Lerosey, I., Ribeiro, A., Deville, A., Coz, C., et al. (2005). Germline mutations of the paired-like. *Cancer Letters*, 228(1-2):51-58.

Bown, N., Cotterill, S., Lastowska, M., O'Neill, S., Pearson, A., & et al. (1999). Gain of Chromosome Arm 17q and Adverse Outcome in Patients with Neuroblastoma. *The New England Journalof Medicine*, 340:1954-1961.

Bresler, S., Weiser, D., Huwe, P., Park, J., Krytska, K., & et al. (2014). ALK Mutations Confer Differential Oncogenic Activation and Sensitivity to ALK Inhibition Therapy in Neuroblastoma. *Cancer Cell*, 26(5):682-94.

Bresler, S., Weiser, D., Huwe, P., Park, J., Krytska, K., & et al.,. (2014). ALK mutations confer differential oncogenic activation and sensitivity to ALK inhibition therapy in neuroblastoma . *Cancer Cell*, 26(5):682-94.

Brodeur, G., & Bagatell, R. (2014). Mechanisms of neuroblastoma regression. *Nature Reviews Clinical Oncology*, 11(12):704-713.

Brodeur, G., Pritchard, J., Berthold, F., Carlsen, N., Castel, V., & et al. (1993). Revisions of the International Criteria for Neuroblastoma Diagnosis, Staging, and Response to Treatment. *Journal of Clinical Oncology*, 11(8):1466-1477.

Brodeur, G., Seeger, R., Schwab, M., Varmus, H., & Bishop, J. (1984). Amplification of N-myc in Untreated Human Neuroblastomas Correlates With Advanced Disease Stage. *Science*, 224(4653):1121-1124.

Buxbaum, A., Haimovich, G., & Singer, R. (2015). In the right place at the right time: visualizing and understanding mRNA localization. *Nature Reviews Molecular Cell Biology*, 16, 95-109.

Cabrita, D., Dobson, C., & Christodoulou, J. (2010). Protein folding on the ribosome. *Current Opinion in Structural Biology*, 20, 33-45.

Campeau , E., Ruhl, V., Rodier, F., Smith, C., Rahmberg, B., Fuss, J., et al. (2009). A versatile viral system for expression and depletion of proteins in mammalian cells. *PLOS one*, 4(8):e6529.

Cech, T. R., & Steitz, J. A. (2014). The Noncoding RNA Revolution—Trashing Old Rules to Forge New Ones. *Cell*, 157(1), 77-94.

Chen, J., Hackett, C., Zhang, S., Song , Y., Bell, R., & Molinaro, A. (2015). The Genetics of Splicing in Neuroblastoma. *Cancer Discovery*, 5(4): 380–395.

Crick, F. (1970). Central Dogma of Molecular Biology. *Nature*, 227, 561-563.

Cui, Q., Shi, H., Ye, P., Li, L., Qu, Q., Sun, G., et al. (2017). m(6)A RNA methylation regulates the self-renewal and tumorigenesis of glioblastoma stem cells. *Cell Reports*, 18:2622–2634.

Dassi, E., Re, A., Leo, S., Tebaldi, T., Pasini, L., Peroni, D., et al. (2014). AURA 2: Empowering discovery of post-transcriptional networks. *Translation (Austin)*, 2(1):e27738.

De Bernardi , B., Gerrand, M., Boni, L., Rubie, H., Canete, A., Di Cataldo, A., et al. (2009). Excellent Outcome With Reduced Treatment for Infants With Disseminated Neuroblastoma Without MYCN Gene Amplification. *Journal of Clinical Oncology*, 27(7):1034-1040.

Delbridge, A., & Strasser, A. (2015). The BCL-2 protein family, BH3-mimetics and cancer therapy. *Cell Death Differentiation*, 22(7): 1071–1080.

Desrosiers , R., Friderici K, & Rottman , F. (1974). Identification of methylated nucleosides in messenger RNA from Novikoff hepatoma cells. *PNAS ISA*, 71: 3971-3975.

Diskin, S., Capasso, M., Schnepp, R., Cole, K., Attiyeh, E., Hou, C., et al. (2012). Common Variation at 6q16 Within HACE1 and LIN28B Influences Susceptibility to Neuroblastoma. *Nature Genetics*, 44(10):1126-1130.

Dobin, A., Davis, C., Schlesinger, F., Drenkow, J., Zaleski, C., Jha, S., et al. (2013). STAR: ultrafast universal RNA-seq aligner. *Bioinformatics*, 29(1):15–21,.

Dominissini, D., Moshitch-Moshkovitz , S., Schwartz, S., Salmon-Divon, M., Ungar, L., Osenberg, S., et al. (2012). Topology of the human and mouse m6A RNA methylomes revealed by m6A-seq. *Nature*, 485: 201-206.

Dreyfuss, G., Kim, N. V., & Kataoka, N. (2002). Messenger-RNA-binding proteins and the messages they carry. *Nature Reviews Molecular Cell Biology*, 3, 195-205.

Du, H., Zhao, Y., He, J., Zhang, Y., Xi, H., & al., e. (2016). YTHDF2 destabilizes m6A-containing RNA through direct recruitment of the CCR4-NOT deadenylase complex . *Nature Communications*, 7:12626.

Feng, C., Liu, Y., Wang, G., Deng, Z., Zhang, Q., Wu, W., et al. (2014). Crystal Structures of the Human RNA Demethylase Alkbh5. *Journal of Biological Chemistry*, 289(17):11571-11583.

Gamazon, E., Pinto, N., Konkashbaev, A., Im, H., Diskin, S., London, W., et al. (2013). Trans-population analysis of genetic mechanisms of ethnic disparities in neuroblastoma survival. *Journal of the National Cancer Institute*, 105(4):302-309.

Gebauer, F., Preiss, T., & Hentze, M. (2012). *From cis-regulatory elements to complex RNPs and back.* Cold Spring Harbor Perspectives in Biology.

Genuth, N., & Barna, M. (2018). Heterogeneity and specialized functions of translational machinery: from genes to organisms. *Nature Reviews Genetics*, 19:431-452.

Geula, S., Moshitch-Moshkovitz, S., Dominissini, D., AlFatah Mansour, A., Kol, N., & et al.,. (2015). m6A mRNA methylation facilitates resolution of naïve pluripotency toward differentiation. *Science*, 347(6225):1002-1006.

Gingras, A., Raught, B., & Sonenberg, N. (1999). eIF4 initiation factors: effectors of mRNA recruitment to ribosomes and regulators of translation. *Annual Review of Biochemistry*, 68:913-963.

Gu, S., Sun, D., Dai, H., & Zhang, Z. (2018). N(6)-methyladenosine mediates the celllular proliferation and apoptosis via microRNAs in arsenite-transformed cells. *Toxicology Letters*, 292:1-11.

Harding, H., Zhang , Y., Bertolotti, A., Zeng, H., & Ron, D. (2000). Perk is essential for translational regulation and cell survival during the unfolded protein response. *Molecular Cell*, 5, 897-904.

Hau, D., Zhao, Y., & et al.,. (2016). YTHDF2 destabilizes m6A-containing RNA through direct recruitment of the CCR4–NOT deadenylase complex . *Nature Communications*, 7:1-11.

Herzog, V., Reichholf, B., Neumann, T., Rescheneder, P., Bhat, P., Burkard, T., et al. (2017). Thiol-linked alkylation of RNA to assess expression dynamics. *Nature Methods*, 14:1198–1204.

Hienonen, T., Sammalkorpi, H., Isohanni, P., Versteeg, R., Karikoski, R., & Aaltonen, L. (2005). A 17p11.2 germline deletion in a patient with Smith-Magenis syndrome and neuroblastoma. *Journal of Medical Genetics*, 42:e3.

Holliday , R., & Pugh, J. (1975). DNA modification mechanism and gene activity during development. *Science*, 187:226-232.

Horiuchi, K., Kawamura, T., Iwanari, H., Ohashi , R., Naito, M., & et al. (2013). Identification of Wilm's tumor 1-associating protein complex and its role in alternative splicing and the cell cyle. *Journal of Biological Chemistry*, 288:33292-33302.

Huang , H. , Weng, H., Zhou, K., Wu, T., Zhao, B., Sun, M., et al. (2019). Histone H3 trimethylation at lysine 36 guides m6A RNA modification co-transcriptionally. *Nature*, 567: 414-519.

Huang, H., Weng, H., & Chen, J. (2020). m6A modification in coding and non-coding RNAS: roles and therapeutic implication in cancer. *Cancer Cell Review*, 37:270-288.

Huang, H., Weng, H., Sun, W., Qin, X., Shi, H., Wu, H., et al. (2018). Recognition of RNA N(6)-methyladenosine by IGF2BP proteins enhances mRNA stability and translation. *Nature Cell Biology*, 20:285-295.

Huang, H., Weng, H., Sun, W., Qin, X., Shi, H., Wu, H., et al. (2018b). Recognition of RNA N(6)-methyladenosine by IGF2BP proteins enhances mRNA stability and translation. *Nature Cell Biology*, 20:285-295.

Huang, M., & Weiss, W. A. (2013). Neuroblastoma and MYCN. *Cold Spring Harbor Perspectives in Medicine*, 3(10):a014415.

Huber, K. (2006). The sympathoadrenal cell lineage: Specification, diversification, and new perspectives. *Developmental Biology*, 298:335–343.

Huber, K. (2008). Persistent expression of BMP-4 in embryonic chick adrenal cortical cells and its role in chromaffin cell development. *Neural Develoment*, 3:28.

Iehara, T., Hamazaki, M., Tajiri, T., Kawano, Y., Kaneko, M., & et al. (2013). Successful treatment of infants with localized neuroblastoma based on their MYCN status. *International JOurnal of Clinical Oncology*, 18:389-395.

Istrail, S., & Davidson, E. (2005). Logic functions of the genomic cis-regulatory code. *PNAS*, 102:4954-4959.

Iyer, L., Zhang , D., & Aravind, L. (2016). Adenine methylation in eukaryotes: apprehending the complex evolutionary history and functional potential of an epigenetic modification. *BioEssays*, 38:27-40.

Jackson, R., Hellen, C., & Pestova, T. (2010). The mechanism of eukaryotic translation initiation and principles of its regulation . *Nature Reviews Molecular Cell Biology*, 11:113-127.

Jacob, F., & Monod, J. (1961). Genetic regulatory mechanisms in the synthesis of proteins. *Journal of Molecular Biology*, 3, 318-356.

Kan, L., Grozhik, A., Vedanayagam, J., Patil, D., Pang, N., & et al. (Communication). The m6A pathway facilitates sex determination in Drosophila . *Nature*, 8:15737.

Kane, S., & Beemon, K. (1987). Inhibition of methylation at two internal N6-methyladenosine sites caused by GAC to GAU mutations. *Journal of Biological Chemistry*, 262(7): 3422-3427.

Ke, S., Pandya-Jones, A., Saito, Y., Fak, J., Vagbo, C., Geula, S., et al. (2017). mRNA modifications are deposited in nascent pre- mRNA and are not required for splicing but do specify cytoplasmic turnover. *Genes & Development*, 31:990-1006.

Kembhavi, S., Shah, S., Rangarajan, V., Qureshi, S., Popat, P., & Kurkure, P. (2015). Imaging in neuroblastoma: an update. *The Indian Journal of Radiology & Imaging*, 25(2):129-136.

Kennedy, E., Bogerd, H., Kornepati, A., Kang, D., Ghoshal, D., & et al. (2016). Posttransctiptional m6A editing of HIV-1 mRNAs enhances viral gene expression. *Cell Host Microbe*, 19:675-685.

Knudson, A., & Strong , L. (1972). Mutation and cancer: neuroblastoma and pheochromocytoma. *American Journal of Human Genetics*, 24:514-522.

Krueger, F. (2012). *Trim Galore: a wrapper tool around Cutadapt and FastQC to consistently apply quality and adapter trimming to FastQ files, with some extra functionality for MspI-digested RRBS-type (Reduced Representation Bisufite-Seq) libraries*. Retrieved from Babraham Bioinformatics: http://www. bioinformatics. babraham. ac. uk/projects/trim_galore/. (Date of access: 28/04/2016

Lamarca, V., Marzo, I., Sanz-Clemente, A., & Carrodeguas, J. (2008). Exposure of any of two proapoptotic domains of presenilin 1-associated protein/mitochondrial carrier homolog 1 on the surface of mitochondria is sufficient for induction of apoptosis in a Bax/Bak-independent manner. *Journal of molecular biology*, 5:325-334.

Le Douarin, N., & Kalcheim, G. (1999). *The neural crest 2nd edn.* Cambridge: Cambridge Univerity Press.

Lee, J. (2009). Lessons from X-chromosome inactivation: lncRNA as guides and theters to the epigenome. *Genes & Development* , 23:1831-1842.

Li, B., Yang, X., Li, P., Yuan, Q., Liu, H., Yuan, J., et al. (2008). IL-4/Stat6 activities correlate with apoptosis and metastasis in colon cancer cells. *Biochemical and Biophysical Research Communication*, 369(2):554-560.

Li, Z., Weng, H., Su, R., Weng, X., Zuo, Z., Li, C., et al. (2017). FTO Plays an Oncogenic Role in Acute Myeloid Leukemia as a N6-Methyladenosine RNA Demethylase. *Cancer Cell*, 31(1): 127-141.

Linder, B., Grozhik, A., Olarerin-George, A., Meydan, C., Mason, C., & Jaffrey, S. (2015). Single-nucleotide-resolution mapping of m6A and m6Am throughout the transcriptome. *Nature Methods*, 12:767–772.

Liu , J., Yue, Y., Han, D., Wang, X., Fu, Y., & et al.,. (2014). A METTL3-METTL14 complex mediates mammalian nuclear RNA N6-adesonine methylation. *Nature Chemical Biology*, 10:93,95.

Liu, N., Dai, Q., Zheng, G., He, C., Parisien, M., & Pan, T. (2015). N(6)-methyladenosine-dependent RNA structural switches regukate RNA-protein interaction. *Nature*, 518:560-564.

Liu, Z., Lu, H., Pastuszny, A., & Hu, C. (2005). Apolipoprotein l6, a Novel Proapoptotic Bcl-2 Homology 3-only Protein, Induces Mitochondria-Mediated Apoptosis in Cancer Cells . *Molecular Cancer Research*, 3(1):21-31.

London, W., Castleberry , R., Matthay, K., Look, A., Seeger, R., Shimada, H., et al. (2005). Evidence for an age cutoff greater than 365 days for neuroblastoma risk group stratification in the Children's Oncology Group. *Journal of Clinical Oncology*, 23(27):6459-6465.

Luo, S., & Tong, L. (2014). Molecular basis for the recognition of methylated adenins in RNA by the eukaryotic YTH domain. *PNAS USA*, 111:13834-13839.

Manolio, T., Collins, F., Cox, N., Goldstein, D., Hindorff, L., Hunter, D., et al. (2009). Finding the missing heritability of complex diseases. *Nature*, 461(7265):747-753.

Maris, J., Hogarty, M., Bagatell, R., & Cohn, S. (2007). Neuroblastoma. *Lancet*, 369,2106-2120.

Marshall, G., Carter, D., Cheung, B., Liu, T., Mateos, M., Meyerowitz, J., et al. (2014). The prenatal origin of cancer. *Nature Reviews Cancer*, 14:277-289.

Marshall, G., Carter, D., Cheung, B., Liu, T., Mateos, M., Meyerowitz, J., et al. (2014). The prenatal origins of cancer. *Nature Reviews Cancer*, 14:277–289.

Marte, B., & Downward, J. (1997). PKB/Akt: connecting phosphoinositide 3-kinase to cell survival and beyond. *Nature Genetics*, 22, 355-358.

Martin, M. (2011). Cutadapt removes adapter sequences from high-throughput sequencing reads. *EMBnet.journal*, 17(1).

Matsushima, W., Herzog, V., Neumann, T., Gapp, K., Zuber, J., Ameres, S., et al. (2018). SLAM-ITseq: sequencing cell type-specific transcriptomes without cell sorting. *Development*, 145(13). pii: dev164640.

Matzke, M., Metzke, A. J., & Kooter, J. M. (2001). RNA: Guiding Gene Silencing. *Science*, 293(5532): 1080-1083.

Mauer, J., Luo, X., Blanjoie, A., Jiao , X., Grozhic, A., & et al.,. (2017). Reversible methylation of m6Am in the 5' cap controls mRNA stability. *Nature*, 541:371-375.

McCarthy, D., Chen, Y., & Smyth, G. (2012). Differential expression analysis of multifactor RNA-Seq experiments with respect to biological variation. *Nucleic Acid Reserach*, 40(10):4288-97.

Mette, M., van der Winden, J., Matzke, M., & Matzke, A. (1999). Production of aberrant promoter transcripts contributes to methylation and silencing of unlinked homologous promoters in trans. *The EMBO Journal*, 18: 241-248.

Meyer, K., Patil, D., Zhou, J., Zinoviev, A., Skabkin, M., Elemento, O., et al. (2015). 5' UTR m(6)A Promotes Cap-Independent Translation. *Cell*, 163(4):999-1010.

Meyer, K., Saletore, Y., Zumbo, P., Elemento, O., Mason, C., & Jaffrey , S. (2012). Comprehensive analysis of mRNA methylation reveals enrichment in 3' UTRs and near stop codons. *Cell*, 149: 1635-1646.

Molenaar, J., Domingo-Fernández, R., Ebus, M., Lindner, S., Koster, J., & et al. (2012). LIN28B Induces Neuroblastoma and Enhances MYCN Levels via let-7 Suppression. *Nature Genetics*, 44(11):1199-206.

Mossé, Y., Laudenslager, M., Longo, L., Cole, K., Wood, A., & Attiyeh, A. (2008). Identification of ALK as a major familial neuroblastoma predisposition gene. *Nature*, 455(7215):930-935.

Muhar, M., Ebert, A., Neumann, T., Umkehrer, C., Jude, J., Wieshofer, T., et al. (2018). SLAM-seq defines direct gene-regulatory functions of the BRD4-MYC axis. *Science*, 360(6390):800-805.

Neumann, T., Herzog, V., Muhar, M., von Haeseler, A., Zuber, J., Ameres, S., et al. (2019). Quantification of experimentally induced nucleotide conversions in high-throughput sequencing datasets. *BMC Bioinformatics*, 20(258).

Neumann, T., Herzog, V., Muhar, M., von Haeseler, A., Zuber, J., Ameres, S., et al. (2019). Quantification of Experimentally Induced Nucleotide Conversions in High-Throughput Sequencing Datasets . *BMC Bioinformatics*, 20(1):258.

Nuchtern, J., London, W., Barnewolt, C., Naranjo, A., McGrady, P., & et al. (2012). A Prospective Study of Expectant Observation as Primary Therapy for Neuroblastoma in Young Infants: A Children's Oncology Group Study. *Annals of Surgery*, 256(4):573-580.

Olsen, P., & Ambros, V. (1999). The lin-4 regulatory RNA controls developmental timing in Caenorhabditis elegans by blocking LIN-14 protein synthesis after the initiation of translation. *Developmental Biology*, 216, 671-680.

Park, J., Bagatell, R., London, W., Maris, J., & Cohn, S. (2013). Children's Oncology Group's 2013 blueprint for research: neuroblastoma. *Pediatric Blood Cancer*, 60(6):985-93.

Park, J., Bagatell, R., London, W., Maris, J., Cohn, S., Mattay, K., et al. (2013). Children's Oncology Group's 2013 Blueprint for Research: Neuroblastoma. *Pediatric Blood Cancer*, 60(6):985-993.

Patil, D., Chen, C., Pickering, B., Chow, A., Jackson, C., & et al. (2016). m6A RNA methylation promotes XIST-mediated transcriptional repression. *Nature*, 537:369-373.

Patterson, D., Gao, D., Trahan, D., Johnson, B., Ludwig, A., & et al.,. (2011). Effect of MDM2 and vascular endothelial growth factor inhibition on tumor angiogenesis and metastasis in neuroblastoma. *Angiogenesis*, 14,255–266.

Pause, A., Belsham, G. J., Gingras, A.-C., Donzé, O., Lin, T.-A., Lawrence Jr, J. C., et al. (1994). Insulin-dependent stimulation of protein synthesis by phosphorylation of 5′ cap function. *Nature*, 371, 762-767.

Peifer, M., Hertwig, F., Roels, F., Dreidax, D., Gartlgruber, M., & et al. (2015). Telomerase Activation by Genomic Rearrangements in High-Risk Neuroblastoma. *Nature*, 526(7575):700-704.

Pendleton, K., Chen , B., Liu , K., Hunter, O., Xie, Y., Tu, B., et al. (2017). The U6 snRNA m6A Methyltransferase METTL16 Regulates SAM Synthetase Intron Retention. *Cell*, 169(5):824-835.

Perry, R., & Kelley, D. (1974). Existence of methylated messenger RNA in mouse L cells. *Cell*, 1: 37,42.

Pestova, T., Kolupaeva, V., Lomakin, I., Pilipenko, E., Shatsky, I., Agol, V., et al. (2001). Molecular mechanisms of translation initiation in eukaryotes. *PNAS*, 98(13):7029-7036.

Ping , X., Sun, B., Wang, L., Xiao, W., Yang, X., & et al.,. (2014). Mammalian WTAP is a regulatory subunit of the RNA N6-methyladenosine methyltransferase. *Cell Research*, 24:177-189.

Pinto, N., Applebaum, M., Volchenboum, S., Matthay, K., Matthay, K., London, W., et al. (2005). Advances in Risk Classification and Treatment Strategies for Neuroblastoma. *Journal of Clinical Oncology*, 33(27):3008-3017.

Preiss, T., & Hentze , M. (2003). Starting the protein synthesis machine: eukaryotic translation initiation. *Bioessays*, 25:1201-1211.

Pugh, T., Morozova O, Attiyeh, E., Asgharzadeh, S., Wei, J., & et al. (2013). The genetic landscape of high-risk neuroblastoma. *Nature Genetics*, 45(3):279-284.

Robinson, M., McCarthy, D., & Smyth, G. (2010). edgeR: a Bioconductor package for differential expression analysis of digital gene expression data. *Bioinformatics*, 26(1):139-40.

Sait, S., & Modak, S. (2017). Anti-GD2 immunotherapy for neuroblastoma. *Expert Review of Anticancer Therapi*, 17(10):889-904.

Sanjana, N., & Zhang, F. (2014). Improved vectors and genome-wide libraries for CRISPR screening. *Nature Methods*, 11(8):783-4.

Schoenberg, D., & Maquat, L. (2012). Regulation of cytoplasmic mRNA decay. *Nature Reviews Genetics*, 13, 246-259.

Scutenaire, J., Deragon, J., Jean, V., Benhmed, M., Raynaud, C., Favory, J., et al. (2018). The YTH domain protein ECT2 is an m6A reader required for normal trichome branches in Arabidopsis. *Pant Cell*, 30:986-1005.

Seeger, R., Brodeur, G., Sather, H., Dalton, A., Siegel, S., Wong, K., et al. (1985). Association of Multiple Copies of the N-myc Oncogene With Rapid Progression of Neuroblastomas. *New England Journal of Medicine*, 313(18):1111-1116.

Selberg, S., Blokhina, D., Aatonen, M., Koivisto, P., Siltanen, A., Mervaala, E., et al. (2019). Discovery of Small Molecules that Activate RNA Methylation through Cooperative Binding to the METTL3-14-WTAP Complex Active Site. *Cell Reports*, 26:3762-3771.

Shayesteh , L., Lu, Y., Kuo, W., Baldocchi, R., Godfrey, T., Collins, C., et al. (1999). PIK3CA is implicated as an oncogene in ovarian cancer. *Nature Genetics*, 21(1), 99-102.

Shi, H., Wei, J., & He, C. (2019). Where, When, and How: Context-Dependent Functions of RNA Methylation Writers, Readers, and Erasers. *Molecular Cell Review*, 74:640-650.

Shima, H., Matsumoto, M., Ishigami, Y., Ebina, M., Muto, A., Sato , Y., et al. (2017). S-Adenosylmethionine Synthesis Is Regulated by Selective N6-Adenosine Methylation and mRNA Degradation Involving METTL16 and YTHDC1. *Cell Report*, 21(12):3354-3363.

Siller, E., DeZwaan, D., Anderson, J., Freeman, B., & Barral, J. (2010). Slowing bacterial translation speed enhances eukaryotic protein folding efficiency. *Journal of Molecular Biology*, 396, 1310-1318.

Singh, B., Kinne, H., Milligan, R., Washburn, L., Olsen, M., & Lucci, A. (2016). Important role of FTO in the survival of rare panresistant triple-negative inflammatory breast cancer cell facing a severe metabolic challenge. *PLoS One*, 11:e0159072.

Singh, G., Pratt, G., Yeo, G., & Moore, M. (2015). The clothes make the mRNA: past and present trends in mRNP fashion. *Annual Review of Biochemistry*, 84, 325-354.

Sledz, P., & Jinek, M. (2016). Structural insights into the molecular mechanism of the m6A writer complex. *eLife*, 5, e18434.

Smith, T., Heger, A., & Sudbery, I. (Research). UMI-tools: modeling sequencing errors in Unique Molecular Identifiers to improve quantification accuracy. *Genome*, 27(3):491-499.

Strother, D., London, W., Schmidt, M., Brodeur, G., Shimada, H., & et al. (2012). Outcome after surgery alone or with restricted use of chemotherapy for patients with low-risk neuroblastoma: results of Children's Oncology Group study P9641. *Journal of Clinical Oncology*, 30(15):1842-1848.

Stutz, F., Bachi , A., Doerks, T., Braun, I., Séraphin, B., Wilm, M., et al. (2000). REF, an evolutionary conserved family of hnRNP-like proteins, interacts with TAP/Mex67p and participates in mRNA nuclear export. *RNA*, 6(4):630-650.

Su, R., Dong, L., Li, C., Nachtergaele, S., Wunderlich, M., Qing, Y., et al. (2018). R-2HG exhibits anti-tumor activity by targeting FTO/m(6)A/MYC/CEBPA signaling. *Cell*, 172:90-105.

Tebaldi, T., Dassi, E., Kostoska, G., Viero, G., & Quattrone, A. (2014). tRanslatome: an R/Bioconductor package to portray translational contro. *Bioinformatics*, 30(2):289-91.

Testa, J., & Bellacosa, A. (2001). AKT plays a central role in tumorigenesis. *PNAS*, 98, 10983-10985.

Theler , D., Dominguez , C., Blatter, M., Boudet, J., & Allain FH. (2014). Solution structure of the YTH domain in complex with N6-methyladenosine RNA: a reader of methylated RNA. *Nucleic Acid Research*, 42:13911-13919.

Tian , J., Ying, P., Ke, J., Zhu, Y., Yang, Y., Gong, Y., et al. (2019). ANKLE1 N6-methyladenosine-related variant is associated with colonrectal cancer risk by maintaining the genomic stability. *International Journal of Cancer*, 11.

Uddin, M., Roy, K., Hosain, S., Khiste, S., Hill, R., Jois, S., et al. (2019). An N(6)-methyladenosine at the transited codon 273 of p53 pre-mRNA promotes the expression of R273H mutant protein and drug resistance of cancer cell. *Biochemical Pharmacology*, 160:134-145.

Unsicker, Z. (1973). Fine structure and innervation of the avian adrenal gland. I. Fine structure of adrenal chromaffin cells and ganglion cells. *Zeitschrift für Zellforschung und mikroskopische Anatomie*, 145:389-416.

Valentijn, L., Koster, J., Zwijnenburg, D., Hasselt, N., van Sluis, P., Volckmann, R., et al. (2015). TERT rearrangements are frequent in neuroblastoma and identify aggressive tumors. *Nature Genetics*, 47:1411,1414.

Venter, C. J., & et al.,. (2001). The sequence of the human genome. *Science*, 291(5507): 1304-1351.

Vogel, K., & Weston, J. (1990). The sympathoadrenal lineage in avian embryos. I. Adrenal chromaffin cells lose neuronal traits during embryogenesis. *Developmental Biology*, 139:1–12.

Vu, L. P., Cheng, Y., & Kharas, M. G. (2018). The Biology of m6A RNA Methylation in Normal and Malignant Hematopoiesis. *Cancer Discovery*, 9(1):25-33.

Vu, L. p., Pickering, B. F., Cheng, Y., Zacara, S., Nguyen, D., Minuesa , G., et al. (2017). The N6-methyladenosine (m6A)-forming enzyme METTL3 controls myeloid differentiation of normal hematopoietic and leukemia cells. *Nature medicine*, 23:1369–1376.

Wang , X., Feng, J., Xue, Y., Guan, Z., Zhang, D., Liu, Z., et al. (2016). Structural basis of N(6)-adenosine methylation by the METTL3-METTL14 complex. *Nature*, 534, 575-578.

Wang, J., Li, Y., Wang, P., Han, G., Zhang, T., Chang, J., et al. (2020). Leukemogenic Chromatin Alterations Promote AML Leukemia Stem Cells via a KDM4C-ALKBH5-AXL Signaling Axis. *Cell Stem Cell*, 27, 81–97.

Wang, P., Doxtader, K. A., & Nam, Y. (2016). Structural Basis for Cooperative Function of Mettl3 and Mettl14 Methyltransferases. *Molecular Cell*, 2:306-317.

Wang, X., Feng, J., Xue, Y., Guan Z, Zhang , D., & et al. (2016). Structural basis of N6-adenosine methylation by the METTL3-METTL14 complex. *Nature*, 534:575-578.

Wang, X., Feng, J., Xue, Y., Guan, Z., Zhang, D., Liu, Z., et al. (2016b). Structural basis of N6-adenosine methylation by the METTL3–METTL14 complex. *Nature*, 534:575–578.

Wang, X., Zhao, B., Roundtree, I., Lu, Z., Han, D., & et al. (2015). N6-Methyladenosine modulates messenger RNA translational efficiency. *Cell*, 161:1388-1399.

Wei, C., Gershowitz, A., & Moss, B. (1975). N6,O2'-dimethyladenosine a novel methylated ribonucleoside next to the 5' terminal of animal cell and virus mRNA. *Nature*, 257:251-253.

Wei, J., Liu, F., Lu, Z., Fei, Q., Ai, Y., He, P. C., et al. (2018). Differential m6A, m6Am, andm1A Demethylation mediated by FTO in the cell nucleus and cytoplsm. *Molecular Cell*, 71:973-985.

Weng, H., Huang, H., Wu, H., Qin, X., Zhao, B. S., Dong, L., et al. (2018). METTL14 Inhibits Hematopoietic Stem/Progenitor Differentiation and Promotes Leukemogenesis via mRNA m6A Modification. *Cell Stem Cell*, 22(2):191-205.

Wickens, M., Goodwin, E., Kimble, J., Strickland , S., & Hentze, M. (2000). *Translational control of gene expression.* New York, USA: Cold Spring Harbour Laboratory Press.

Wojtas, M., Pandey, R., Mendel, M., Homolka, D., Sachidanandam, R., & Pillai, R. (2017). Regulation of m6A Transcripts by the 3'→5' RNA Helicase YTHDC2 Is Essential for a Successful Meiotic Program in the Mammalian Germline. *Molecular Cell*, 68(2):374-387.

Xing, L., & Bassell, G. (2013). mRNA localization: an orchestration of assembly, traffic and synthesis. *Traffic*, 14, 2-14.

Xu, C., Liu, K., Ahmed, H., Loppnau, P., Schapira, M., & Min, J. (2015). Structural basis for the discriminative recogniton of N6-methyladenosine RNA bythe human YT521-B homology domain family of protein. *Journal of Biological Chmistry*, 290:24902-24913.

Yang, F., Jin, H., Que, B., Chao, Y., Zhang, H., Ying, X., et al. (2019). Dynamic m(6)A mRNA methylation reveals the role of METTL3-m(6)A-CDCP1 signaling axis in chemical carcinogenesis. *Oncogene*, 38:4755-4772.

Yu, G., & He, Q. (2016). ReactomePA: an R/Bioconductor package for reactome pathway analysis and visualization. *Molecular BioSystem*, 12(2):477-9.

Yu, G., Wang, L., Han, Y., & He, Q. (2012). clusterProfiler: an R package for comparing biological themes among gene clusters. *OMICS*, 16(5):284–287.

Yu, J., Vodyanik, M., Smuga-Otto, K., Antosiewicz-Bourget, J., Frane, J., Tian, S., et al. (2007). Induced Pluripotent Stem Cell Lines Derived From Human Somatic Cells. *Science*, 318(5858):1917-20.

Zc3h13/Flacc is required for adenosine methylation by bridging the mRNA-binding factor Rbm15/Spenito to the m6A machinery component Wtap/Fl(2)d. (n.d.). *Genes & Development*.

Zhang, J., Bai, R., Li, M., Ye, H., Wu, C., Wang, C., et al. (2019). Excessive miR-25-3p maturation via N(6)-methyladenosine stimulated by cigarette smoke promotes pancreatic cancer progression. *Nature Communications*, 10:1858.

Zhang, S., Wei, J., & et al.,. (2016). MYCN controls an alternative RNA splicing program in high-risk metastatic neuroblastoma. *Cancer Letters*, 371(2): 214-224.

Zheng, G., Dahl, J., Niu, Y., Fedorcsak, P., Huang, C., & et al.,. (2013). ALKBH5 is a mammalian RNA demethylase that impacts mRNA metabolism and mouse fertility. *Mololecular Cell*, 49: 18-29.

Zhong, S., Li, H., Bodi, Z., Button, J., Vespa , L., & et al. (2008). MTA is an Arabidopsis messenger RNA adenosine methylase and interacts with a homolog of a sex-specific splicing factor. *Plant Cell*, 20:1278-1288.

Zhong, S., Li, H., Bodi, Z., Button, J., Vespa , L., & et al.,. (2008). MTA is an Arabidopsis messenger RNA adenosine methylase and interacts with a homolog of a sex-specific splicing factor. *Plant Cell*, 20:1278-1288.

Zhou, K. I., Shi, H., Lyu, R., Wylder, A. C., Matuszek, Z., Pan, J. N., et al. (2019). Regulation of Co-transcriptional Pre-mRNASplicing by m6A through the Low-Complexity protein hnRNPG. *Molecular Cell*, 76:70-81.

Zhou, Z., Luo, M., Straesser, K., Katahira, J., Hurt, E., & Reed, R. (2000). The protein Aly links pre-messenger-RNA splicing to nuclear export in metazoans. *Nature*, 407(6802):401-405.

Zhu, S., Lee, J., Guo, F., Shin, J., Perez-Atyade, A., Kutok, J., et al. (2012). Activated ALK collaborates with MYCN in neuroblastoma pathogenesis. *Cancer Cell*, 21:362–373.

Zimmermann, K., Yancopoulos, G., Collum, R., Smith, R., Kohl, N., Denis, K., et al. (1986). Differential expression of myc family genes during murine development. *Nature*, 319:780–783.